PRODUCTION OF NANO ALUMOXANE FROM ALUMINUM HYDROXIDE

A THESIS SUBMITTED TO
THE GRADUATE SCHOOL OF NATURAL AND APPLIED SCIENCES
OF
MIDDLE EAST TECHNICAL UNIVERSITY

BY

KORHAN SEZGİKER

IN PARTIAL FULFILLMENT OF THE REQUIREMENTS
FOR
THE DEGREE OF MASTER OF SCIENCE
IN
CHEMICAL ENGINEERING

JANUARY 2010

Approval of the thesis:

PRODUCTION OF NANO ALUMOXANE FROM ALUMINUM HYDROXIDE

submitted by **KORHAN SEZGİKER** in partial fulfillment of the requirements for the degree of **Master of Science in Chemical Engineering Department, Middle East Technical University** by,

Prof. Dr. Canan Özgen _____
Dean, Graduate School of **Natural and Applied Sciences**

Prof. Dr. Gürkan Karakaş _____
Head of Department, **Chemical Engineering**

Prof. Dr. Güngör Gündüz _____
Supervisor, **Chemical Eng. Dept., METU**

Assist. Prof. Dr. Bora Maviş _____
Co-supervisor, **Mechanical Eng. Dept., Hacettepe Univ.**

Examining Committee Members:

Prof. Dr. Işık Önal _____
Chemical Engineering Department, METU

Prof. Dr. Güngör Gündüz _____
Chemical Engineering Department, METU

Assist. Prof. Dr. Serkan Kıncal _____
Chemical Engineering Department, METU

Prof. Dr. Abdullah Öztürk _____
Metallurgical and Materials Engineering Department, METU

Assist. Prof. Dr. Burcu Akata Kurç _____
Micro and Nano Technology Department, METU

Date: 15.01.2010

I hereby declare that all information in this document has been obtained and presented in accordance with academic rules and ethical conduct. I also declare that, as required by these rules and conduct, I have fully cited and referenced all material and results that are not original to this work.

Name, Last name : KORHAN SEZGİKER

Signature :

ABSTRACT

PRODUCTION OF NANO ALUMOXANE FROM ALUMINUM HYDROXIDE

Sezgiker, Korhan

M.S., Department of Chemical Engineering

Supervisor: Güngör Gündüz, Prof. Dr.

Co-Supervisor: Bora Maviş, Assist. Prof. Dr.

January 2010, 114 pages

Alumina (Al_2O_3) is one of the most widely used engineering ceramic. It can be used in a wide range of applications like electrical/thermal insulation, wear resistance, structural refractories, cutting tools, abrasives, catalyst carriers and coatings. A traditional ceramic process has several steps (i.e. powder synthesis and processing, shape forming, drying, organic burnout and densification). Accessing powders with sizes in the range of a couple of micrometers down to several tens of nanometers is considered critical in attaining higher densities in the final ceramic bodies. Besides since significant shrinkage can be observed in the thermal treatment steps due to the excessive use of additives (e.g. binders, solvents and plasticizers) in the powder processing and forming steps, it is important to take remedies that would increase the solids loading in the initial mixtures. In addition, most of the conventional additives and solvents used in these steps are toxic and it is

necessary to replace them with the environmentally benign aqueous-based alternatives.

Alumoxanes could be used as a benign aqueous-based alternative to be used as a ceramic precursor or an agent. They are a group of compounds that have nano sized boehmite cores encapsulated with the organic groups used in its production steps.

In this research work, alumoxane nano particles which can be used as precursors for nano-alumina were developed starting from aluminum trihydroxide. As a preconditioning step, grinding was applied to decrease the aluminum hydroxide particle size (≤ 60 μm) to submicron sizes. This process was followed by the glycothermal ageing step, and organic derivative of boehmite was obtained. The amorphous particles thus obtained were further treated mechanochemically in a high energy ball mill with organic chemicals like acetic acid, methoxy acetic acid, stearic acid and L-lysine. After this step the observed sizes of the particles were as low as 10-100 nm. The effects of organic molecules used in each step were studied by FTIR spectroscopy and their effectiveness in exfoliation of hydroxide layers were identified with dynamic light scattering from processing solutions dispersed in aqueous medium. Moreover, in each step, structural analyses were carried out by XRD.

Keywords: alumoxane, organic derivative of boehmite, mechanochemistry, glycothermal process, nano alumina precursor

ÖZ

ALÜMİNYUM HİDROKSİTTEN NANO ALÜMOKSAN ÜRETİMİ

Sezgiker, Korhan
Yüksek Lisans, Kimya Mühendisliği Bölümü
Tez Yöneticisi: Güngör Gündüz, Prof. Dr.
Ortak Tez Yöneticisi: Bora Maviş, Yard. Doç. Dr.

Ocak 2010, 114 sayfa

Alümina (Al_2O_3), yaygın olarak tercih edilen seramik malzemelerin başında gelmektedir. Çeşitli uygulama alanlarında (elektriksel/ısıl yalıtımda, aşınma direncinin ve çizilme dayanımının gerektiği alanlarda, kesme aletlerinde, yüzey kaplamalarında) kullanılabilir. Geleneksel seramik işleminde uygulanan üretim basamakları, toz üretimi ve işlemesi, şekil verme işlemi, kurutma, organiklerden kurtulma ve sinterleme olarak adlandırılabilir. Bu doğrultuda, seramik üretiminde kullanılacak tozların mikron boyutları yerine nano boyutlarda üretilmesi ile elde edilecek son seramik cisminin daha yoğun bir yapıya sahip olması çok kritik bir noktadır. Bunun yanında, çözücü, bağlayıcı ve plastikleştirici ajanlarının aşırı kullanımından dolayı ısıl işlem basamaklarında dikkate değer büzülmeler gözlenebilir. Bu sorunun çözülmesi için seramik karışımındaki katı oranının artırılması büyük bir önem arzetmektedir. Ayrıca, seramik üretim basamaklarında eklenen ajanların ve

çözücülerin çoğu toksiktir ve bu sorunun çözümü için bu tür maddelere alternatif olan su bazlı ajanların kullanılması gerekmektedir.

Alümokzan, su bazlı yapısıyla, zararlı organikler içeren çeşitli seramik öncüllerine güzel bir alternatif olabilir. Alümoksan, nano boyutlu böhmit (AlOOH) çekirdeğine sahip, yüzeyi sentez sırasında kullanılan organik gruplarla çevrilmiş olan yapılardır.

Bu araştırmada, alüminyum hidroksitten başlanarak nano alümina öncülü olarak kullanılabilen nano alümoksan elde edilmiştir. Alüminyum hidroksit parçacıkları (≤ 60 μm), öncelikle ön öğütme basamağından geçerek 500 nm civarında olan parçacık boyutlarına indirilmiştir. Bundan sonra, glikotermal işleme sokulmuş ve 200 nm parçacık boyutlarında olan böhmitin organik türevleri elde edilmiştir. Bu amorf yapıdaki parçacıklar, farklı organik kimyasallar (asetik asit, metoksi asetik asit, stearik asit ve lisin) ortamında değirmende öğütülerek mekanokimyasal işleme sokulmuştur. Bu işlemden sonra elde edilen alümoksan parçacıklarının boyutları 10-100 nm arasına düşmüştür. FTIR spektroskopisi ile kullanılan organik moleküllerin etkileri incelenmiştir. Bunun yanında, dinamik ışık saçılımı ile de parçacıkların boyutları ve organiklerin hidroksit tabakalarındaki ayrılmalar üzerine etkileri incelenmiştir. Ayrıca, elde edilen parçacıkların yapısal analizleri XRD ile yürütülmüştür.

Anahtar Sözcükler: alümoksan, böhmitin organik türevleri, mekanokimya, glikotermal işlem, nano alümina öncülü

To My Parents and İrem

ACKNOWLEDGEMENTS

I would like to express my deepest gratitude to my supervisor Prof. Dr. Güngör Gündüz for his expertise and guidance throughout my studies. I cannot thank him enough for his encouragement, understanding, patience, and for these enlightening two years during which I had the chance to work with him.

I would like to express my sincere thanks to my co-supervisor Assist. Prof. Dr. Bora Maviş for his endless helps, great ideas guiding the research discussions, and for his enthusiastic motivating speech during my thesis research period. I would also like to thank Prof. Dr. Üner Çolak for his invaluable guidance and support.

Concerning the characterization analyses during my research study, technical assistance of METU Central Laboratory, Metallurgical and Materials Engineering and Chemical Engineering in addition to HU Geological Engineering and Mining Engineering staff are greatly appreciated.

I would like to thank to my laboratory friends İrem Vural, Gülden Eroğlu, Simge Çınar, Burcu Berna Topuz, Anisa Coniku, Nasser Khazeni, Sevinç Sevim Kahya, Nagihan Keskin, Berker Özerciyes, Nihan Karakoç, Erkan Biber, Ahmet Göktaş for their collaborative, motivating and friendly manner.

I would like to thank all of my friends for always standing by me during this difficult accomplishment. My special thanks go to Ali Can Kızılkaya, Ayça Arınan, Ayşegül Çiftçi, Berker Fıçıcılar, Elif Karatay, Turhan Bayraktar, Muhlis Yiğit Soysal, Şafak Bayram and Kadri Buğra Özütemiz for their unique and valuable friendship and all the memories we had in these two years.

I am also thankful to my parents for their perpetual love and for the support they provided me all the time.

Last but not least, the thanks I owe to İrem Vural cannot be expressed by words. She has been my greatest motivation not only through my research studies, but also through my entire recent two years. I am thankful to her for her endless support and faith in me.

This work was supported by METU (BAP-07.02.2009.00.01 – Scientific Research Project) and HU (0601602003 – Scientific Research Project).

TABLE OF CONTENTS

LIST OF TABLES

TABLES

LIST OF FIGURES

FIGURES

LIST OF SYMBOLS AND ABBREVIATIONS

AA	Acetic Acid
ATH	Aluminum Trihydroxide
B	Boehmite
BPR	Ball to Powder Ratio (by weight)
D	Diameter (mm)
d(50)	Mass median diameter (nm)
CA	Carboxylic Acid
DTA	Differential Thermal Analysis
EG	Ethylene Glycol
FT-IR	Fourier Transform Infrared Spectroscopy
GT	Glycothermal Process
IPOH	Isopropyl Alcohol
LPR	Liquid to Powder Ratio (by mol)
Ly	Lysine
Ly-A	Lysine Alumoxane
MAA	Methoxy Acetic Acid
MA-A	Methoxy Acetate Alumoxane
MAO	Methyl Alumoxane
MC	Mechanochemical Process
MEAA	Methoxy Ethoxy Acetic Acid
MEA-A	Methoxy Ethoxy Acetate Alumoxane
MEEAA	Methoxy Ethoxy Ethoxy Acetic Acid
MEEA-A	Methoxy Ethoxy Ethoxy Acetate Alumoxane
ODB	Organic Derivative of Boehmite
PB	Pseudo Boehmite
PCS	Photon Correlation Spectroscopy
PG	Pre-Grinding

p-HB-A	para Hydroxy Benzoate Alumoxane
PS	Particle Size
PSA	Particle Size Analysis
PSD	Particle Size Distribution
SA	Stearic Acid
SEM	Scanning Electron Microscopy
T	Temperature (°C)
TGA	Thermogravimetric Analysis
W	Weight (g)
XRD	X-Ray Diffraction
V	Volume (ml)
µm	Micrometer

CHAPTER 1

INTRODUCTION

Advanced ceramics are considered as a class of materials to be used in high technology applications. Alumina can be considered as one of the widely used engineering ceramic due to their superior properties (e.g., high hardness, corrosion resistance, high thermal stability, and oxidation and chemical resistance) [1-2].

Alumina, (Aluminum oxide – Al_2O_3) can be used in a wide range of applications like electrical/thermal insulation, wear resistance, structural refractories, cutting tools, abrasives, adsorbents, catalyst carriers, coatings, and structural prostheses.

Alumina has several unstable transition phases but the most stable phase is named corundum (α-alumina) which could be produced by the direct calcination of aluminum hydroxide over 1200°C.

From conventional Bayer Process, alumina can be produced with impurities and nonhomogeneous particle size distribution. Thus, pure and nano sized alumina powder synthesis plays the key role in the production of advanced alumina ceramics. Several alumina precursors were introduced in the literature. The most widely used ones are aluminum alkoxides [3-5] and aluminum salts [6-7] as a bottom-up process. Processes of aluminum alkoxides and/or salts are represented in Figure 1.1 by the red route.

Additionally, aluminum metal was used to produce nano sized alumina particles [8].

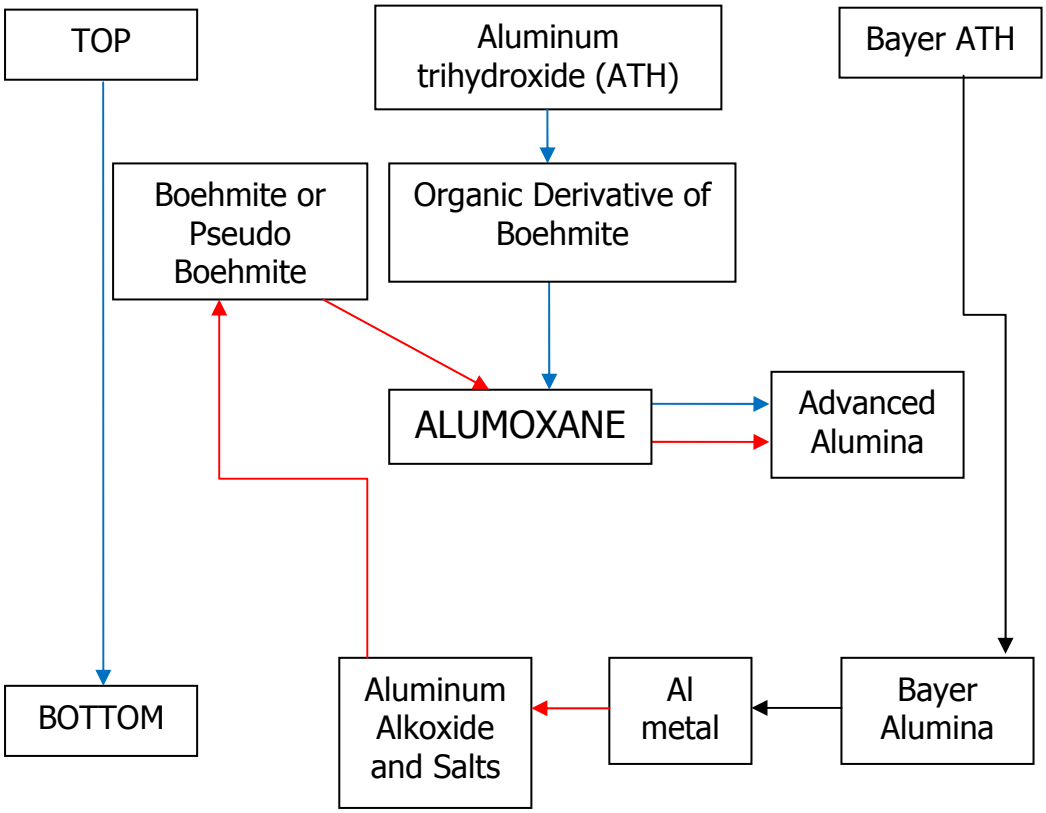

Figure 1.1 Simplified schematic representation of alternative alumoxane production (red arrows for the general alumoxane route by Barron et al and blue arrows for this study).

However, there are disadvantages of using such alumina precursors (aluminum alkoxide and salts). Aluminum alkoxides are costly due to the complicated production method. Additionally, aluminum salts have some problems in terms of enviromental regulations since corrosive gases are released upon the calcination of the precursor [8-9]. On the other hand, aluminum hydroxide is readily available at low cost and has no corrosive

effects and environmentally benign. Therefore, it becomes a good alternative for the alumina precursor production.

In ceramic production, one of the most critical steps is densification. When heat treatment is applied, significant shrinkage can be observed due to the excess amount of additives used throughout the production. To minimize that, solids loading have to be altered to achieve more ceramic yield during the powder production and shape forming steps. Moreover, toxic reagents are used during these steps. Thus, to overcome those problems environmentally benign aqueous based alumoxanes were introduced [10].

Alumoxanes were presented as aqueous based nano alumina precursors. Due to the reasons mentioned above, they were considered to be used instead of aluminum alkoxides, which are the typical precursors of nano alumina particles [10-13].

Alumoxanes had been produced by reflux method in aqueous medium with the chemical reagents; pseudo boehmite and carboxylic acids [10]. Solvent free synthesis [14] was also introduced to produce alumoxane by applying shear and high temperature on carboxylic acid and boehmite. Molecular representation of the alumoxane was demonstrated in Figure 1.2 [10].

Boehmite is the core structure of alumoxane. Therefore, it is the starting material for the production of alumoxane as well as aluminum alkoxides. Boehmites can be produced by sol-gel, hydro/glyco/alcothermal processes [11-12, 15-19]. By using glycol/alcothermal processes, organic derivatives of boehmites (ODB), with poor crystalline structure, can be produced [15-16].

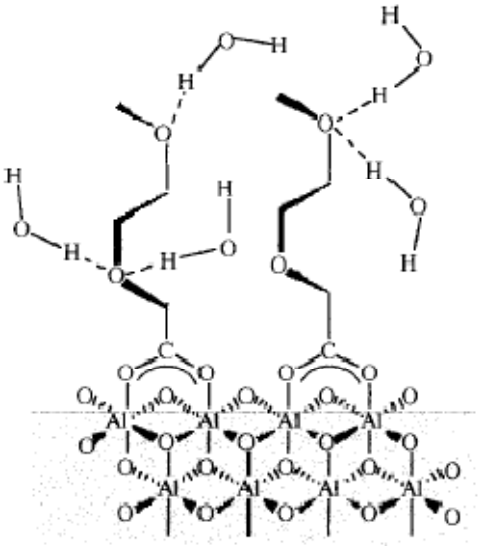

Figure 1.2 Schematic representation of carboxylic acid substituted alumoxane [10].

In this study, aluminum trihydroxide (ATH), $Al(OH)_3$, was used as a starting material to synthesize novel alumoxane that could be further used in the synthesis of nano alumina particles. This process can be represented as a top-down approach which was started from the intermediate product of Bayer Process which is ATH. ATH was first ground to have required particle sizes and then it was fed into the glycothermal process. After glycothermal reaction, organic derivative of boehmite (ODB) was produced. Further process was applied mechanochemically on ODB particles in the medium of the selected carboxylic acids in a high energy ball mill to produce alumoxane. The originality of this current study was obtaining alumoxane by the adaptation of a new approach as an alternative to the reflux and the solvent free methods.

CHAPTER 2

LITERATURE REVIEW

In this chapter, conventional alumina and nano-alumina production methods, different nano-alumina precursors, boehmite/pseudo boehmite/organic derivative of boehmite and their production methods and alumoxane synthesis will be introduced.

2.1 Alumina: Phase Transition and Production Methods

Aluminum forms sesqui-oxide with rhombohedral (corundum) structure having aluminum atom octahedrally coordinated with oxygen atoms [20-21].

The phase transition of alumina starting from various of hydroxides (gibbsite - γ-$Al(OH)_3$, bayerite - α-$Al(OH)_3$, boehmite - γ-AlO(OH) and diaspore - α-AlO(OH)) was shown in Figure 2.1. It was observed that at low temperatures (250-900°C), crystal structures of alumina are χ, η, γ, ρ, and at high temperatures (900-1150°C), they are δ, κ, θ alumina. Further heating process results in α-Al_2O_3 (corundum) and it is called α-alumina and cannot be named under transition aluminas. The phases formed at lower temperatures are named under pseudomorphs [22]. δ, κ, and θ alumina phases are defined as high temperature polymorphs [23]. Phase transition starting from aluminum hydroxides to the transition aluminas with respect to temperature and pressure was represented in Figure 2.2.

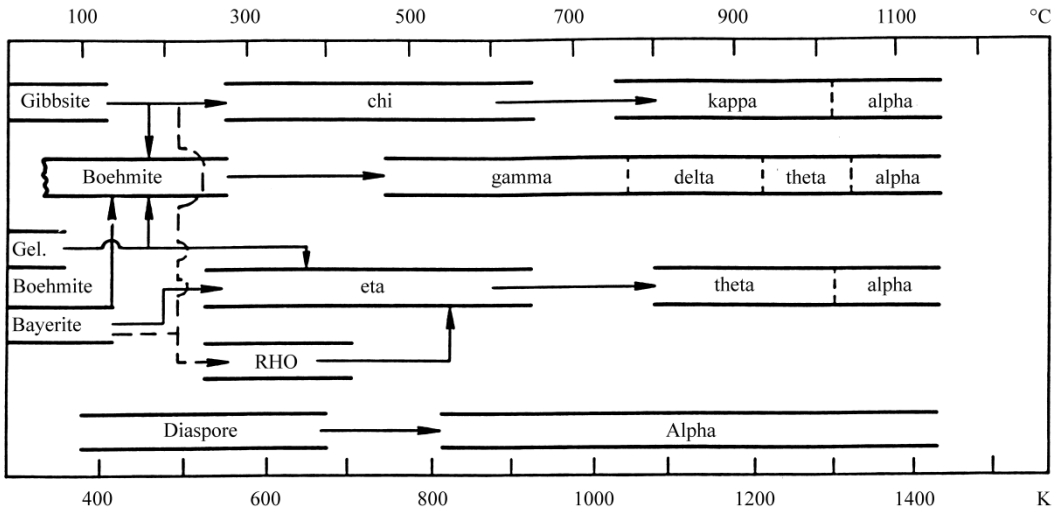

Figure 2.1 Thermal transformation sequences of aluminum hydroxides [22].

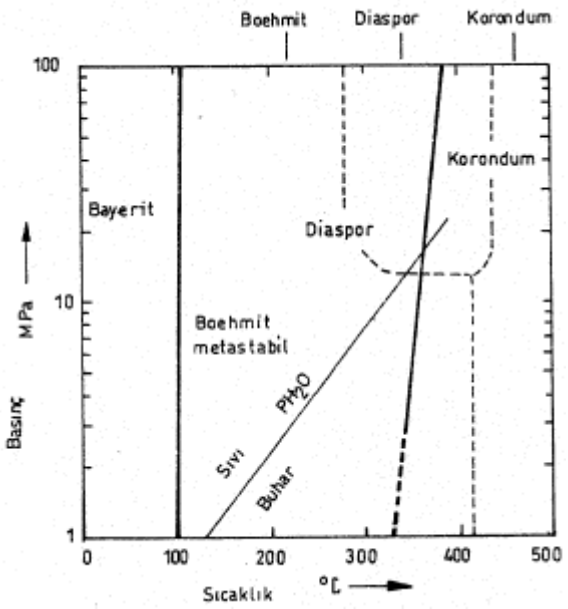

Figure 2.2 Phase diagram of aluminum hydroxides [24].

Alumina can be synthesized by different methods. Conventional alumina can be produced mainly by the Bayer Process to be used as an aluminum precursor. As the process is represented in Figure 2.3, alumina is produced by the calcination process of the aluminum trihydroxide in the rotary kiln [25]. The product of the Bayer Process cannot be used in advanced ceramic applications due to its impurities and over-micrometer sized inhomogeneous particle size distribution. Yet, the prerequisites of the materials to be used in the advanced ceramic applications are being ultra-pure and finely mono-dispersed alumina particles.

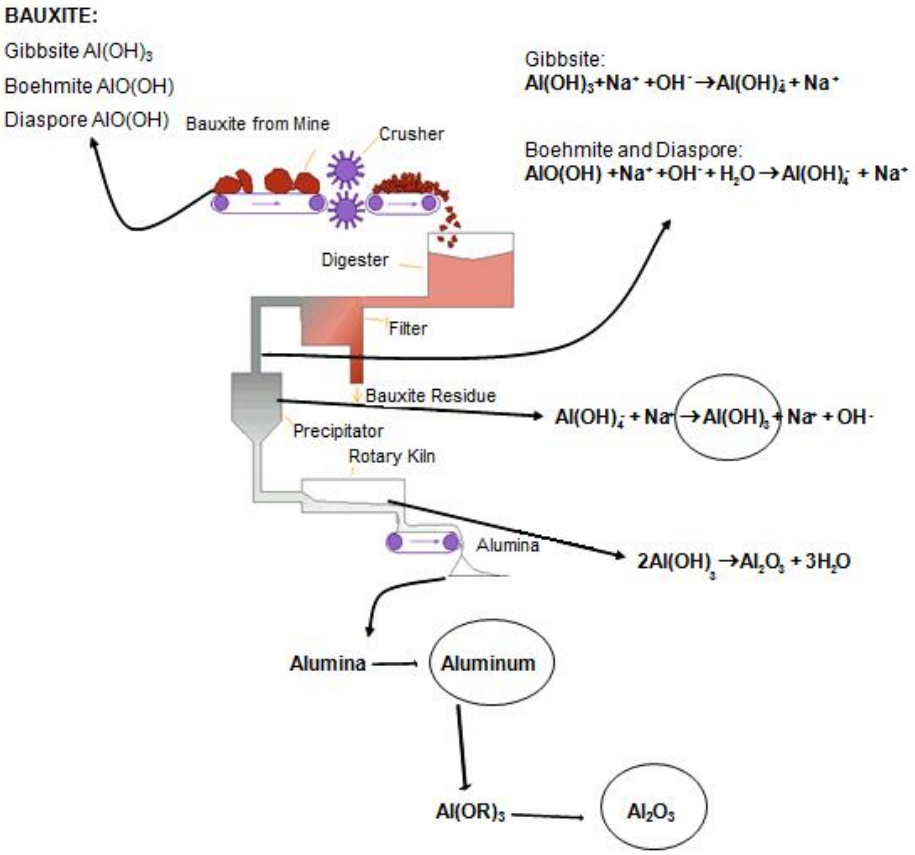

Figure 2.3 Schematic representation of Bayer Process.

To produce high purity and fine alumina from Bayer ATH, several approaches were developed [26-28]. These approaches were applied to reduce the final impurity due to Bayer soda and to produce finer but not nano sized alumina particles.

Additionally, Mazloumi and his coworkers produced nano sized (≤ 100 nm) alumina particles starting from the Bayer liquor (sodium aluminate solution). In that study, to obtain nano size with high purity alumina, a dispersant agent (Tiron, [29-31]) was used during the sol-gel process and after the produced gel was observed calcination was further applied [9].

Apart from starting with ATH, several alumina precursors (e.g., alumina salts, aluminum alkoxide, and aluminum metal) can be used with different chemical routes to produce high purity and better dispersed α-alumina particles [9].

Wu and his collaborators produced nano α-alumina particles around 40 nm by sol-gel method starting with aluminum salt - $Al(NO_3)_3$ – and using dispersant to avoid agglomeration [6]. In another study, alumina precursor was produced starting from $Al(NO_3)_3$ and mineral oil, by emulsion evaporation method and further calcination resulted in micrometer sized (1-10 μm) spherical α-alumina particles [7].

Moreover, Thiruchitrambalam et al. developed a process to produce α-alumina at 1000 °C starting with aluminum metal to obtain boehmite and further processing it by sol-gel method with the addition of HNO_3 [8].

Another approach was developed to produce alumina precursor starting from aluminum alkoxides in the presence of surfactants to produce a gel further processed in hydrothermal reactor at 100 °C for a day. After hydrothermal

process, the obtained powder was calcined at 500 °C to yield nano-structured γ-alumina particles [3].

Alumina powders, synthesized with various chemical routes had to be followed by some other processes to be used in ceramic applications. In a conventional ceramic process, powder synthesis is followed by processing steps of the shape forming, drying, organic burn-out, and densification. Accessing powders with sizes in the range of a couple of microns down to several tens of nanometers is considered critical in obtaining higher densities in the final ceramic bodies. Besides, since significant shrinkage can be observed in the thermal treatment steps due to the excessive use of additives (e.g., binders, solvents and plasticizers) in the powder processing and shape forming steps [2], it is important to find the solution that would increase the solids loading in the initial mixtures. In addition, most of the conventional additives and solvents used in these steps are toxic and it is necessary to replace them with the environmentally benign aqueous-based alternatives such as alumoxanes [10].

2.2 Alumoxane: Structure and Production Methods

Alumoxanes were first introduced by Adrianov to define species containing an oxo (O^{2-}) bridge binding two aluminum atoms (Al-O-Al) [32]. Then, it was proposed as linear and cyclic structures composed of three coordinate Al atoms demonstrated in Figure 2.4 (A and B) [33]. Moreover, multi-cyclic structures composed of four coordinate Al atom were demonstrated in Figure 2.4 (C and D) [33-34].

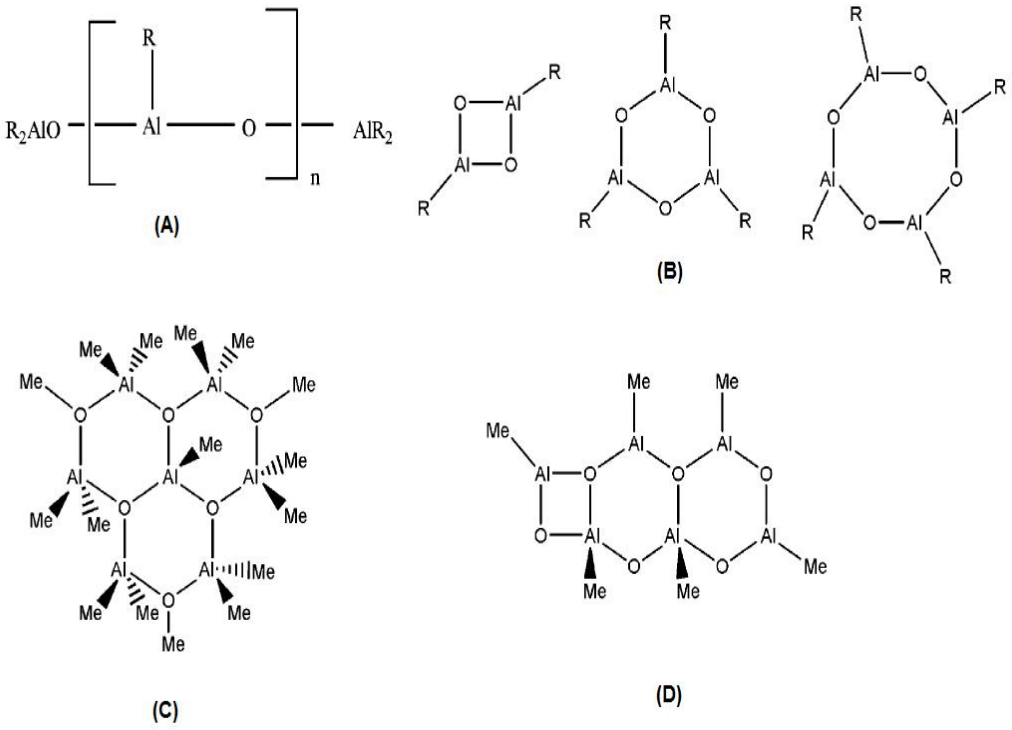

Figure 2.4 Structural proposals of metylalumoxanes (MAO) [33].

Alumoxanes can be determined as the intermediate product in the hydrolysis process of organoaluminum compounds (e.g., aluminum alkoxide) to ATH (bottom-up approach) [35]. In other words, alumoxanes are a group of compounds that are characterized by aluminum-oxygen cores, which resembles the structure of boehmite (AlOOH), surrounded with organics [36-37]. In Figure 2.5, simplified Al-O core structure was demonstrated.

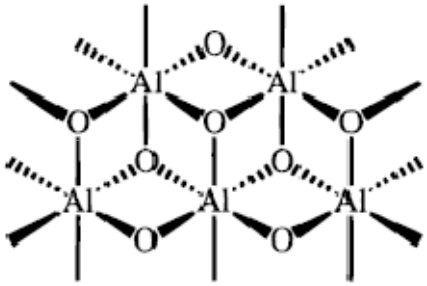

Figure 2.5 Al-O core structures in alumoxanes [10].

Moreover, production of alumoxanes directly from boehmite was represented as a top-down approach and the proposed reaction of $AlO(OH)_n$ with carboxcylic acid (CA) was shown in Equation 1 [10]. As it was seen from the reaction mechanism, alumoxanes could be named under metal carboxylates (e.g., neutralization of metal hydroxides/oxides/carbonates with fatty acids) [38].

$$[Al(O)OH)]_n \xrightarrow{HO_2CR} [Al(O)_x(OH)_y(O_2CR)_z]_n \quad (1)$$

Another demonstration of the formation of carboxylated alumoxanes was represented schematically in Figure 2.6.

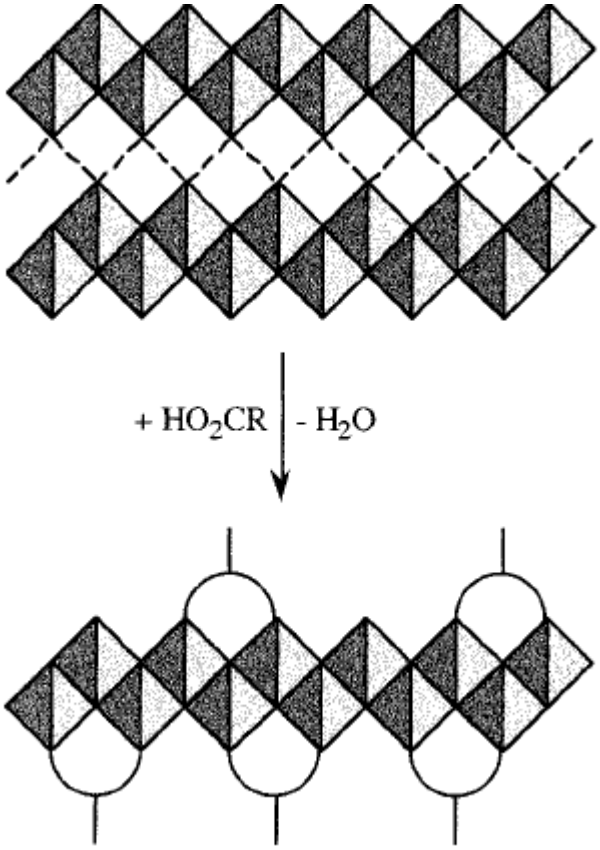

Figure 2.6 Representation of boehmite reacted with CA (shaded triangles for the side view of Al-O octahedra and semicircle with bar for CA) [10].

Alumoxanes have been offered as aqueous based nano alumina precursors and considered to be less costly and less toxic than the aluminum alkoxides, which are the typical precursors of nano alumina particles [10-13]. Alumoxanes were produced by starting directly from boehmite (B) and pseudo-boehmite (PB) [10, 13].

In another study, starting point was from commercial pseudo-boehmite various CAs (Acetic acid - AA, methoxy acetic acid - MAA, methoxy ethoxy acetic acid - MEAA and methoxy ethoxy ethoxy acetic acid - MEEAA) were

added. They were refluxed in water for 24 – 72 hours. After obtaining a clear solution, they were centrifuged for 1 hour and decanted. As a final step, it was dryed to obtain the alumoxane particles. The products' particle size had time dependency and the PS distribution became more homogenous having particle sizes around 10-25 nm after 50 hours of reflux time [10].

Similarly, p-hydroxy benzoate alumoxane (p-HB-A) and lysine alumoxane (Ly-A) were prepared by reflux method of those organics and pseudo-boehmite in water overnight. The average particle sizes were measured as 394 and 400 nm, respectively [13].

2.3 Applications of Alumoxanes

The alumoxanes produced with different CAs were used in diverse applications. Mainly, they were tried to be adapted as an alumina precursor. It was used as a preceramic binder in traditional tape casting and as a infiltration agent being an environmentally benign precursor and increasing the ceramic yield [10]. In addition to this, hollow α-alumina spherical particles were introduced by alumoxanes [39]. To investigate its processability as 3-D ceramic feature, A-Alumoxane and MEEA-Alumoxane were used as a precursor for the green body and it was observed that shrinkage and cracking were reduced by altering the solid content as nano-particle in the ceramic green body [40]. Additionally, to strengthen the porous alumina particles, nano sized A-alumoxane and MEEA-alumoxane have been used as alumina precursors [1, 41].

Nano composites and inorganic-organic hybrid materials were produced by using p-HB Alumoxane and Ly-Alumoxane with the presence of epoxide resin

and a hardener [13]. Moreover, those alumoxanes were investigated as a filler material in carbon fiber/epoxy composites [42].

Nano sized alumoxanes were applied as inorganic-organic hybrid filler to the polymeric systems to obtain scratch and abrasive resistant coating materials, especially in automotive industry [43].

Boczkowska et al. produced urea-urethane nanocomposite (20-100 nm) with the addition of modified MAO demonstrated in Figure 2.7 as filler material [44].

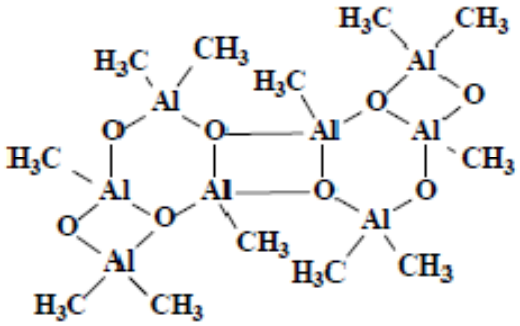

Figure 2.7 Simplified representation of MAO core [44].

To use alumoxanes in polymer matrices, surface modifications can be applied by bonding the appropriate functional groups onto alumoxane structure which was the key role throughout the polymer/alumoxane composite production [45-46].

Some studies were carried out to produce polymer/alumoxane nano composites to apply on bone tissue engineering [47-48]. Moreover,

heterogeneous polyolefin catalysts were introduced based on metallocene/MAO by using carboxylated alumoxane (p-HB-A) nano particles as a substrate [49]. Furthermore, A-alumoxanes were introduced to produce alumina based membranes to have higher porosity and permeability with being environmentally benign [50].

2.4 Boehmite/Pseudo Boehmite and Organic Derivatives of Boehmite

Boehmite, which is an intermediate hydroxide of aluminum and typically used in preparation of membranes, catalysts, and coatings [51], can be produced by sol-gel technique as well as hydro/glyco/alcothermal methods [11-12, 15-19]. It has been demonstrated that pseudo-boehmite which can be considered as partly crystalline boehmite. It can be used in synthesis of alumoxanes with different organic groups (e.g. carboxylic acid) [10, 13-14].

Boehmite could be produced by hydrothermal and sol-gel method starting with different materials; aluminum salts, aluminum hydroxides, aluminum metal, and aluminum alkoxides [9].

In hydrothermal method, process temperature, time, and pH of the medium were critical parameters to obtain different particle size distribution and morphology. Starting from aluminum salt (aluminum acetate), boehmite sol was produced by hydrothermal route at 200-300 °C for 1-10 hours [52]. Schmidt and his coworkers started with aluminum salt ($AlCl_3.5H_2O$) and prepared a solution with the addition of surfactant and ammonium hydroxide to adjust the pH around 10. To the produced gel with co-precipitation, alumina seeds (4 %) were added and were introduced to hydrothermal reactor. After 1 hour process at 190 °C, the average particle size of the

synthesized α-alumina powder was observed as 66 nm with the spherical morphology [53]. Additionally, aluminum nitrates were treated hydrothermally in the range of 160-220 °C within a stirred reactor. If the temperature was taken as 160 °C, pseudo boehmite was produced. However, the increasing process temperature resulted in production of crystallized boehmite. [54].

Another starting material to produce boehmite is aluminum alkoxide which could be used with hydrothermal synthesis. In another study, aluminum tri-sec-butoxide and aluminum tri-tert-butoxide were separately introduced to the reactor with HCl medium at 150 °C to produce 100-500 nm sized boehmite particles [55]. Additionally, Tannenbaum and his coworkers produced boehmite starting from aluminum alkoxide by hydrolysis and further processing by sol-gel method,. They obtained 20-30 nm boehmite particles by using surfactant throughout the process [4].

Moreover, another form of boehmite which is namely "organic derivatives of boehmite" could be synthesized by glyco/alcothermal methods from aluminum hydroxide (ATH) and aluminum alkoxides in various glycols or alcohols medium [11-12, 15-19].

Inoue and his co workers investigated the hydro/alcothermal process products obtained from ATH having different particle sizes. The ATH sample was processed at 250 °C for 2 hours in pressurized reactor and the several synthesized products were investigated structurally. Selected solvents were water, alcohols (2-8 carbon alcohols), and mineral oil. It was observed that with the particle size of ATH decreasing from 80 μm to 0.2 μm, the gibbsite to boehmite transformation percent decreased, but those gibbsite were transformed into poorly crystallized χ-alumina [17].

In another study of Inoue, reactions of aluminum compounds (aluminum hydroxide, aluminum alkoxide, and aluminum salts) in several organic solvents (alcohols, glycols and amino alcohols) were investigated [11].

Moreover, in mineral oil at 250-300 °C over 2 hours of time, aluminum alkoxide (aluminum isopropoxide) was transformed into χ-alumina and further calcination resulted in α-alumina formation without any transformation to κ-alumina. The χ-alumina obtained had particle sizes of 9-10 nm and after the calcination processes, it only increased to 15 nm [12].

Apart from alkoxides, Inoue and his coworkers found that by the reaction of ATH in ethylene glycol (EG) at 250 °C under the vapor pressure of EG, a compound having an empirical formula of $AlO(OCH_2CH_2OH)_{0.31}(OH)_{0.69}$ was observed [16, 56]. This product was named as glycol derivative of boehmite, which was demonstrated in Figure 2.8. The critical parameter was the feed particle size of ATH. If it was under 0.2 μm, the transformation of ATH to glycol derivative of boehmite was completed [11, 16, 19].

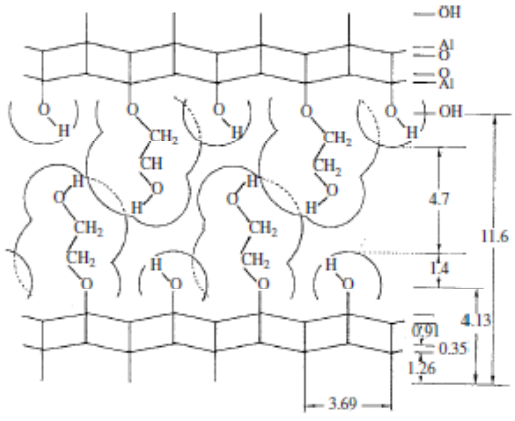

Figure 2.8 Structure of glycol derivative of boehmite [11].

Additionally, alkoxyalumoxanes (alkyl derivative of boehmite) were obtained by the reaction aluminum metals or aluminum alkoxides in alcohols at 250 °C. This structure was composed of the alkyl groups covalently bonded to boehmite layers [15].

2.5 Alternative Method to Produce Alumoxane: Solvent-Free Synthesis

As it was mentioned earlier, alumoxanes were synthesized by the reflux of the pseudo-boehmite with several carboxylic acids in aqueous medium and the synthesis time was long period like 1 to 3 days.

As an alternative, Barron and his co workers stated to produce alumoxane with a solvent free method using a rheometer. With shear and the temperature, the organics (L-lysine-, stearate-, and p-hydroxybenzoate-derived materials) were introduced to boehmite and the alumoxane particles were produced when the temperature above 80 °C. The particle size (PS) of the alumoxanes were under 5 nm and the process time was 20-250 minutes [14].

As a summary, alumoxanes could be produced by both reflux method [10, 13] and solvent free method [14] with the addition of selected organics.

Within the scope of this study, alumoxane would be produced by the mechanochemical treatment of the glycothermally processed ATH with the selected organics (carboxylic acids). This process route was shown in Figure 1.1 (blue arrows) as a top-down approach.

CHAPTER 3

EXPERIMENTAL

In this chapter, mechanochemical treatment of organic derivatives of boehmites (ODBs) from aluminum hydroxide (ATH) will be described including all materials used and production steps followed. Details of characterization methods utilized in each step are included.

3.1 Materials

Materials used and their functions in the processes are; ATH as a starting material, ethylene glycol (EG) as the grinding and glycothermal medium, acetic acid (AA), methoxy acetic acid (MAA), stearic acid (SA) and lysine (Ly) as functional or supporting reagents in the grinding mediums.

3.1.1 Aluminum Hydroxide (ATH)

For the production of ODBs that would be treated mechanochemically, ATH is selected as a starting material. It was reagent grade and purchased from Merck. Some of the properties of ATH are given in Table 3.1.

Table 3.1 Properties of ATH used in this work.

Chemical Formula	$Al(OH)_3 \cdot xH_2O$
Molecular Weight (g/mol)	78.00
Appearance	White solid

3.1.2 Glycothermal Process Medium

Ethylene glycol is used as the medium in the glycothermal process. It is also used for the preparation of pre-grinding medium. It is purchased from Merck. Structural formula and some of the properties of EG are given in Figure 3.1 and Table 3.2.

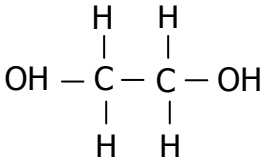

Figure 3.1 Structural formula of EG.

Table 3.2 Properties of EG used in this work.

Chemical Name	Ethylene Glycol
Chemical Formula	$C_2H_4(OH)_2$
Molecular Weight (g/mol)	62.07
Density (g/ml)	1.112
Weight Percentage	99
Appearance	Liquid

3.1.3 Functional or Supporting Reagents Used in Grinding Mediums

AA, MAA, SA and Ly are used in the preparation of mediums for pre-grinding and mechanochemical treatment steps. AA, MAA and SA were purchased from Merck. Lysine monohydrate was purchased from Fluka. Their structural formulas and some of the properties are given in Figure 3.2 and Table 3.3.

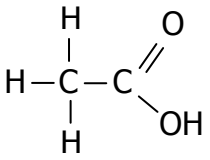

(a) AA

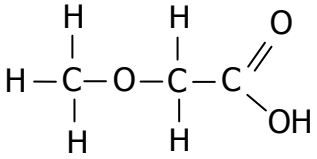

(b) MAA

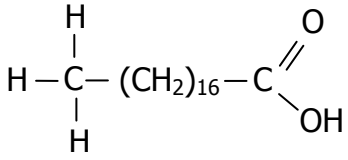

(c) SA

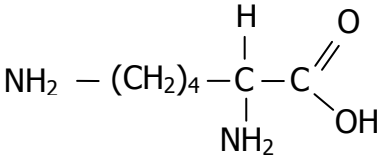

(d) Ly

Figure 3.2 Structural formulas of (a) AA, (b) MAA, (c) SA and (d) Ly.

Table 3.3 Properties of AA, MAA, SA and Ly used in this work.

Chemical Name	Chemical Formula	Molecular Weight (g/mol)	Density (g/ml)	Wt %	Physical State
Acetic Acid	CH_3CO_2H	60.05	1.05	99.8	Liquid
Methoxy Acetic Acid	$CH_3OCH_2CO_2H$	90.08	1.174	97	Liquid
Stearic Acid	$CH_3(CH_2)_{16}CO_2H$	284.48	0.847	97	Solid
Lysine Monohydrate	$H_2N(CH_2)_4CH(NH_3)CO_2H.H_2O$	164.21	-	98	Solid

3.2 Production Steps

Mechanochemical treatment of ODBs starting from ATH includes three steps: i) pre-grinding, ii) glycothermal and iii) mechanochemical treatment. In the following sections, aim of these steps will be described and detailed experimental procedures will be given. However, in order to gain experience in the processes and characterization methods applied in each step, some preliminary experiments were carried on for each step. Therefore first those studies will be covered.

3.2.1 Preliminary Studies

For use in the glycothermal step of the process, the ATH ($Al(OH)_3$) from commercial supplier had to be ground. The initial particle size of this product was around 150 μm, and it was ground down to sizes around 1-0.5 μm with a grinding step that would be named hereof, 'pre-grinding step' which is short for 'preliminary grinding'. Particle size is an important parameter in the

boehmite production under glycothermal conditions. Moreover, such a step needed to be included due to the lack of a mixing system in the pressurized reactor. Thus, to have a homogeneous mixture in the reactor at all times, the sizes of particles needed to be small enough for their homogeneous dispersion since the only mixing action was supplied through the Brownian motion of these small particles at high temperature.

In the pre-grinding step, a high energy ball mill (Retsch PM100) was used to decrease the particle size and to have a narrow particle size distribution. A simplified representation of the mill chamber is supplied in Figure 3.3.

Figure 3.3 Representative sketch of the high energy ball mill used.

In order to have a standard experimental procedure in the primary experiment sets, a series of experiments were performed. In these experiments pre-grinding medium is prepared with the addition of ATH to the selected organic reagent as grinding medium. The feed solution is mixed with a magnetic stirrer until a homogeneous mixture is obtained (for 15-20 minutes). Feed was then poured into the grinding bowl with the grinding

balls. After the grinding process, the feed was washed and it was separated from the balls with a proper sieve. Obtained solution was centrifuged and the collected powders were dried at 60 °C. Grinding procedure is summarized in Figure 3.4 and the conditions of preliminary experiments are summarized in Table 3.4.

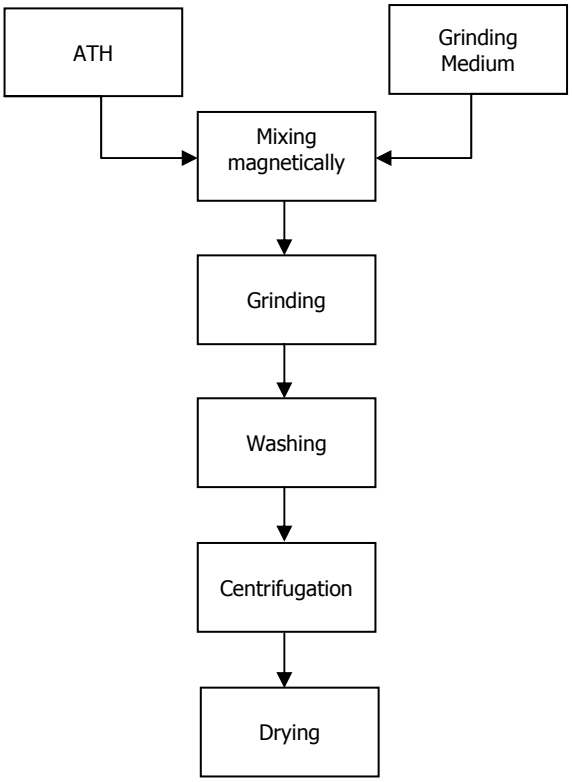

Figure 3.4 Flow-chart of the preliminary grinding process.

Table 3.4 Two step and one step pre-grinding studies with the selected parameters*.

Grinding Type	Sample #	Step 1				Step 2			
		D_{ball} (Ømm)	Time (min)	Speed (rpm)	Grinding Medium	D_{ball} (Ømm)	Time (min)	Speed (rpm)	Grinding Medium
Two Step	PG-A	10	10	500	IPOH	3	40	400	IPOH
	PG-B	10	10	500	IPOH	3	10	500	IPOH
	PG-C	10	10	500	IPOH	3	60	500	EG
One Step	PG-D	-	-	-	-	3	40	500	EG
	PG-E	-	-	-	-	3	40	500	EG+AA
	PG-F	-	-	-	-	3	100	500	AA

* Grinding media was selected as WC (tungsten carbide). For 10 mm balls, ball weight was 232.5 gr and for 3 mm balls, ball weight was 622.9 gr. Ball to powder ratio (BPR) by weight was taken as 12. Grinding jar capacity was 125 ml. 80 ml was its utility volume.

Ground ATHs were treated in EG at high temperature in a pressurized vessel in the step that follows pre-griding. This treatment step was named as 'glycothermal step'. Inoue and his co-workers reported production of organic derivatives of boehmites with the glycothermal method [16, 56]. In their work, they used ATH powders with different particle size ranges as a starting material and carried the glycothermal process at 250°C. The preliminary studies on glycothermal process were started with the benchmark values from the study of Inoue et al. To determine the required reaction time for complete transformation, a series of experiments were performed in a stainless steel pressurized reactor with a three liter capacity. Picture of the reactor used can be seen in Figure 3.5. The reaction medium was additionally put in a glass cylinder which has approximately 250 ml capacity. This was done to limit the reaction volume to a reasonable value so that a pre-ground batch could be used in more than one run. Gap between the stainless steel liner and the glass was filled with the solvent used in the glycothermal process (i.e. EG). Schematic representation of the experimental set-up is given in Figure 3.6.

Figure 3.5 Picture of the pressurized reactor.

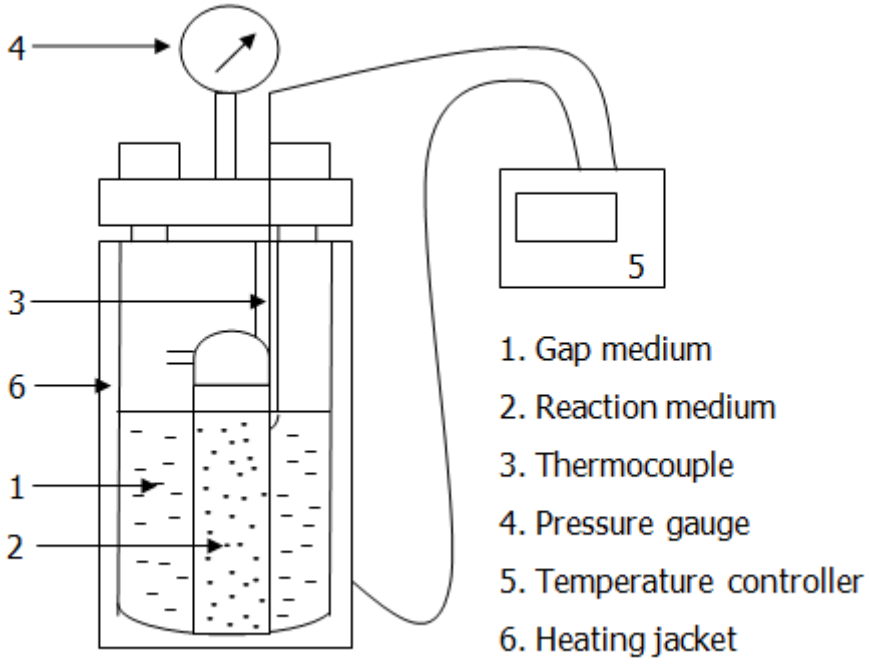

Figure 3.6 Schematic representation of the pressurized reactor set-up.

The experimental procedure of the glycothermal process was standardized upon the evaluation of the results of preliminary studies. In all experiments solids' loading in the feed of the reactor was kept at 10 wt% ATH, balance being EG. Prepared feed was mixed with a magnetic stirrer for about an hour following with the ultrasonic mixing step. Ultrasonication was continued for 5 minutes with 50% power. After the glycothermal feed solution was prepared, the gap was filled with EG and the glycothermal digestion process was continued for 2 or 6 hours at 250 °C. When the process was completed, feed was centrifuged from the EG and this step was followed with several washing and centrifugation steps. Obtained powder was then dried at 60 °C to be used in the final mechanochemical treatment step. In Figure 3.7 a summary of the applied procedure is given and the conditions studied in preliminary studies are summarized in Table 3.5.

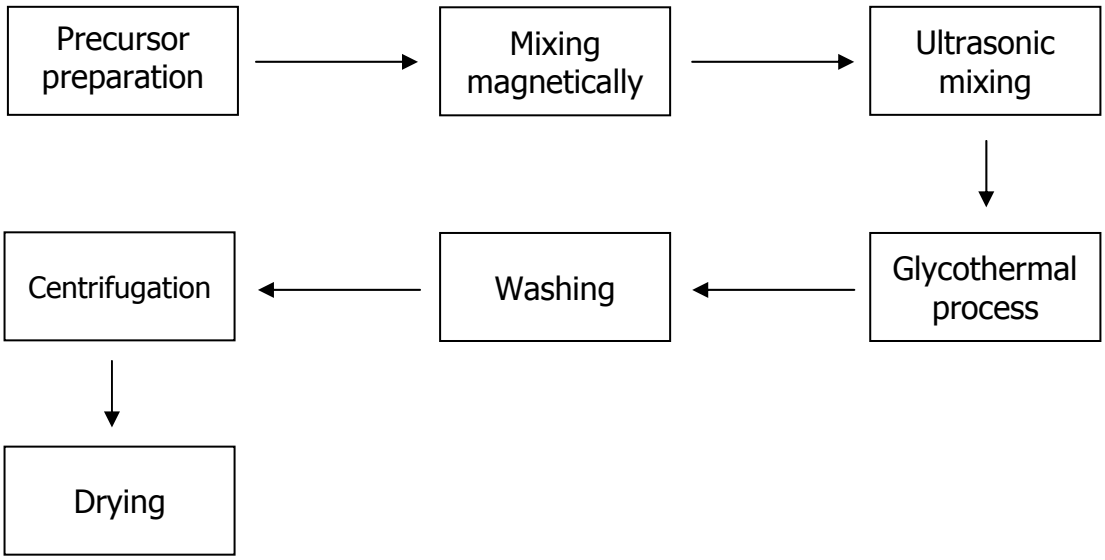

Figure 3.7 Flow-chart of the glycothermal digestion procedure.

Table 3.5 Experimental conditions of the preliminary glycothermal studies.

Sample #	Feed ATH	T (°C)	Time	wt% ATH	pH initial	pH final
GT-1	PG-A	250	2	10	7.2	-
GT-2	PG-C	250	6	10	7.6	7.6
GT-3	PG-E	250	6	10	4.8	7.9
GT-4	PG-F	250	6	10	4.5	6.5

In order to reduce the size of particles obtained from glycothermal digestion, the glycothermal product, ODB was treated mechanochemically in the same high energy ball mill using the grinding mediums; AA and MAA. An experimental procedure similar to the one applied in pre-grinding step (Figure 3.4) was followed in this step. The prepared feed solutions were more viscous than the solutions prepared for the pre-grinding due to the nano-sized feed powder (ODB). Thus, while preparing the feed, vigorous mixing accompanied with slow addition of the feed powder was necessary. In order to standardize the mechanochemical step, some preliminary experiments were performed which are summarized in Table 3.6.

Table 3.6 Preliminary studies on mechanochemical grinding with the selected parameters*.

Sample #	Feed ODB	Time (min)	Speed (rpm)	Grinding Medium
MC-1	GT-2	180	500	MAA
MC-2	GT-3	120	500	AA
MC-3	GT-4	180	500	AA

* Grinding media was selected as WC (tungsten carbide) balls with 3 mm diameter. Weight of the balls were 622.9 gr. Grinding jar capacity was 125 ml. BPR (by weight) was kept constant as 20. Liquid to powder ratio by moles (LPR) was kept constant as 1.

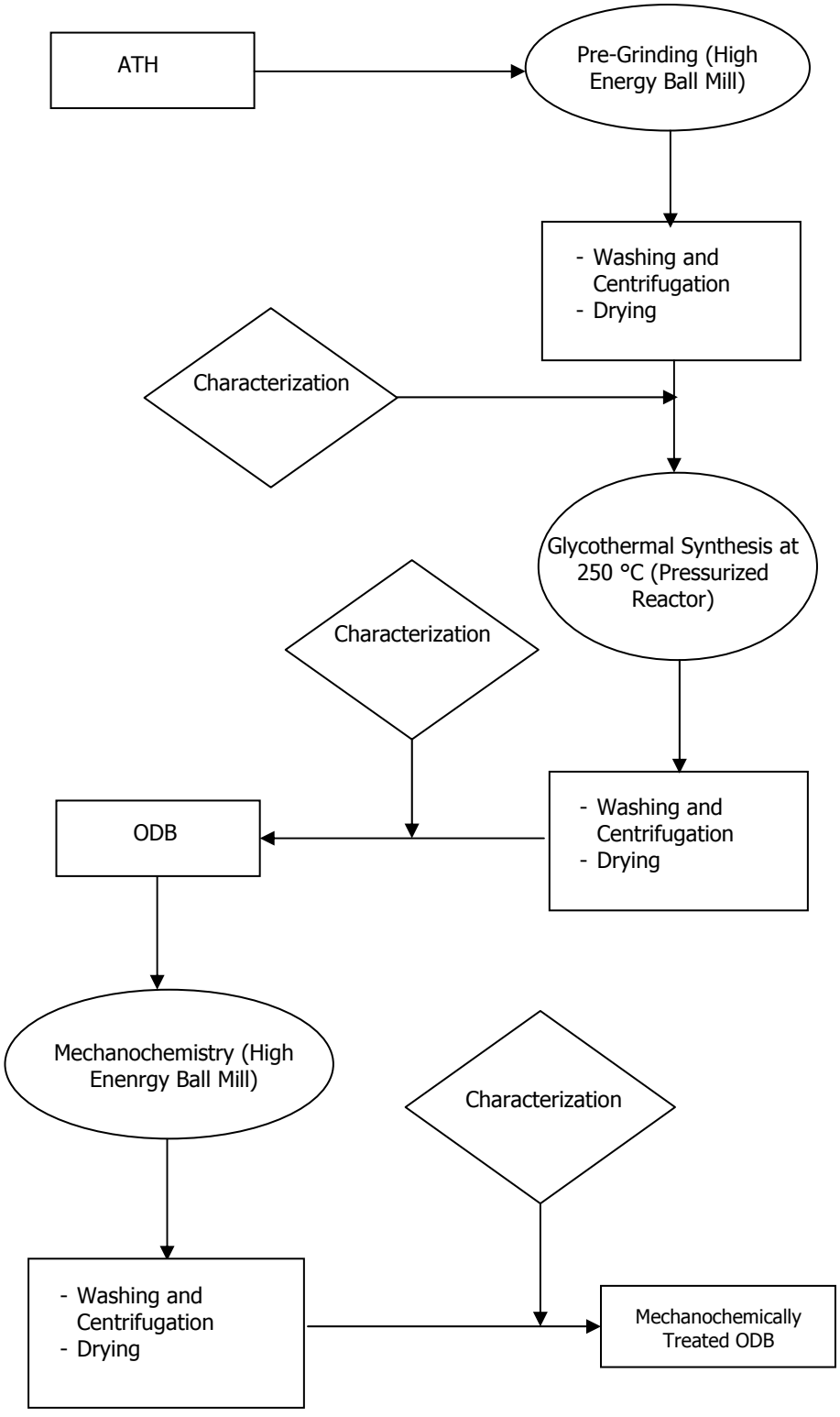

Figure 3.8 Flow-chart of the three-step procedure developed for the production of mechanochemically treated ODBs.

A summary of all the steps of the process are given in flow-chart that is presented in Figure 3.8.

3.2.2 Pre-Grinding in Mixtures of EG and Organic Reagents

A procedure of pre-grinding of ATH was standardized after the evaluation of the preliminary studies. Feed solution was prepared with the same procedure used in preliminary experiments and experimental conditions of the samples prepared are summarized in Table 3.7. By nature, this step is a wet grinding step. Since AA and MAA are in liquid state, no additional liquid addition was needed yet, being in solid state SA and Ly are mixed with ethanol (EtOH) and deionized water (DIW), respectively, before they are fed into the grinding jar.

Table 3.7 Pre-grinding conditions*.

Sample #	Wt_{Powder} (gr)	LPR (by mol)	V_{Liquid} (ml)	Grinding Medium
PG-AA (PG-E)	51.910	1	37.77	EG+AA
PG-MAA	51.910	1	44.27	EG+MAA
PG-SA	51.910	1	38.16	EG+SA+EtOH
PG-Ly	51.910	1	33.76	EG+Ly+DIW

* Grinding media was selected as WC (tungsten carbide) balls with 3 mm diameter. Weight of the balls were 622.9 gr. Grinding jar capacity was 125 ml. BPR (by weight) was kept constant as 12. Grinding speed was taken as 500 rpm and grinding time was 40 minutes for each sample.

3.2.3 Glycothermal Process

After evaluation of the preliminary experiments on glycothermal step, reaction time was kept constant at 6 hours. Obtained powder was named as organic derivative of boehmite (ODB). The experimental procedure used was identical to the one used in the preliminary studies. In Table 3.8, the glycothermal process conditions are summarized.

Table 3.8 Experimental conditions of the standardized glycothermal studies.

Sample #	Feed ATH	T (°C)	Time	wt% ATH	pH initial	pH final
GT-AA	PG-AA (PG-E)	250	6	10	4.8	7.9
GT-MAA	PG-MAA	250	6	10	3.9	5
GT-SA	PG-SA	250	6	10	9	6.85
GT-Ly	PG-Ly	250	6	10	5.7	8.75

3.2.4 Mechanochemical Treatment

With the standardized experimental procedure, a series of mechanochemical grinding treatments were performed with AA, MAA, SA and Ly as the grinding medium. Due to the same reason mentioned in the description of pre-grinding step, SA and Ly were fed into the grinding jar with their solvents, namely EtOH and DIW, respectively.

The experimental procedure applied is shown in Figure 3.4 and the experimental conditions are summarized in Table 3.9.

Table 3.9 Experimental conditions of mechanochemical treatment step*.

Sample #	Feed ODB	Time (min)	Speed (rpm)	Grinding Medium
MC-AA	GT-AA	120	500	AA
MC-MAA	GT-MAA	180	500	MAA
MC-SA	GT-SA	180	500	SA+EtOH
MC-Ly	GT-Ly	180	500	Ly+DIW

* Grinding media was selected as WC (tungsten carbide) balls with 3 mm diameter. Weight of the balls were 622.9 gr. Grinding jar capacity was 125 ml. BPR (by weight) was kept constant as 20.

3.3 Heat Treatment of Mechanochemically Treated ODBs

Two types of heat treatment were carried out on mechanochemically treated ODBs to identify the alumina phases that would form. Briefly MC-AA, MC-MAA, MC-SA and MC-Ly were calcined at 500 and 1200 °C for 3 hours in a cubic furnace. Sample codes are tabulated in Table 3.10 given below.

Table 3.10 Sample codes of the heat treated ODBs.

Sample ID	Feed ID	Time (h)	Temperature (°C)
B-HT1	B	3	500
MC-AA-HT1	MC-AA	3	500
MC-MAA-HT1	MC-MAA	3	500
MC-SA-HT1	MC-SA	3	500
MC-Ly-HT1	MC-Ly	3	500

Table 3.10 (continued)

Sample ID	Feed ID	Time (h)	Temperature (°C)
B-HT2	B	3	1200
MC-AA-HT2	MC-AA	3	1200
MC-MAA-HT2	MC-MAA	3	1200
MC-SA-HT2	MC-SA	3	1200
MC-Ly-HT2	MC-Ly	3	1200

3.4 Characterization Methods

In each step of production characterization of the products were carried out by different characterization methods. They are FT-IR (Fourier Transform Infrared Spectroscopy), PSA (Particle Size Analysis), SEM (Scanning Electron Microscope), XRD (X-ray Diffraction) and TGA-DTA (thermogravimetric analyses and differential thermal analyses).

3.4.1 FT-IR (Fourier Transform Infrared Spectroscopy) Analysis

With the FT-IR spectroscopy, the identifying features of the functional or supporting reagents were followed after each step of the process. FT-IR spectra were collected by IR Prestige-21 SHIMADZU FT-IR spectrometer in the Department of Chemical Engineering, METU. Samples for the analysis were prepared in solid forms by mixing them in KBr pellet. 200 mg of pellet mixtures were prepared with a vacuum press. In each pellet, 1 wt% sample was included.

3.4.2 PSA (Particle Size Analysis)

The particle size (PS) and zeta potential values can give detailed information on the stability and dispersion mechanism in a colloidal solution. In each production step, to control the particle size and understand the particle behavior in the solutions several zeta potential and particle size measurements were carried out in a wide angle particle size analyzer (Malvern Zetasizer Nano Instrument – Model No: ZEN3500, Malvern Instruments Ltd.). The specification of the measurement range is between 1 nm and 5 μm (5000 nm). Two types of cuvettes were used during the measurements:

- Size cell: Only used for the particle size measurements
- Zeta cell: Used for the particle size and zeta potential measurements

In preliminary studies, only size cell was used but throughout the progress of the study, information of the zeta potential was required. Therefore, some particle size measurements were performed with using both size cell and zeta cell. After the evaluation of the results, zeta cell was selected to make all measurements.

Sample preparation has an important affect on the measured data. Thus, with modifications to the measurement method some improvements were achieved throughout this study. In preliminary experiments, the measurement sample was prepared by mixing the dried powder in an aqueous solution and decreasing its pH to 3.5 to 2.5 with AA. Then the prepared solution was treated with ultrasonic horn to have better particle dispersion. In order to have colloidal suspension stable against agglomeration, pH of alumina-ATH-boehmite suspensions should not be close to the iso-electric point of these oxides, which is between 8 and 9.

Depending on the zeta potential of the particles before measurement the pH adjustment mentioned above was necessary. However, no matter how well the particles are dispersed, in some cases the primary particle sizes observed in SEM micrographs could not be measured from the PSA. In order to have distributions more representative of the primary sizes a different sample preparation method was adapted. In this method, particles were taken from their solutions without drying. Then, they were mixed with DIW and centrifuged at 6000 rpm for 10 minutes. The centrifugate parts (liquid) of them were taken as samples for measurements and as a final step, ultrasonic mixing is applied for 2-5 minutes in order to have better dispersion. With this method the quality of particle size measurements was improved. Additional details of the methodic differences in measurement are explained in Appendix A. All measured data is reported as d(50) values. d(50) values corresponds to the cumulative particle size under which 50 % of all particles lies and could also be named as mass median diameter.

3.4.3 SEM (Scanning Electron Microscope) Analysis

Morphological characterization of products was carried out by the scanning electron microscopes either in Central Laboratory, METU (Model No: Quanta FEI 400F Field Emission SEM instrument) or in Geological Engineering Department, HU (Zeiss Evo 50).

3.4.4 XRD (X-ray Diffraction) Analysis

The structural analyses were carried out by using the X-Ray Diffraction instrument located at Department of Metallurgical and Materials Engineering, METU (Model No: RIGAKU – D/Max-2200/PC) by using CuKα (λ = 0.154 nm)

at 40 kV and 40 mA. All patterns were collected between 2θ values of 10^{o} and 80^{o}.

3.4.5 Thermal Analysis (DTA-TGA)

DTA (Differential Thermal Analysis) and TGA (Thermogravimetric Analysis) were used for thermal analyses of the samples. A Setaram thermal analyses system located in HU Mining Engineering Department was utilized for analyses. Heating rate in all analyses was constant at 10 °C/min and all analyses were conducted in air. Samples were heated in an alumina crucible. Results of thermal analyses are given in Appendix D.

CHAPTER 4

RESULTS AND DISCUSSIONS

4.1 Preliminary Studies

4.1.1 Preliminary Grinding Step

A preliminary grinding step (pre-grinding) was needed to decrease the size of particles fed to the glycothermal step of the alumoxane production process. Therefore preliminary studies for alumoxane production started with an effort on the optimization of this pre-grinding step. These exploratory studies were carried out either in two steps or one step as explained in Table 3.4.

First, rotation speed and duration were studied as parameters to be optimized. The particle size analysis (PSA) results of the two step pre-grinding are given in Figure A.1 (Appendix A). By increasing the rotation speed from 400 rpm (PG-A) to 500 rpm (PG-B), d(50) could be decreased from 500 nm to 400 nm. The additional observation was that this decrease in particle size could be achieved in a much shorter time with the stated increase in rotation speed. Therefore in the rest of the study rotation speed was kept at 500 rpm. By increasing the grinding time up to 70 minutes at 500 rpm and using ethylene glycol (EG) as the grinding medium instead of isopropyl alcohol (IPOH), even a smaller d(50) of 330 nm could be achieved with the conditions of PG-C. Due its higher viscosity use of EG would possibly help also in decreasing the contamination from grinding medium abrasion. In addition instead of a two-step pre-grinding, a one-step grinding would save

considerable time. Therefore a second group of pre-grinding conditions were tested by a straightforward one-step procedure using EG as the grinding medium. It can be followed from Figure A.1 that in 50 minutes with PG-C conditions the d(50) could be decreased down to 400 nm. Using 40 minutes as the duration, when a one-step pre-grinding was applied, the d(50) decreased to 450 nm (PG-D in Figure 4.1). When result obtained from PG-C was compared with that from PG-D, it was concluded that a one-step pre-grinding would decrease the sizes as effectively as the initially experimented two-step counterpart. Therefore in the following experiments a one-step pre-grinding was applied to the feed.

The effect of organic chemical used as the grinding medium was investigated further by comparing EG with an organic acid, namely acetic acid (AA). The results obtained from EG (PG-D), EG in combination with AA (PG-E) and AA alone (PG-F) are summarized in Figure 4.1. Grinding medium formed by mixing EG and AA gave the smallest sizes (d(50) was 400 nm) in shortest time (30 minutes). Within the same duration, with EG, d(50) remained around 550 nm and in 40 minutes it decreased to only around 450 nm. A value around 450 nm could be achieved in AA only after 60 minutes. Therefore, the pre-grinding medium was selected as the EG and AA mixture. It was also concluded that for a more effective grinding, the medium could be formed by combining the organic reagents that would be used in the final mechanochemical step with EG. It should also be noted here that the particles size measurements from samples that represent intermediate grinding durations are taken from aqueous solutions in which the particles were directly dispersed, whereas measurements from the final samples were taken in two different ways as explained in Appendix A. Appendix A also includes a discussion on why in some cases, with increased grinding duration the already-decreased particles sizes would tend increase.

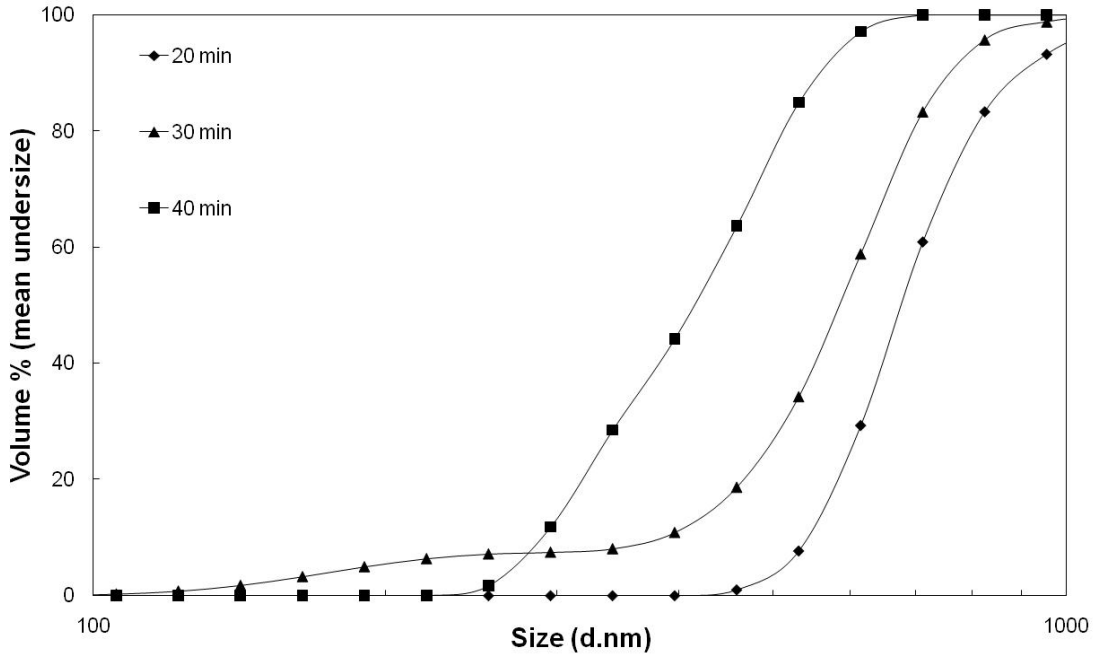
100
80
60
40
20
0
Volume % (mean undersize)
20 min
30 min
40 min
100
1000
Size (d.nm)

(a) PG-D

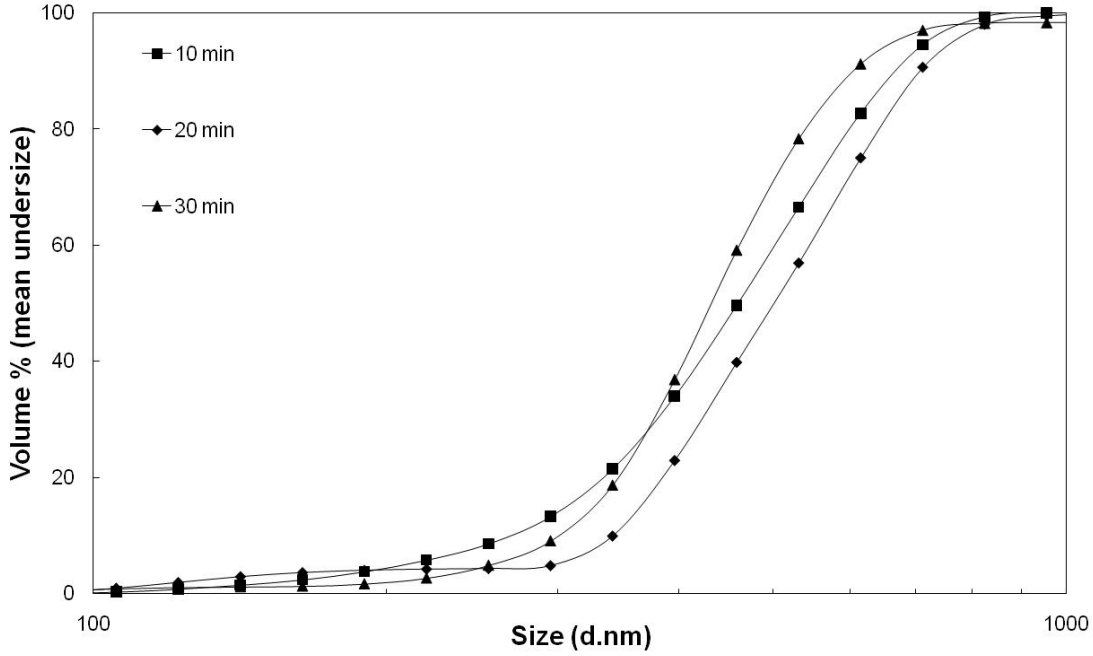
100
80
60
40
20
0
Volume % (mean undersize)
10 min
20 min
30 min
100
1000
Size (d.nm)

(b) PG-E

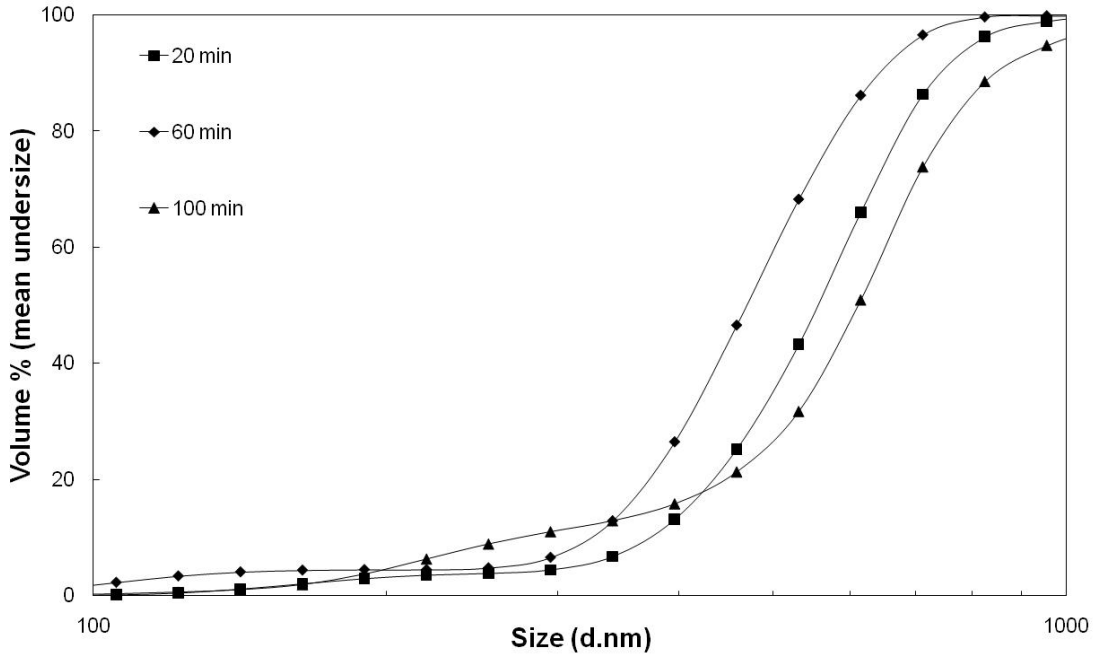

(c) PG-F

Figure 4.1 Cumulative particle size distribution of ATH particles subjected to a one-step pre-grinding in the preliminary studies; **(a)** PG-D: EG, **(b)** PG-E: EG and AA mixture, **(c)** PG-F: AA.

To support the PSA results, pre-ground particles were further analyzed by SEM. In Figure 4.2, the SEM micrographs of the samples ground under the pre-grinding conditions PG-C, PG-E and PG-F are given along with those of ATH before any grinding. From the SEM micrographs of ATH before grinding it can be observed that the initial particles sizes are around 50-60 μm and although there are a few particles with sizes above micrometer, the majority of them could be decreased down to sub-micrometer range with the pre-grinding step applied. With the pre-grinding step, besides a significant decrease in particle size, also a reasonable homogenization of the particle size distribution was achieved.

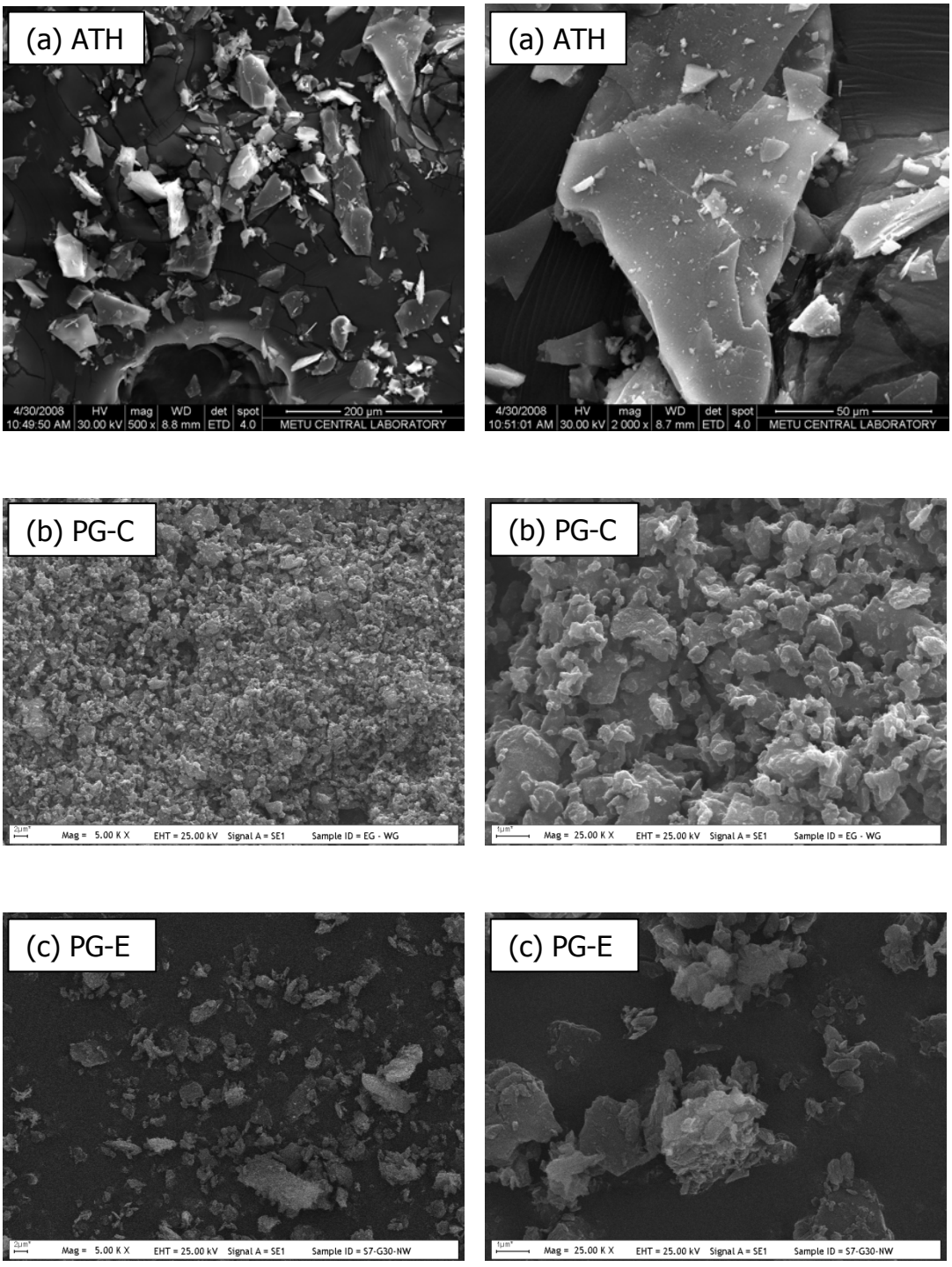

Figure 4.2 SEM micrographs of ATH particles and ATH particles subjected to pre-grinding in the preliminary studies; **(a)** ATH, **(b)** PG-C, **(c)** PG-E, **(d)** PG-F.

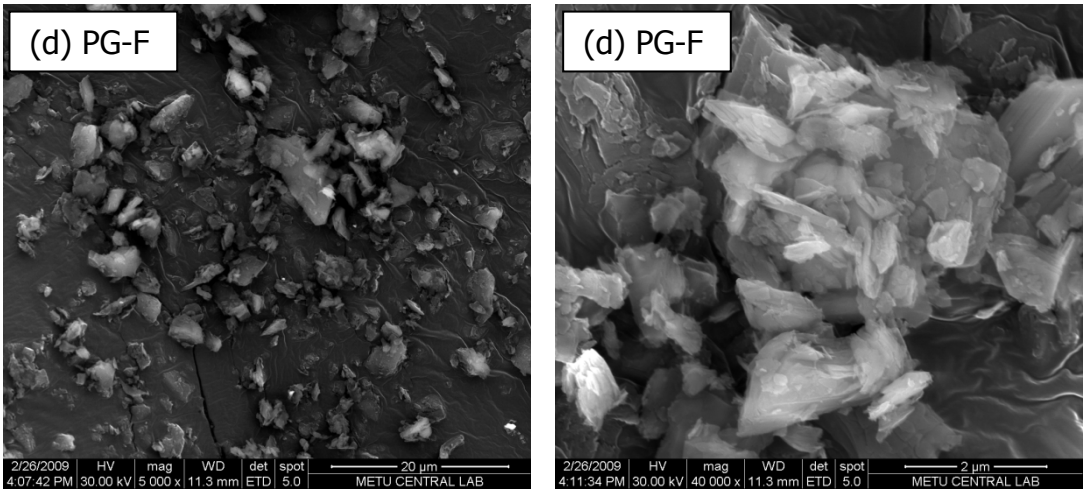

Figure 4.2 (Continued)

It can be inferred from the SEM micrographs given in Figure 4.2 that the primary particle sizes achieved under PG-C conditions are lower than any other condition studied. This is probably due to the two steps applied in its preparation. Yet, conditions PG-E and PG-F yielded the required particle size reduction for the next step, which is glycothermal processing step. In addition, a slight exfoliation among ATH layers was observable in the micrographs taken from pre-ground samples. The finely ground particles were in an agglomerated state due to reasons discussed in Appendix A. The agglomerate sizes were around 1-2 µm and they were formed by nano-sized (≤ 500 nm) primaries.

After the pre-grinding step, structural analysis of the particles was carried out. XRD patterns of samples pre-ground under the conditions of PG-B, PG-C, PG-E and PG-F are given along with that of raw ATH in Figure 4.3.

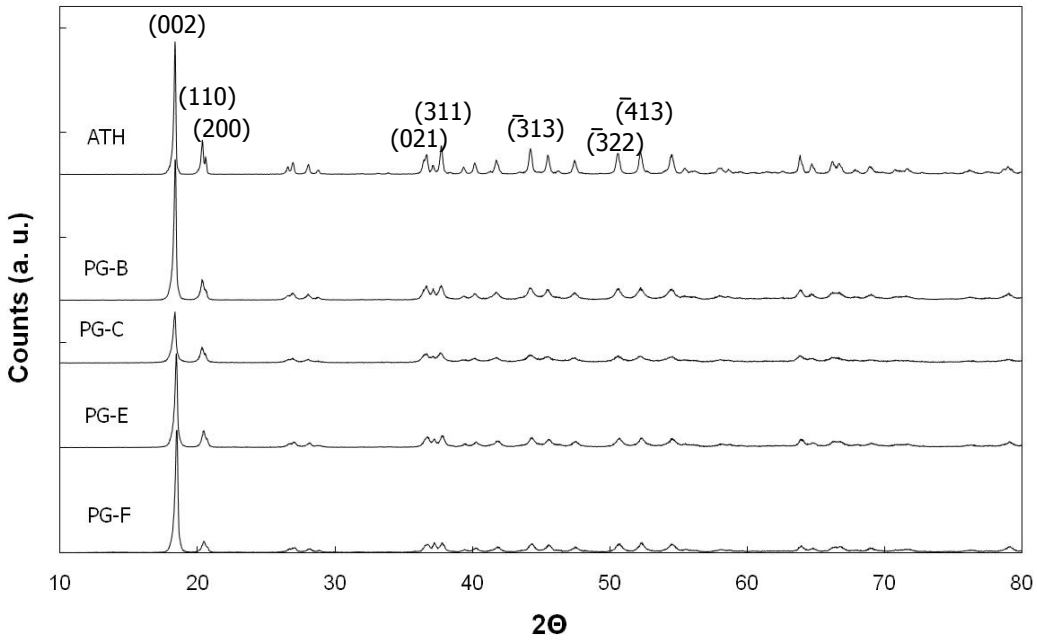

Figure 4.3 XRD patterns of ATH and ATH particles subjected to pre-grinding in the preliminary studies.

ATH has a layered structure and the layers are stacked in z-axis. The plane that cuts the unit cell by half along the z-axis has the indices (002). In the XRD patterns, (002) plane shows itself at a 2Θ value of 18.27° (Appendix C). While a shift to lower 2Θ values in this peak's position would correspond to a larger interlayer separation possibly due to intercalating species, a general relative intensity decrease would indicate that the length of crystals along this so-called layer stacking direction have become shorter. The loss of integrity among layers and formation of layers those are much thinner can also be termed as 'exfoliation'. While there are no pre-grinding conditions, in which there is a sensible shift (i.e. 'intercalation') in the (002) peaks, it would be fair to say that PG-C and PG-E conditions have caused considerable 'exfoliation' compared to other conditions, PG-C being the most effective.

These results are coherent with the results from PSA and SEM analysis and as stated above; to save time in pre-conditioning steps PG-E was chosen as the optimum pre-grinding condition. It should be also mentioned that none of the conditions change the crystal structure of the feed material (i.e. the ground particles still show the crystal structure of ATH after this step).

4.1.2 Glycothermal Step

After the preconditioning step, glycothermal process was applied to the pre-ground ATH particles prepared in different conditions. This step was carried out in a pressurized reactor that was set at 250°C, EG being the reaction medium. Digestion was proceeded for different time periods (namely, 2 (GT-1) and 6 (GT-2) hours) to determine the glycothermal process time required for the complete transformation of ATH to a poorly crystallized boehmite-like phase. In Figure 4.4, the XRD patterns collected from GT-1 and GT-2 are plotted along with the patterns collected from ATH and a well-crystallized boehmite (B) (refer to Appendix B) synthesized in our laboratory within the context of a different project.

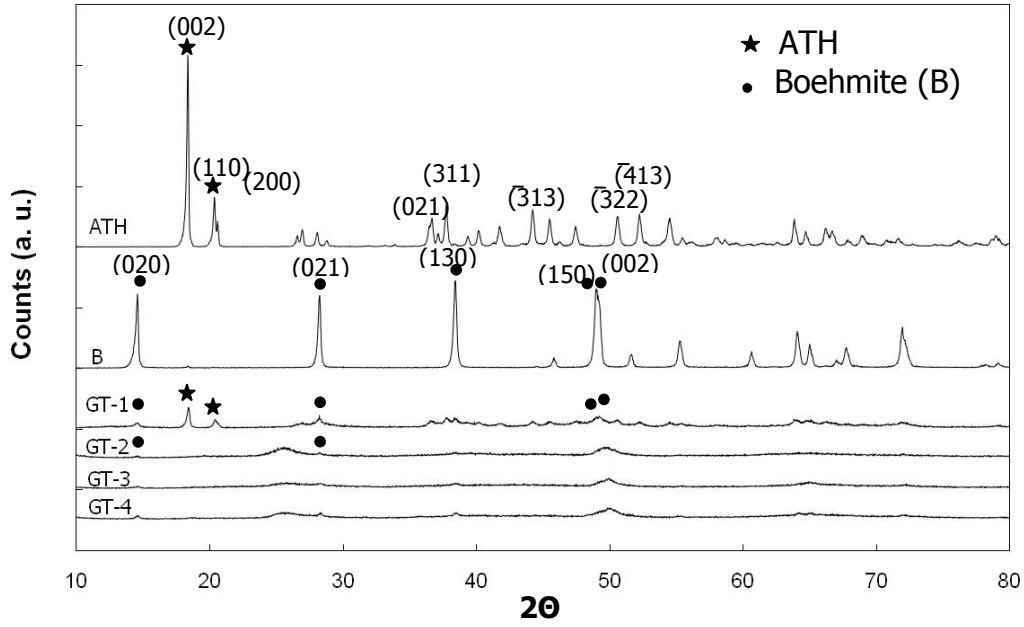

Figure 4.4 XRD patterns of the products obtained after 2 (GT-1) and 6 (GT-2, GT-3 and GT-4) hours of glycothermal processing.

When the XRD patterns in Figure 4.4 were examined, it was observed that time required for the near complete transformation of ATH to a poorly crystallized boehmite was about 6 hours. When ATH was processed for 2 hours, there were still some ATH peaks denoting remnant ATH in GT-1. Nevertheless, after 6 hours of process time, there were no peaks that can be ascribed to ATH. It can also be seen that the product that is forming as ATH is digested has some peaks which coincide in position with that of highly crystalline boehmite as expected [16]. However it is clear that this transformation product is in an extremely poor crystallized state. This intermediate digestion product was named as 'organic derivative of boehmite – ODB' after Inoue et al. [16]. Similar XRD patterns were also observed for samples GT-3 and GT-4, processing conditions of which can be found in Table 3.5. Glycothermal digestion products GT-1 and GT-2 were also

analyzed by means of particle size analyzer. Results are presented in Figure 4.5.

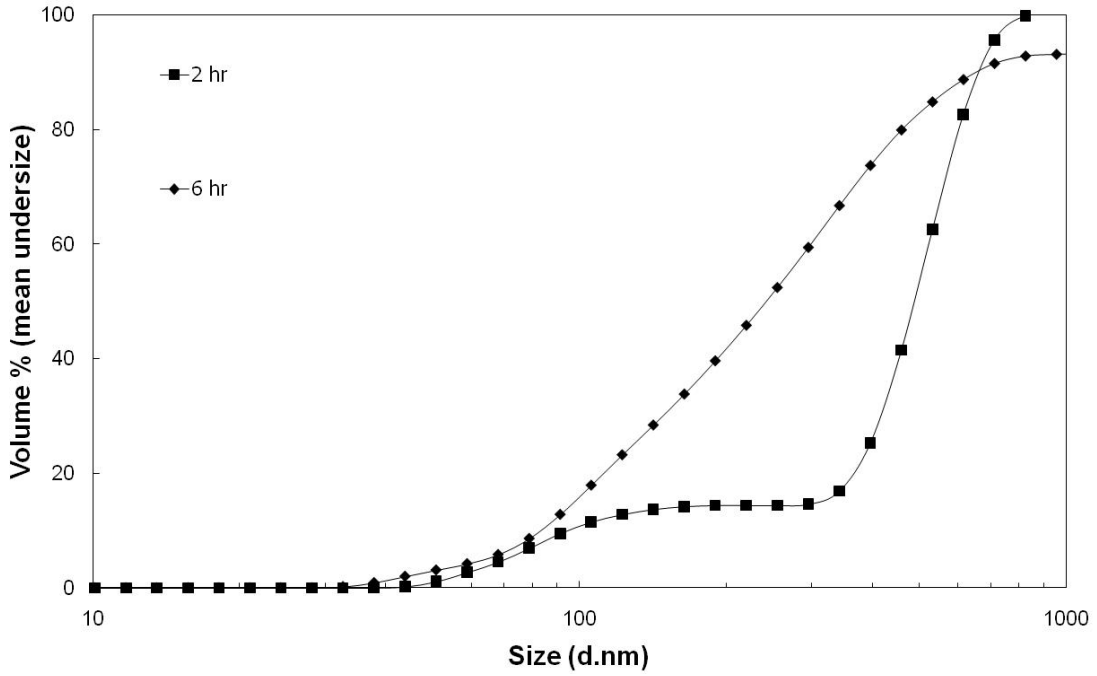

Figure 4.5 Cumulative particle size distribution of glycothermally processed ATH particles; GT-1: 2 hours and GT-2: 6 hours.

It was observed that in 2 hours (GT-1) sample, d(50) of the particles were around 450 nm and the distribution was bi-modal (with 100 nm and 500 nm as the average sizes) giving a sense of partial transformation from ATH to ODB as also indicated by XRD results. In contrast, after a 6 hours treatment (GT-2), d(50) values were decreased to 250 nm with a wide mono-modal distribution. In other words, as the transformation of ATH to ODB proceeded the initially formed 100 nm particles were grown and increased to an average particle size around 250 nm. The particle size analysis result from

the centrifugate of 6 hour digested sample is given in Figure A.3. The width of the mono-modal distribution was in fact much smaller according to this more representative measurement. Stating in other words, there is a certain amount of agglomeration among particles that is difficult to disturb upon direct dispersion in water. A detailed explanation is given in relevant parts of Appendix A.

SEM analysis was also carried out in order to investigate the morphologies and agglomeration behavior of the produced particles. In Figure 4.6, effect of digestion time on primary particle size and morphology of the glycothermal product (ODB) is presented.

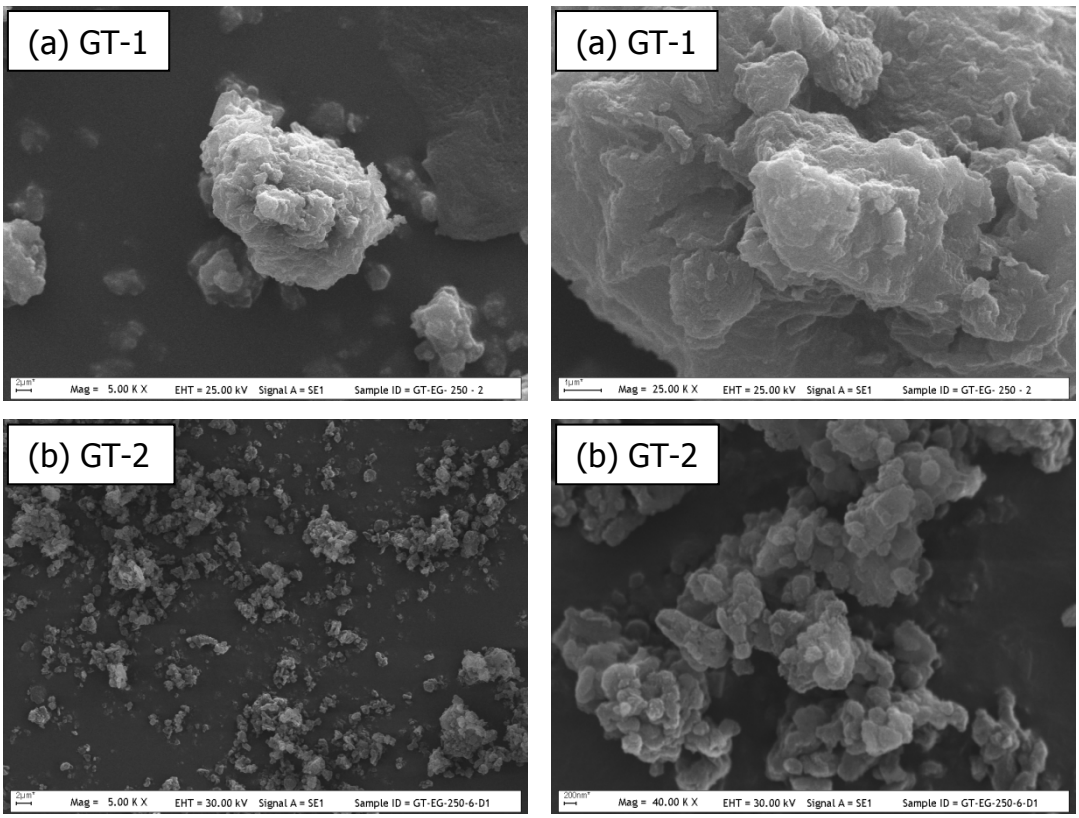

Figure 4.6 SEM micrographs of glycothermally processed ATH particles; **(a)** GT-1: 2 hours, **(b)** GT-2: 6 hours, **(c)** GT-4: 6 hours.

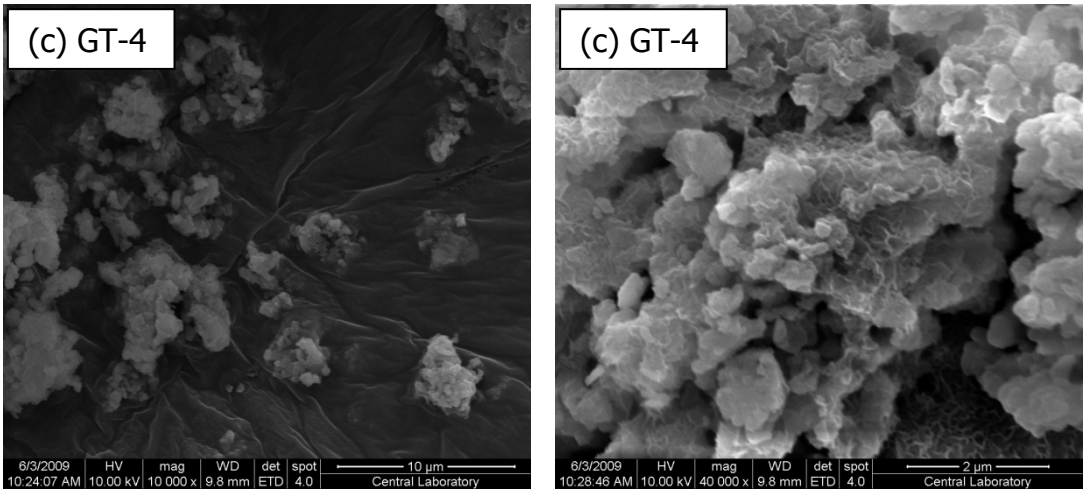

Figure 4.6 (Continued)

When the SEM micrographs of GT-1 and GT-2 are compared, it is observable that complete transformation of ATH into ODB resulted in homogenously distributed smaller and spherical particle sizes. GT-2 and GT-4 had similar and homogeneous particle size distribution around 200-300 nm, while GT-1 had an inhomogeneous bimodal particle size distribution around 400 nm and 100 nm which is in line with the particle size analysis presented in Figure 4.5.

Optimum glycothermal processing time was set as 6 hours for the rest of the study upon examination of the preliminary results.

4.1.3 Mechanochemistry Step

After production of ODB particles, they were treated mechanochemically in the high energy ball mill with AA and MAA (methoxy acetic acid) as the grinding mediums. A series of preliminary experiments were performed, conditions of which were given in Table 3.6. Since these were preliminary

trials, no special effort was given to use ODB's produced under same conditions. In MC-1, GT-2 was processed with MAA medium, whereas AA was used with MC-2 and MC-3. Feeds of MC-2 and MC-3 were GT-3 and GT-4, respectively. Using the mechanochemical processing method developed in these preliminary experiments, different types of alumoxanes were produced as will be explained in the forthcoming sections. In Figure 4.7 XRD patterns taken from two of the mechanochemically processed powders are given with the reference patterns of ATH and B.

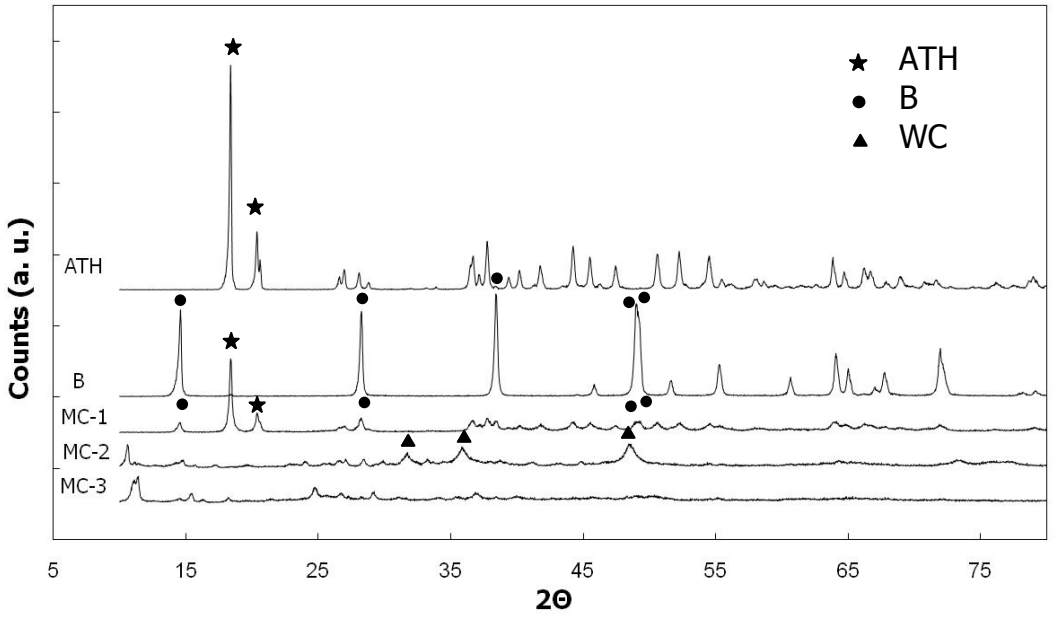

Figure 4.7 XRD patterns of mechanochemically processed ODB's.

Boehmite has a layered structure resembling that of ATH. However, in boehmite structure layers are stacked along y-axis. Within the layers Aluminum atoms are octahedrally coordinated by oxygen and hydroxyl. The layers are formed by edge-sharing octahedra like in ATH, however in

boehmite the tips of octahedra are aligned with x-axis. The plane that cuts the unit cell by half along the y-axis has the indices (020). In the XRD patterns, (020) plane shows itself at a 2Θ value of 14.5°. It was reported that boehmites produced at temperatures lower than 100^{o}C tend to show 'pseudo-boehmite' structure, which is nothing but finely crystalline boehmite particles that consist of the same or similar octahedral layers grew in the xz plane. Nevertheless the layers lack three-dimensional order because the number of unit cells along the y-axis is restricted. Specific to boehmite (i.e. not all clays behave similarly) a decrease in crystallite size along y-axis, not only broadens the (020) peak, but also shifts it up to 5^{o} 2Θ towards low 2Θ values. This is also accompanied by excessive hydration of the structure. Water can intercalate in between the stacks of crystallites or may adsorb on the crystallite surfaces. If an ordered intercalation between crystallites is the case, the shifts to higher 2Θ values can be justified. If the number of octahedral layers along y-axis is restricted to one, then (020) peak is expected to vanish in XRD patterns, although peaks that correspond to planes that has (hkl) or (h0l) type of indices shall remain. Conversely the crystallites can be consisted of more than one layer. In this case, provided that the number of layers in each crystallite is similar, then the broadening expected for a certain amount of shift to higher 2Θ values shall be limited, whereas if crystallites are formed by stacking of different number of octahedral layers (for example, 75% can consist of 2 layers and 25% 3 layers) then both the shift and broadening would expected to be more [57].

When the XRD patterns of MC-2 and MC-3 are examined, it can be seen that the ODB produced in a poorly crystallized state in the previous step starts to form new crystalline peaks upon processing in the final mechanochemical step. The peaks form at lower 2Θ values. It can be hypothesized that the mechanical agitation brings the crystallites into order along the stacking axis of boehmite, but with a much larger interlayer spacing. In other words, the

organic reagent used in the grinding medium starts to bring the layers into order by intercalating in between them. In the cases presented in Figure 4.7 this is acetic acid. One other important feature is that the emerging peaks are broad compared to highly crystalline products, however they are not as broad as typically observed, shifted and broadened peaks in 'pseudo-boehmites'. This complies with the possibility that new crystallites have similar sizes. With increasing grinding time the shifts get smaller, which could mean that intercalates are in a much ordered state in between the layers. In the case of 180 minutes grinding duration, (020) peak show a tooth tip that signals the existence of at least two distinct, but close crystallite sizes along the y-axis. However from the data it cannot be concluded whether these different-sized crystallites are individually separated (i.e. each crystallite has a specific separation distance along its y-axis) or they exist in a stacking sequence that is 'interstratified' (i.e. each crystallite host two or more distinct regions along its y-axis, such that interlayer separation is changing in each individual zone). In addition, a systematic decrease in the intensities of higher order peaks indicates that the crystals have limited sizes in the xz plane. This increases the expectation that more elongated crystallite morphologies would be observed in MC-3.

As explained in Appendix A, as the grinding proceeds finer and finer particles can be produced. However due to their increased surface area and thus chemical potential, fine particles have a natural tendency to agglomerate. In the grinding jar as the mechanochemical agitation proceeds, continuously exfoliated and separated layers would constantly agglomerate back and as the XRD results suggest, depending on the grinding medium and duration this agglomeration could as well be termed as 'ordering along y-axis' in some cases. Although the layers might restack into a different order, the new crystallites would still be so small that they would also continue to agglomerate among themselves. Therefore while the measurements taken

from the centrifugates collected on top of the washed products would represent the approximate crystallite sizes, the ones taken from the solutions, in which particles are directly dispersed, would give an idea about the agglomeration state of these crystallites. In Figure 4.8 particle size analyses of mechanochemically treated ODB particles made by both methods are given. Measurements from the particles directly dispersed in water are given as straight lines and the measurements carried out from the centrifugate part of the grinding mediums are given as dashed lines. The curves denoted as "0 min", represent the size distribution of the feed material, which is in this case the ODB particles that were obtained from the glycothermal step.

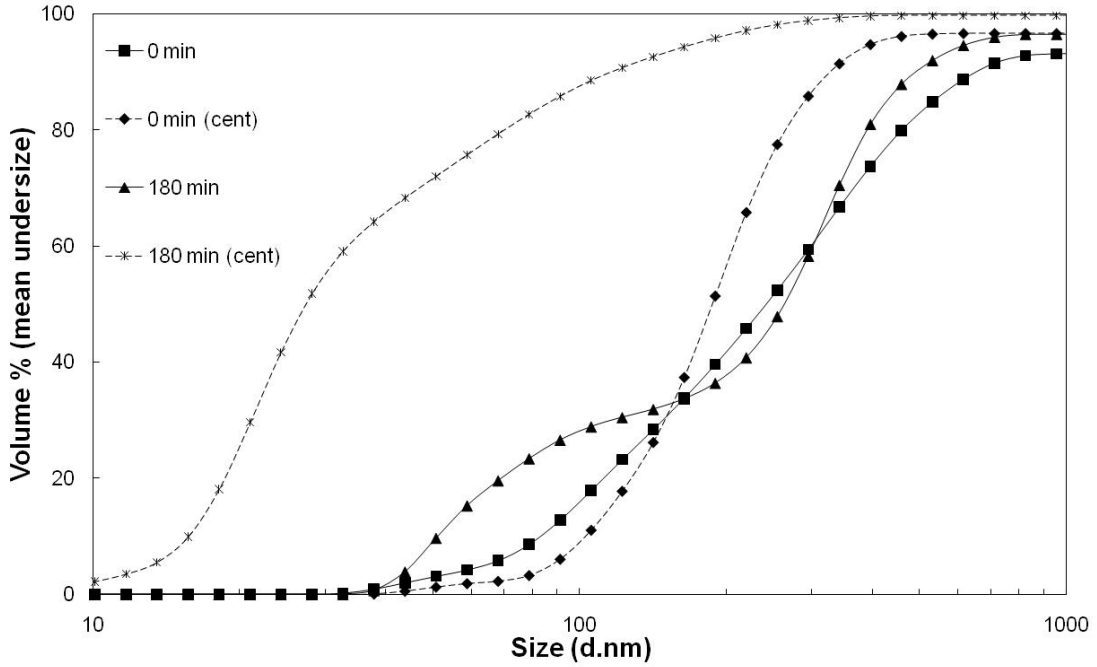

(a) MC-1

Figure 4.8 Cumulative particle size distribution of mechanochemically processed ODB's; **(a)** MC-1, **(b)** MC-2, **(c)** MC-3.

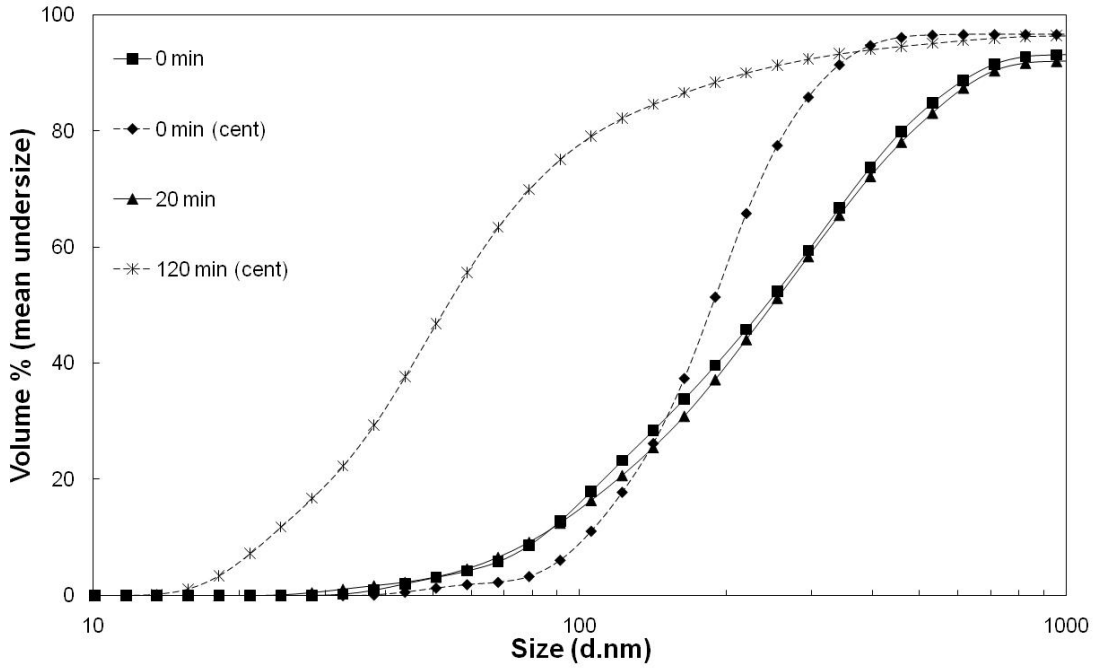

(b) MC-2

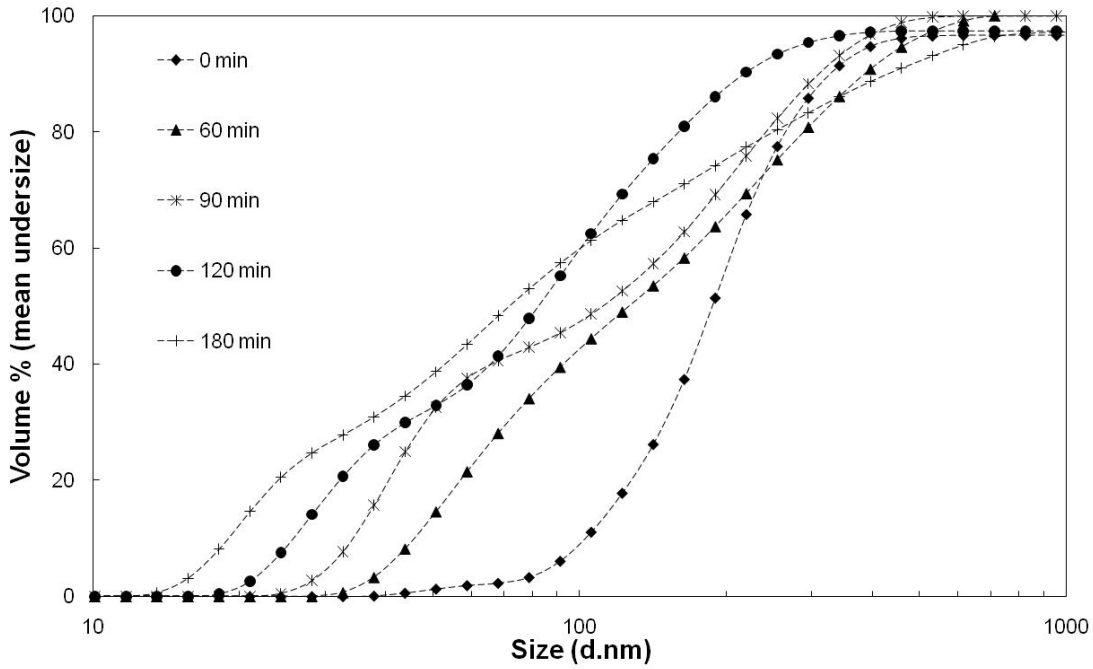

(c) MC-3

Figure 4.8 (Continued)

It was observed from Figure 4.8 that d(50) values were decreased to 30 nm, 50 nm and 70 nm under the grinding conditions MC-1, MC-2 and MC-3, respectively. When MAA was the grinding medium, the cumulative particle size distribution was bimodal with averages being 26 nm and 116 nm. When the treatment in AA medium was 120 minutes, distribution was mono-modal and yet increasing the time to 180 minutes resulted in two different average values, 40 nm and 178 nm. With longer durations, observation of a bimodal distribution could be explained by the agglomeration small particles and the coexistence of primary crystallites with the agglomerated ones. On the other hand, emergence of bimodality could also indicate a change in aspect ratio of the crystallites as evidenced by XRD results discussed above.

To support the PSA and XRD results SEM analyses were performed. In Figure 4.9, SEM micrographs of particles obtained under the MC-1, MC-2 and MC-3 conditions are presented.

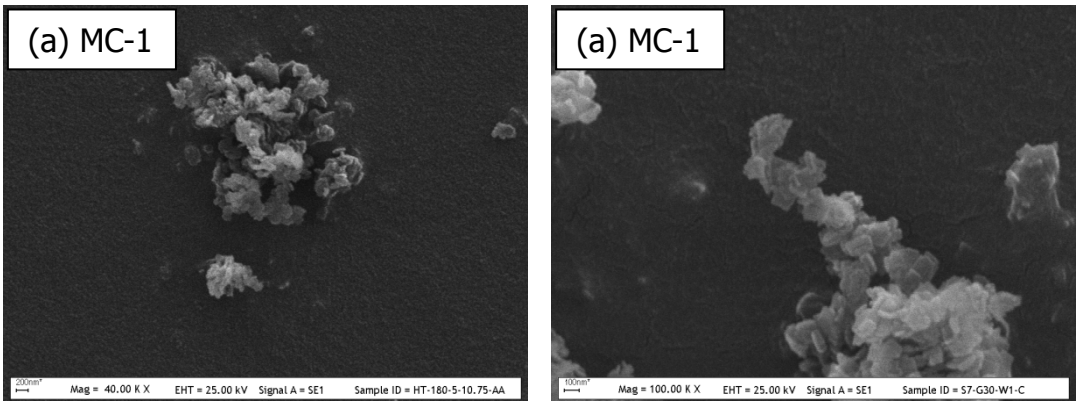

Figure 4.9 SEM micrographs of mechanochemically processed ODB's; **(a)** MC-1, **(b)** MC-2, **(c)** MC-3.

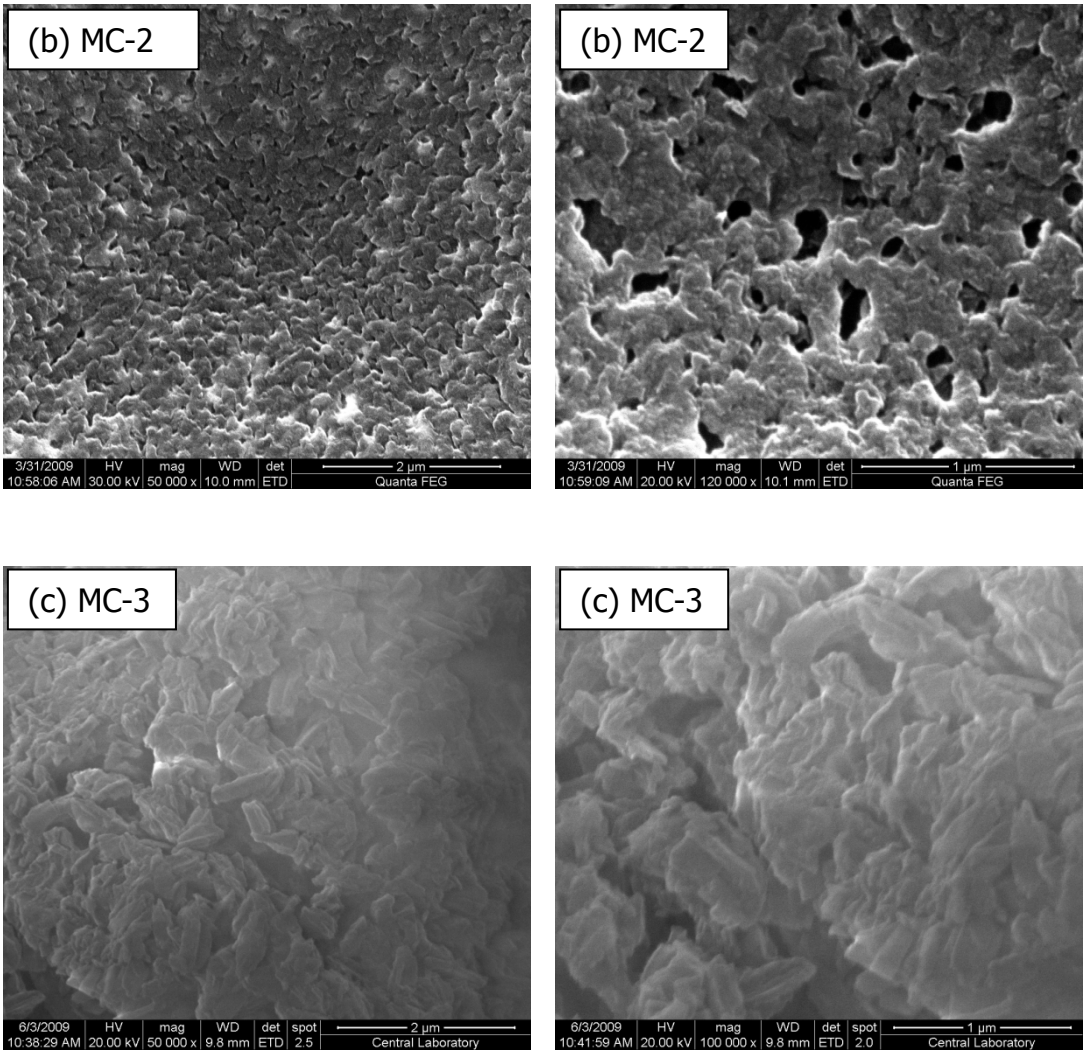

Figure 4.9 (Continued)

Observations from the SEM micrographs complement the PSA and XRD results well. Mechanochemical treatment with MAA resulted in crystallites that are less than 100 nm, but crystallites showed a high degree of agglomeration. Micrographs of MC-2 were taken from a sample prepared by drying the powders directly from their grinding medium. This facilitated the easy analysis of primary crystallites that agglomerate to form secondary particles and the monodisperse nature of the distribution under this mechanochemical treatment condition could be verified. SEM analysis of MC-

3 was performed from the dried powders like MC-1. It was clear that the crystallites were in an agglomerated state. It was intriguing that the aspect ratio of the majority of crystallites was large compared to ones obtained in the preceding conditions. This was in full agreement with the XRD and PSA results.

To conclude the preliminary experiments and characterization of the products obtained, FT-IR spectra of samples representing each step was taken. FT-IR spectra taken from a pre-ground ATH (PG-E), an ODB (GT-2) and a mechanochemically treated ODB (MC-2) are given along with reference spectra from B, ATH, AA and EG in Figure 4.10.

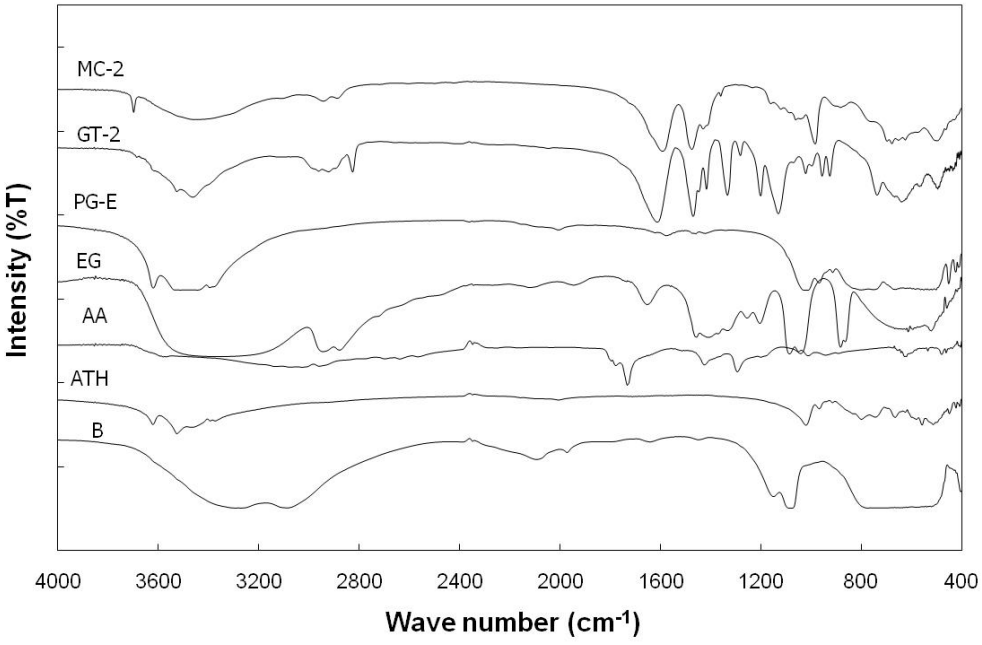

Figure 4.10 FT-IR spectra of PG-E, GT-2 and MC-2 given with the reference spectra from B, ATH, AA and EG that are used in various synthesis steps.

It is observable from the spectra that after pre-grinding ATH in EG-AA mixture (PG-E), the characteristic absorption peak due to free stretching of O-H's in ATH is still present at 3650 cm^{-1}. However the other O-H stretching peaks around 3550 and 3500 cm^{-1} are broadened considerably which is due to the excessive hydrogen bonding of these groups. This can be taken as positive evidence for formation of nanoparticles after grinding, since such deformed stretching vibrations of O-H's have also been encountered in nano particles or upon the formation of amorphous structures due to the increased number of crystal surfaces that are available for further hydrogen bonding [58]. The peaks around 400-900 cm^{-1} are related to Al-O (AlO_6 and AlO_4) stretching vibrations. The broadening of these peaks reveals again the nanoparticle formation. In addition to that, the broad peak around 500 cm^{-1} belong to the pseudo lattice Al-O stretching vibrations in AlO_4 tetrahedron [58]. As a conclusion, it is clear that the pre-grinding step does not modify the ATH structure as also evidenced from XRD results, but decreases the sizes to ultrafine range.

Glycothermal product (GT-2) can be analyzed by comparing it to the boehmite. Boehmite has characteristic IR bands at 1070, 760, 615 and 480 cm^{-1} [19]. While, the first two are assigned to hydrogenic mode, others are assigned for the structural vibrations of boehmite layers [59-61]. These peaks are also preserved in the spectrum of GT-2. 1070 and 760 cm^{-1} peaks are slightly shifted to left and weakened, while others are in their original positions. Moreover, observation of absorption bands at around 2920 cm^{-1} and 2820 cm^{-1} which belong to C-H stretching indicates the incorporation of EG moieties. In addition to those peaks, the peaks around 1500-800 cm^{-1} regions are also observed due to EG incorporation. Furthermore, the observation of broadened 3500 cm^{-1} and 500 cm^{-1} peaks in GT-2 indicates the amorphous or nanoparticulate nature of the product [58].

In MC-2 spectra the nature of broad peaks around 3500 cm^{-1} and 570 cm^{-1} does not change, which explains the agglomerated nature of extremely small crystallites [58]. Characteristic EG peaks' intensities observed in ODB are lowered due to the AA incorporation to the ODB structure, while EG is being replaced. Moreover while characteristic boehmite peaks are disappearing, the characteristic sharp acetate alumoxane peaks around 3300 cm^{-1} and 1070 cm^{-1} emerges. In addition to that, the two peaks observed around 1600 cm^{-1} and 1460 cm^{-1} evidence that the carboxylates are bonded to boehmite crystallite surfaces in the bridging mode [10].

After the evaluation of results of preliminary experiments a process flow-chart was developed for the mechanochemical treatment of the glycothermally processed ATH particles. This is summarized in Figure 3.8. In summary, in pre-grinding a medium formed by mixing EG with the selected organic reagents (e.g AA, MAA, SA and Ly) will be used and the glycothermal step will be carried out at 250°C for 6 hours, which will then be followed by a mechanochemical grinding step with the same organics reagents used in the pre-grinding step.

4.2 Pre-Grinding in Mixtures of EG and Organic Reagents

According to the grinding parameters that were determined in preliminary experiments a set of samples were prepared in conditions defined in Table 3.7. Grinding mediums denoted as PG-AA, PG-MAA, PG-SA and PG-Ly correspond to mixtures of EG with AA, MAA, SA and Ly, respectively. All pre-grinding experiments were carried out as a one step process and continued for 40 minutes. As it may be noticed, sample denoted as PG-AA is a sample that was prepared under conditions similar to sample PG-E presented in

preliminary studies. Pre-ground ATH particles were structurally characterized by XRD and patterns are presented in Figure 4.11.

When XRD patterns from pre-ground samples are compared with the pattern from raw ATH, it can be seen that a slight decrease in the intensity of the most intense peak of ATH (002). While the least intensity decreasing is observed in the sample prepared with SA (PG-SA), decreasing of intensity is the most in Ly treated sample (PG-Ly). Treatments with AA (PG-AA) and MAA (PG-MAA) represent the intermediate cases. Therefore it can be concluded that different organic reagents used besides EG imparted variable exfoliation capacities towards ATH and provided the means of producing starting materials with variable sizes.

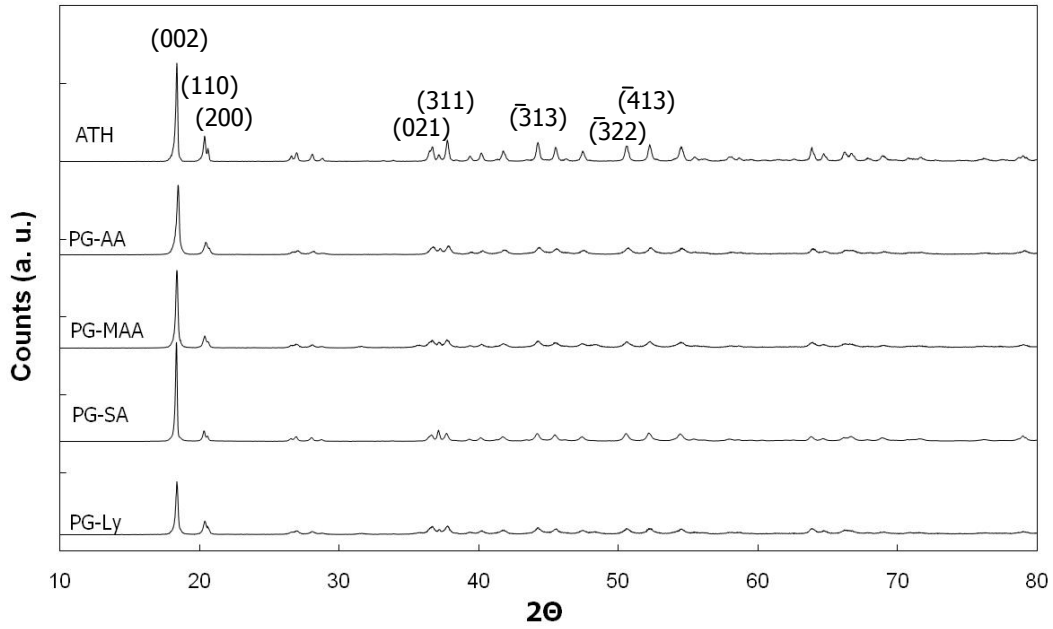

Figure 4.11 XRD patterns of raw ATH and ATH particles subjected to pre-grinding in mixtures formed between EG and; AA (PG-AA), MAA (PG-MAA), SA (PG-SA) and Ly (PG-Ly).

In addition to structural characterization of the pre-ground powders, particle size (PCS) and morphology (SEM) analyses were carried out. PSA results of the samples are given in Figure 4.12. Cumulative distribution plots drawn with straight lines mean that those analyses are made from powders that were dispersed in aqueous medium, and the dashed lines refer to the measurements taken from the centrifugate of grinding medium.

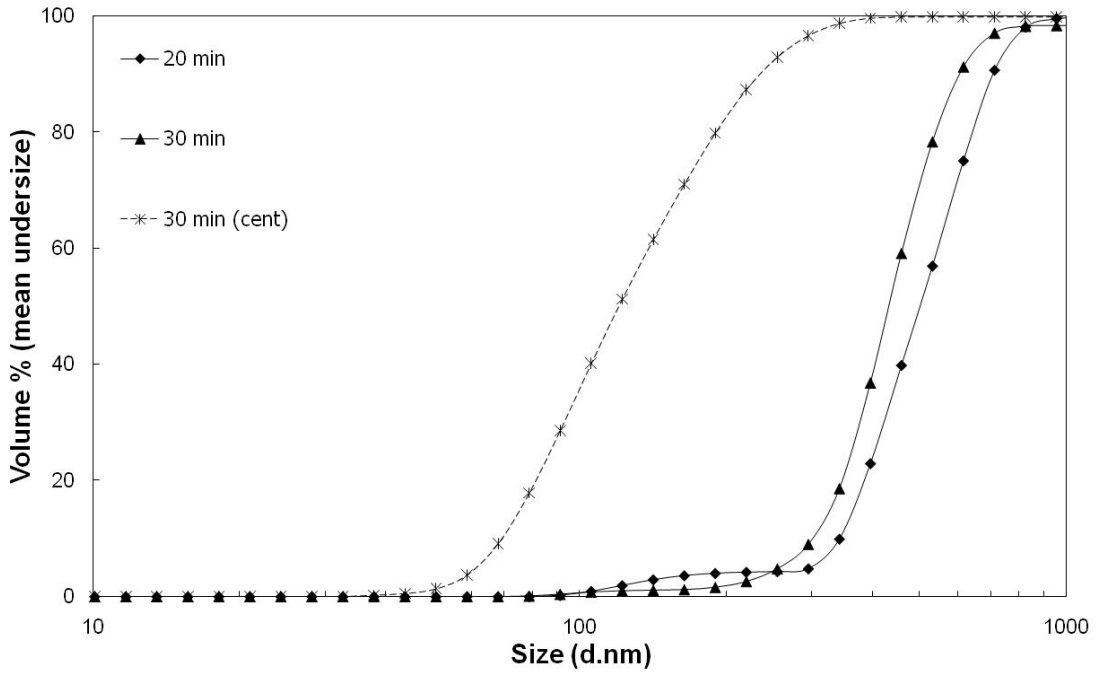

(a) PG-AA

Figure 4.12 Cumulative particle size distribution of ATH particles subjected to pre-grinding in mixtures formed between EG and; **(a)** AA (PG-AA), **(b)** MAA (PG-MAA), **(c)** SA (PG-SA) and **(d)** Ly (PG-Ly).

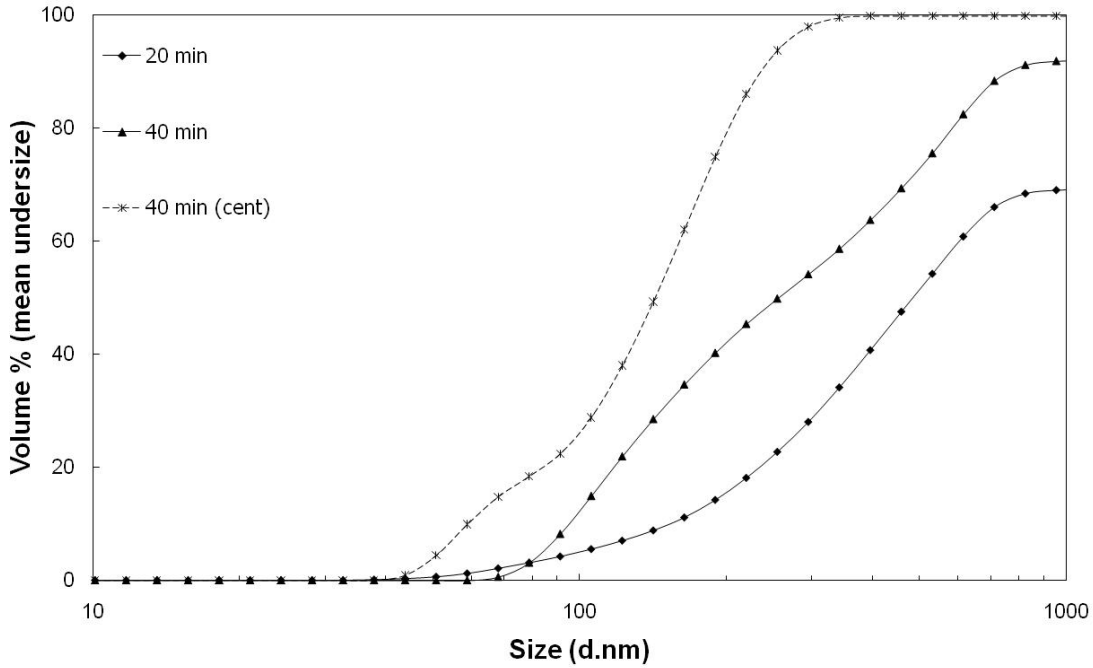

(b) PG-MAA

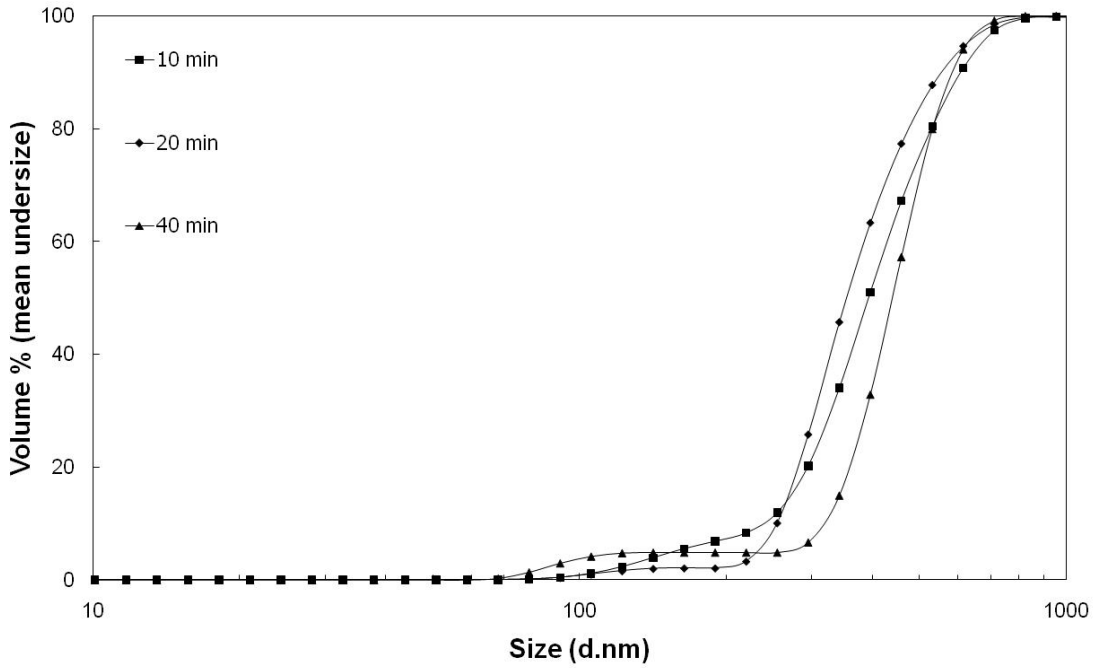

(c) PG-SA

Figure 4.12 (Continued)

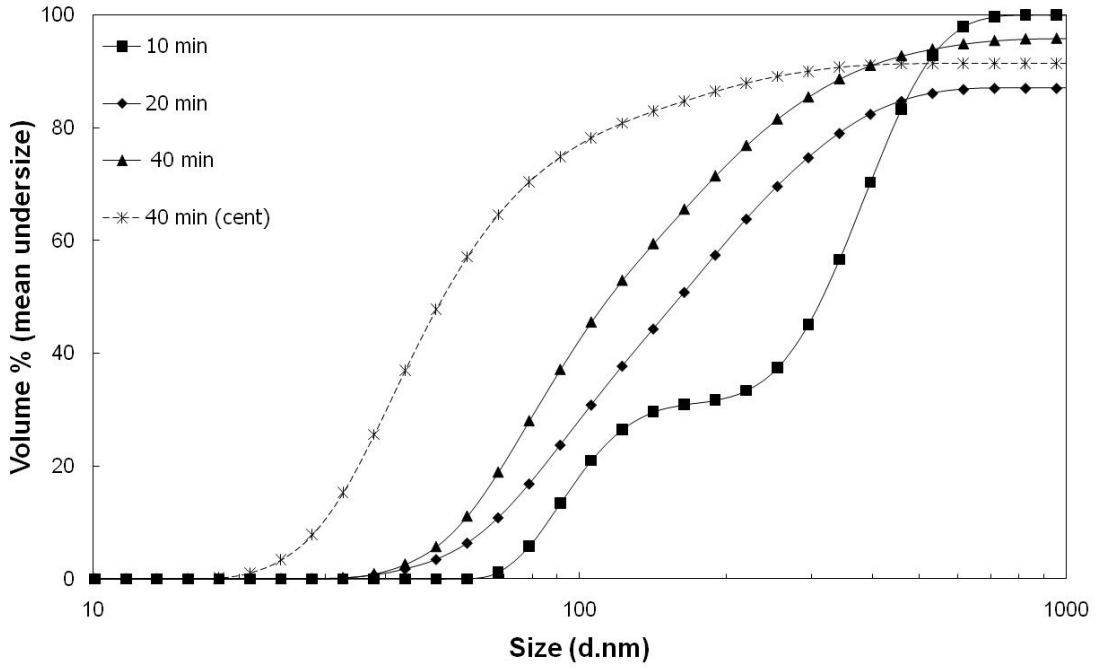

(d) PG-Ly

Figure 4.12 (Continued)

It was observed from Figure 4.12 that in the pre-grinding steps applied ATH particles sizes could be decreased from several tens of microns to micron to sub-micron levels. Grinding with AA gives d(50) values around 400 nm in 30 minutes as discussed in the results of preliminary studies. The centrifugate of the same sample gives a value of 120 nm. Grinding in combination with MAA, d(50) value is observed to be around 250 nm in 40 minutes. The centrifugate of this sample gives a d(50) value of around 140 nm. It can be said that these two conditions give similar results. In the case of pre-grinding in SA added grinding medium, d(50) value remained around 420 nm. It is clear that SA do not provide the most effective grinding conditions nevertheless, the sizes obtained are still suitable for further processing in glycothermal step. In Ly supported medium the observed d(50) values are the lowest. The measurement from plain dispersions give a d(50) of 120 nm and the d(50) of

the centrifugate is around 75 nm. As a final observation it would be important to note that while mediums supported with AA, SA and Ly yield mono-modal particle size distributions, ones with MAA yields a bimodal distribution. Pre-ground particles were further analyzed by SEM and micrographs that were taken are presented in Figure 4.13.

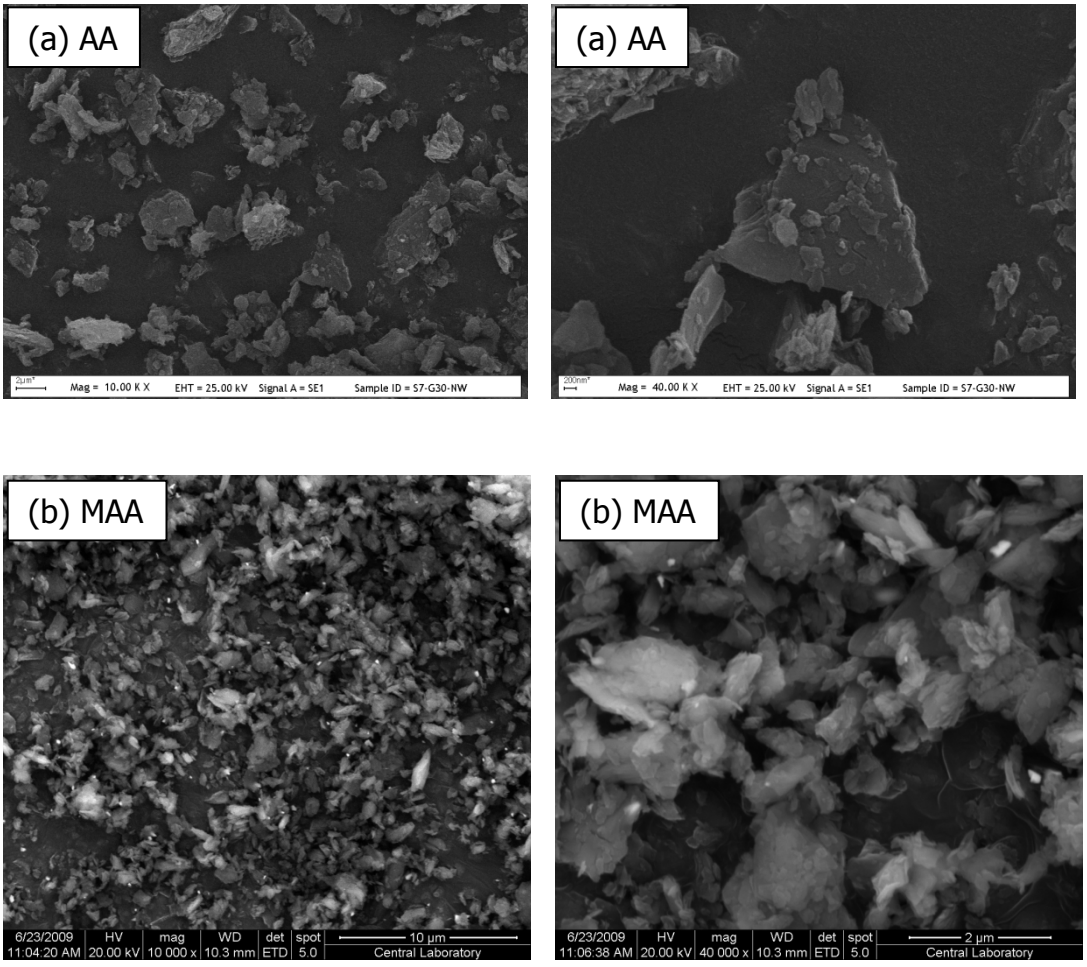

Figure 4.13 SEM micrographs of ATH particles subjected to pre-grinding in mixtures formed between EG and; **(a)** AA (PG-AA), **(b)** MAA (PG-MAA), **(c)** SA (PG-SA) and **(d)** Ly (PG-Ly).

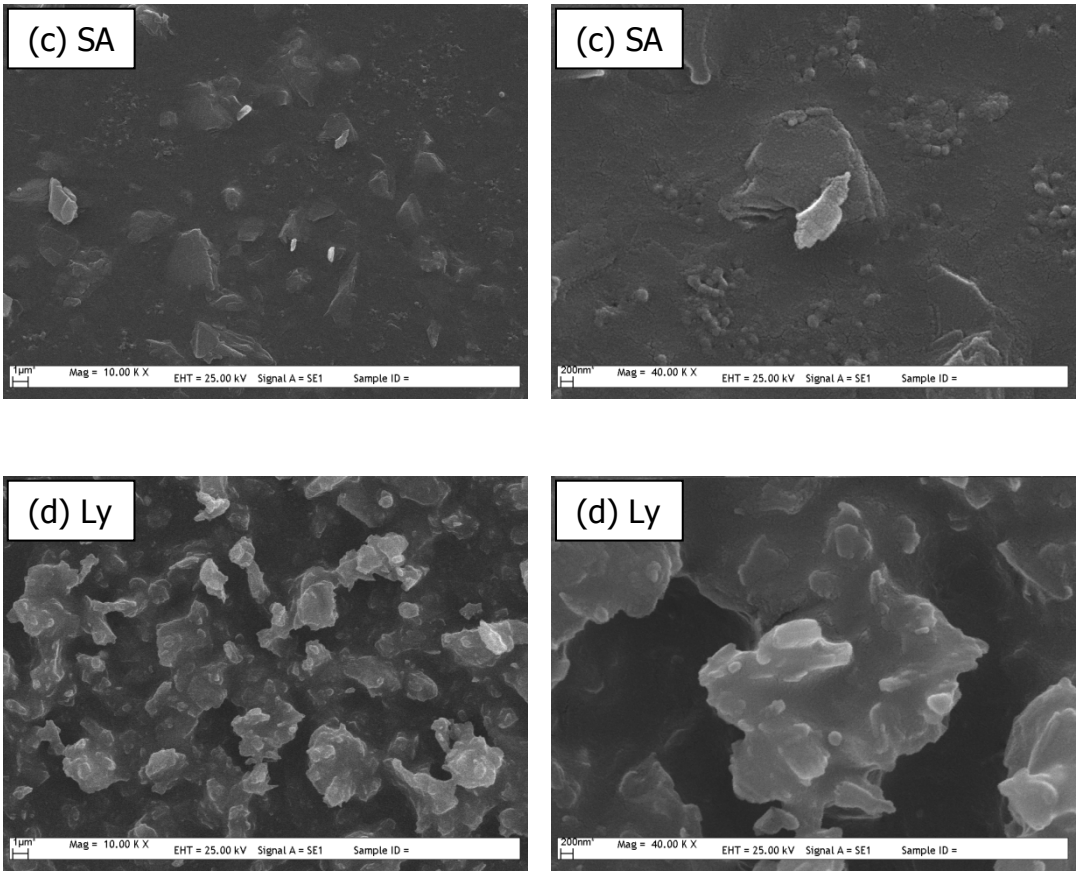

Figure 4.13 (Continued)

The correlation between SEM analyses results and PSA results was remarkable. Particle size observations from AA and MAA mediums indicate similar homogenization levels and particle morphology. In SA and Ly supported mediums it seems like finer sizes were achieved however, these fines are in a much more agglomerated state. It is plausible that the sizes of unbroken pieces in SA medium are similar to those in AA medium. However the PSA results from even the centrifugate of SA medium indicates larger sizes. It is highly probable that relatively long alkyl chains that adsorb on the particle surfaces cause extensive agglomeration even in the well-dispersed state of particles and make the measured sizes larger in the SA treated case. On the contrary, in Ly supported medium the size of the particles left

unbroken were much smaller than in any other mediums. This is in accordance with the conclusions driven from XRD and PSA results. Although it was the first process step in alumoxane production, the observed difference in morphology of particles treated in Ly supported medium is noteworthy.

FT-IR spectra given in Figure 4.14 reveal some information about the degree of interaction between the molecules of reaction medium and the particles. The main features of FT-IR spectra obtained from pre-ground samples are similar and broadened peaks around 3500 cm^{-1} and 570 cm^{-1} can again be taken as a sign of nanoparticle formation as it is also observed in XRD, PSA and SEM analyses [58]. In addition it is peculiar that the organic reagent adsorption is observable in all samples to a certain extend. Nevertheless it is the most in pre-grinding in SA supported medium. This explains the excessive agglomeration in this specific sample. As a conclusion, it can be said that, in view of the particle size distributions although grinding in Ly supported medium gave the best exfoliation and size reduction conditions, in all samples required particle size reduction for glycothermal step was achieved.

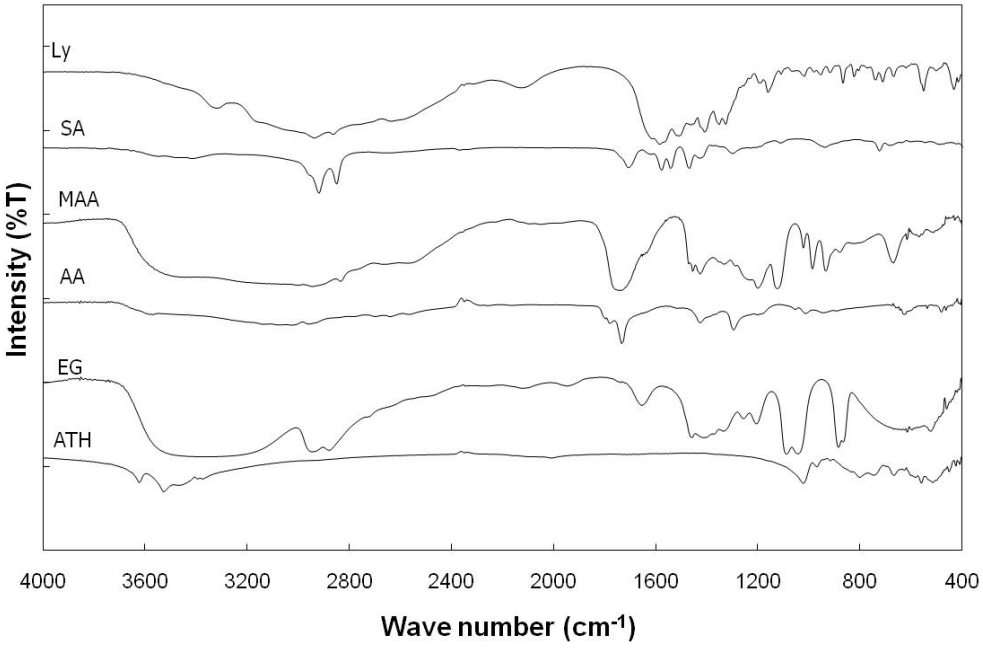

(a)

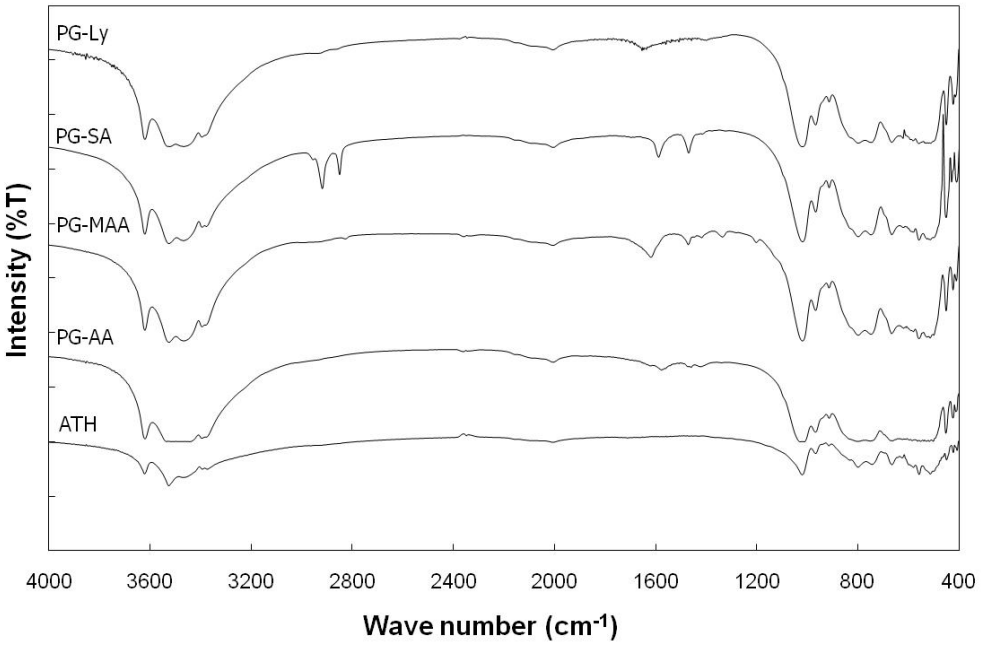

(b)

Figure 4.14 FT-IR spectra of **(a)** organic reagents used (EG, AA, MAA, SA, Ly), and **(b)** ATH particles subjected to pre-grinding in mixtures formed between EG and; AA (PG-AA), MAA (PG-MAA), SA (PG-SA) and Ly (PG-Ly).

4.3 Glycothermal Treatment of Ground Particles

Utilizing the reaction conditions optimized in preliminary studies, pre-ground ATH particles were treated at 250°C in EG medium for 6 hours. Experimental conditions of the ODB productions in this step were given in Table 3.8. Briefly, GT-AA, GT-MAA, GT-SA and GT-Ly correspond to glycothermally digested samples feeds of which were prepared by pre-grinding in AA, MAA, SA and Ly supported mediums. Initial identification of the produced ODB structures was done by XRD analyses, results of which are given in Figure 4.15.

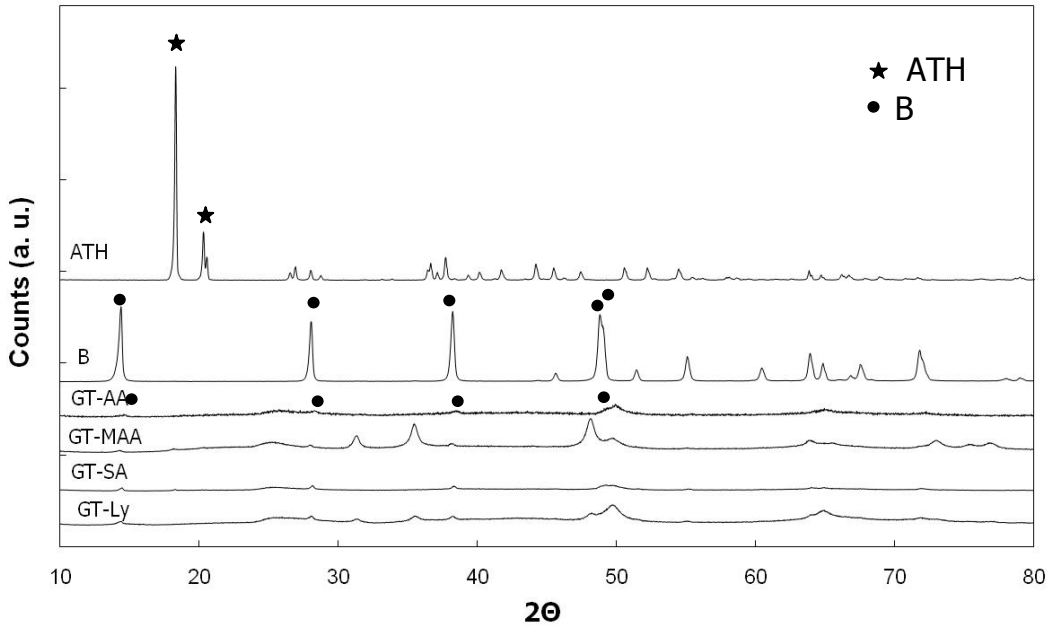

Figure 4.15 XRD patterns of ODBs produced from pre-ground particles in mixtures formed between EG and; AA (GT-AA), MAA (GT-MAA), SA (GT-SA) and Ly (GT-Ly).

It was observed from Figure 4.15 that in all samples digestion in the glycothermal step have been completed to a large extend. Loss of intensity in especially the (020) peak positioned at 2Θ value of 14.50^{o} denotes the loss of integrity among the layers stacked along y-axis. The peaks that denote crystallization in the xz plane appear at higher 2Θ values. The fact that these peaks are broad also implies that crystal dimensions within the planes are limited. However the behavior of (200)/(220) peak couple around 2Θ value of 50^{o} and (231)/(002) peak couple around 2Θ value of 65^{o} in GT-MAA (MAA) and GT-Ly (Ly) is peculiar. First the relatively higher intensities denote a slightly higher crystal growth tendency parallel to those planes. In addition the couples being separated more than their normal positions in highly crystalline boehmites signals an enlarging of the distances between planes represented by short 2Θ valued peak of the couple and a shorter distance between planes represented by the other peak of the couple. More interesting is that the relative intensity differences between the individual peaks in the couples are carried in both peak couples in both GT-MAA and GT-Ly. Although exact differences between the samples can only be understood with more careful structural analyses, XRD data clearly indicate that additive used in the medium of pre-grinding step along with EG definitely has an effect on the structure of the ODB that will be forming in the preceding step.

Results of SEM analyses carried out in addition to the structural analyses of ODB particles are given in Figure 4.16.

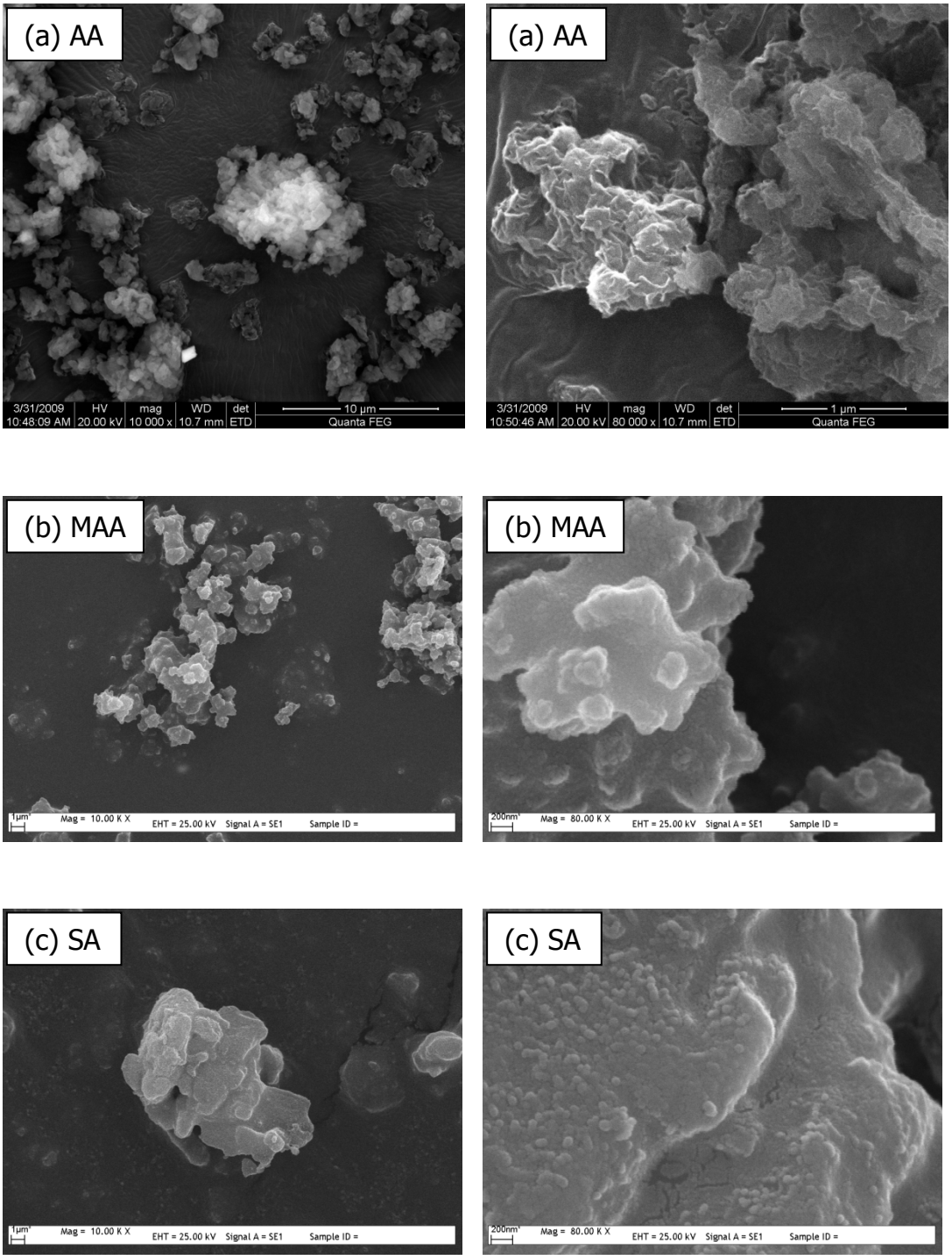

Figure 4.16 SEM micrographs of ODBs produced from pre-ground particles in mixtures formed between EG and; **(a)** AA (GT-AA), **(b)** MAA (GT-MAA), **(c)** SA (GT-SA) and **(d)** Ly (GT-Ly).

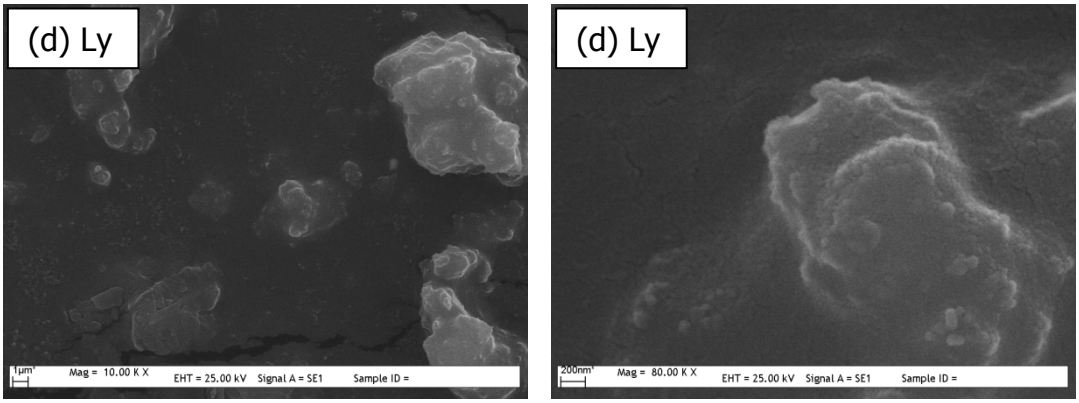

Figure 4.16 (Continued)

Effect of the different feeds on particle morphologies of the ODBs produced in this step was similar except in AA pre-ground sample. Those ODBs seem to have a cabbage-like structure, while the others are formed from sphere-like primaries. All ODBs were highly agglomerated with even some particles around 5 µm, yet they were formed of primary crystallites with sizes around 200 nm.

FT-IR analyses results given in Figure 4.17 displays the molecular level effects of glycothermal digestion process.

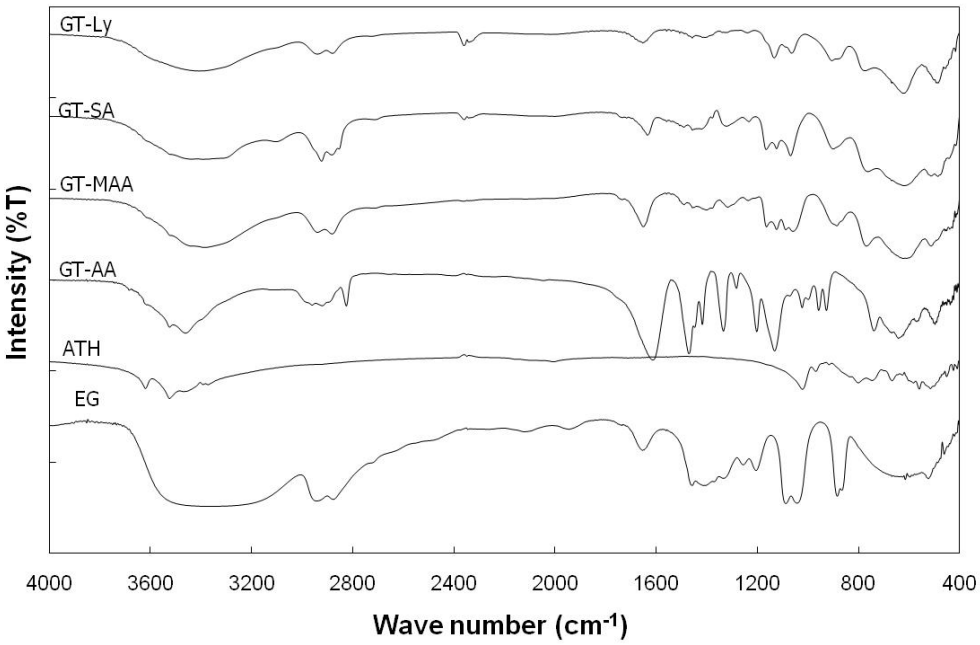

Figure 4.17 FT-IR spectra of ODBs produced from pre-ground particles in mixtures formed between EG and; AA (GT-AA), MAA (GT-MAA), SA (GT-SA) and Ly (GT-Ly).

FT-IR spectra of ODBs show the transition of ATH-type of layers into boehmitic layers upon the digestion in EG. This can be followed from the vanishing sharp lattice O-H stretches (3650 cm^{-1}), which can normally be seen in ATH structures, in the ODB spectra. Instead, a broad peak centered around 3400 cm^{-1} emerges in all ODBs. This is a positive indication of hydroxyls that are excessively hydrogen bonded. It is claimed in literature that EG is intercalated within the layers of ethylene glycol derivative of boehmites [16]. The XRD results presented above are in contrary to this claim because the (020) peak position do not shift to smaller 2Θ values in any of the ODBs produced in this study. Therefore, the crystallites are probably formed of layers that are separated with a distance similar to those in highly crystalline boehmites. On the other hand, the number of crystallites,

in which boehmitic octahedral planes are stacked coherently under these digestion conditions should be severely limited (i.e. (020) intensities are extremely low and widths are extremely large). As explained in Appendix B, boehmite is the thermodynamically stable phase under high temperatures and pressures. Any ATH would have a tendency to transform to boehmite under hydrothermal or glycothermal conditions. Since in EG loaded medium, the surfaces of the freshly transformed boehmites would be prone to blockage by the EG molecules in the digestion medium, it is likely that an octahedral boehmite layer freshly forming in solution would not be coherently stacked with another one, but just excessively hydrogen bonded with another through the free hydroxyls of the adsorbed EG molecules. The small boehmite crystallites observed in the XRD patterns are probably the cores of relatively larger ATH particles that has not been exposed to the EG reaction medium during digestion. Thus those crystallites in the cores are probably not intercalated with EG molecules and the exposed ones are probably limited to singular layers that randomly agglomerate.

The effect of supporting organic reagent in the pre-grinding medium shows itself in the molecular level interactions as well as it does in the crystal structure. Basically in each ODB there seems to be a variable amount of EG adsorption on the crystal surfaces which can be understood from the peaks that can be ascribed to EGs, namely C-H stretches between 2800 and 2900 cm^{-1} and the O-H stretches around 1650 cm^{-1} (these are not lattice hydroxyls). However quantitative analyses of adsorption level after each step is beyond the scope of this study as much as its scientific attraction.

4.4 Mechanochemistry Step

In the final step, using the same reagents used in pre-grinding step glycothermally produced ODBs were treated in the high energy ball mill. Mechanochemical treatments named as MC-AA, MC-MAA, MC-SA and MC-Ly were carried out as indicated in Table 3.9 with AA, MAA, SA and Ly, respectively. XRD patterns of the final products are given in Figure 4.18.

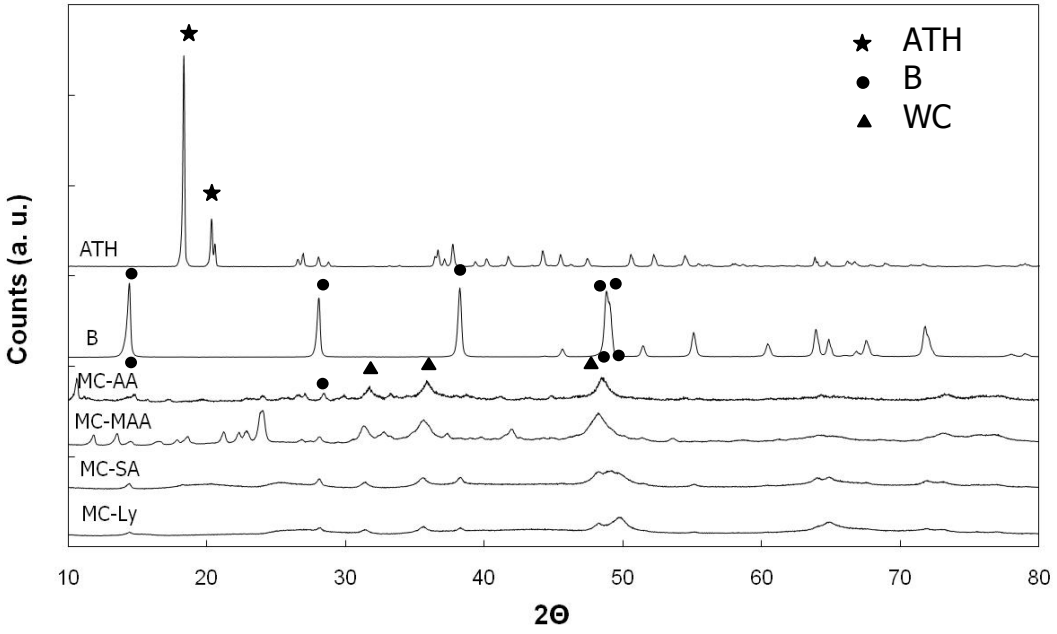

Figure 4.18 XRD patterns of the mechanochemically treated ODB particles; MC-AA: AA, MC-MAA: MAA, MC-SA: SA and MC-Ly: Ly.

In SA and Ly treated samples the crystal structure is not rendered compared to the ODC step. Therefore it could be said that SA has no effect on restacking of the layers due to the existence of long alkyl chains, and similarly the amino acid Ly leads to a different series of interactions with the

remnant EG hydroxyls that its effect on crystallinity of the final product is null. On the other hand, AA and MAA treated cases had lead to unforeseen re-stacking of the layers along the y-axis. While the restacking in AA case is interestingly regular with a large interlayer spacing, the MAA case seems to trigger formation of ATH-like layers accompanied with possibly three different boehmitic stacking configurations, least encountered among them being the ones with separations similar to highly crystalline boehmite. Although reasons of these different results are difficult to discuss further with the data in hand, possible effects of the observed structures, as seen in calcination steps, recall for different functions that could be driven from these precursors.

Some additional peaks which could not be ascribed to either boehmite or ATH can be observed when AA and MAA treated cases are analyzed in detail, namely peaks at 2Θ values of 32°, 37°, 46° and 67°. Those peaks could be due to the transition aluminas like δ-alumina, σ-alumina, γ-alumina and η-alumina that are possibly forming as a side product in the mechanochemical treatment.

In Figure 4.19, cumulative particle size distributions from particles that were mechanochemically treated in AA, MAA, SA and Ly are given.

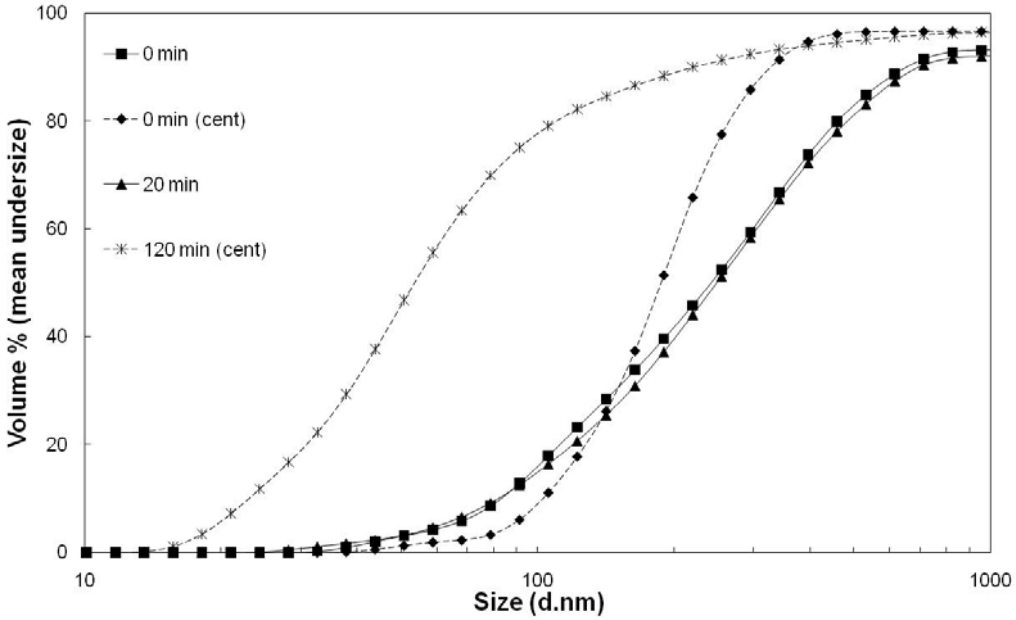

(a) MC-AA

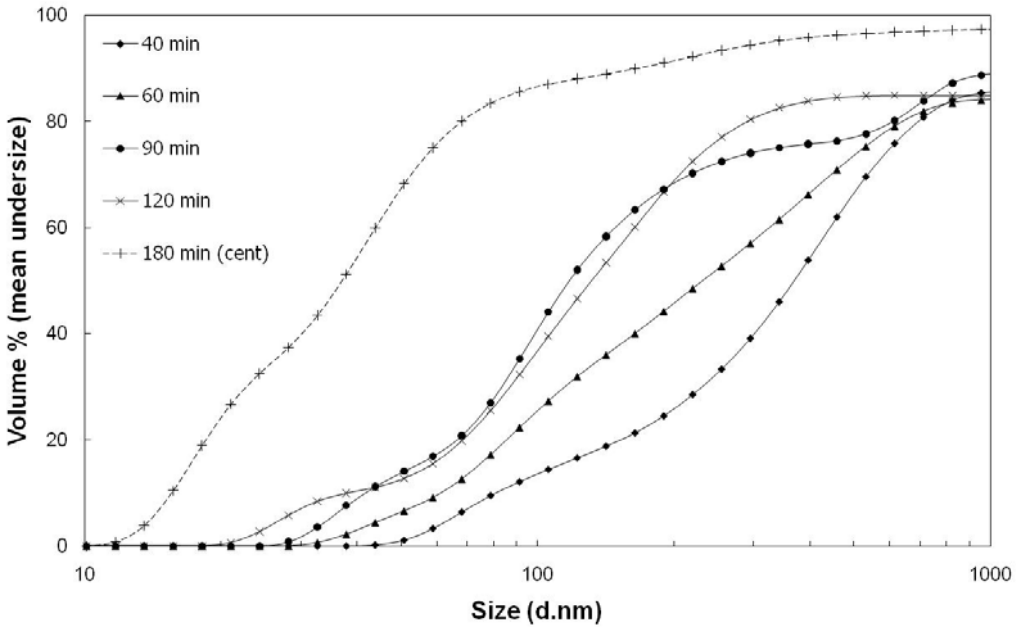

(b) MC-MAA

Figure 4.19 Cumulative particle size distribution of mechanochemically treated particles; **(a)** MC-AA: AA, **(b)** MC-MAA: MAA, **(c)** MC-SA: SA, **(d)** MC-Ly: Ly.

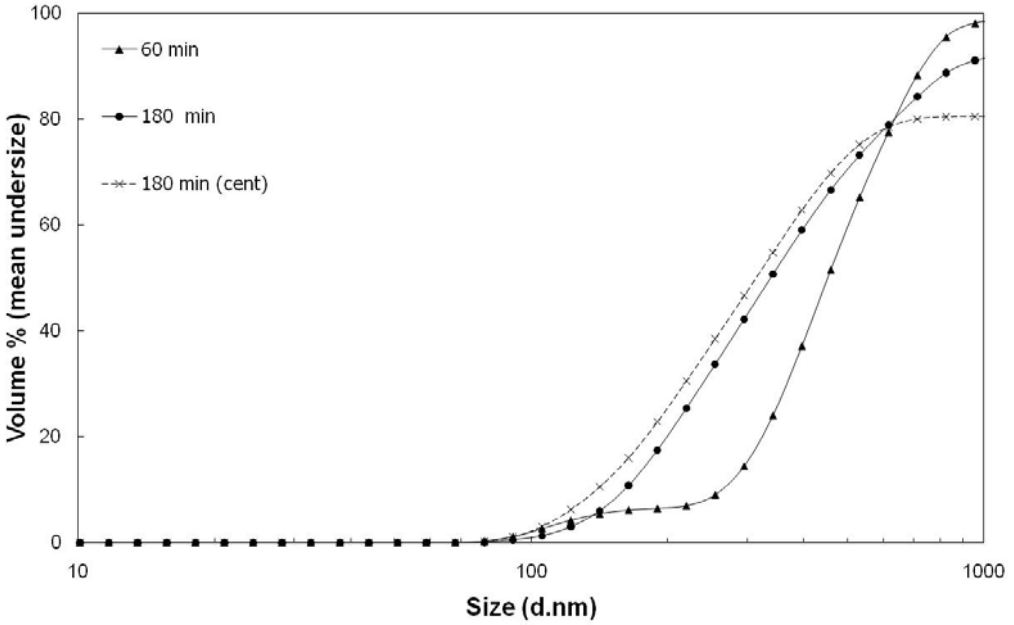

(c) MC-SA

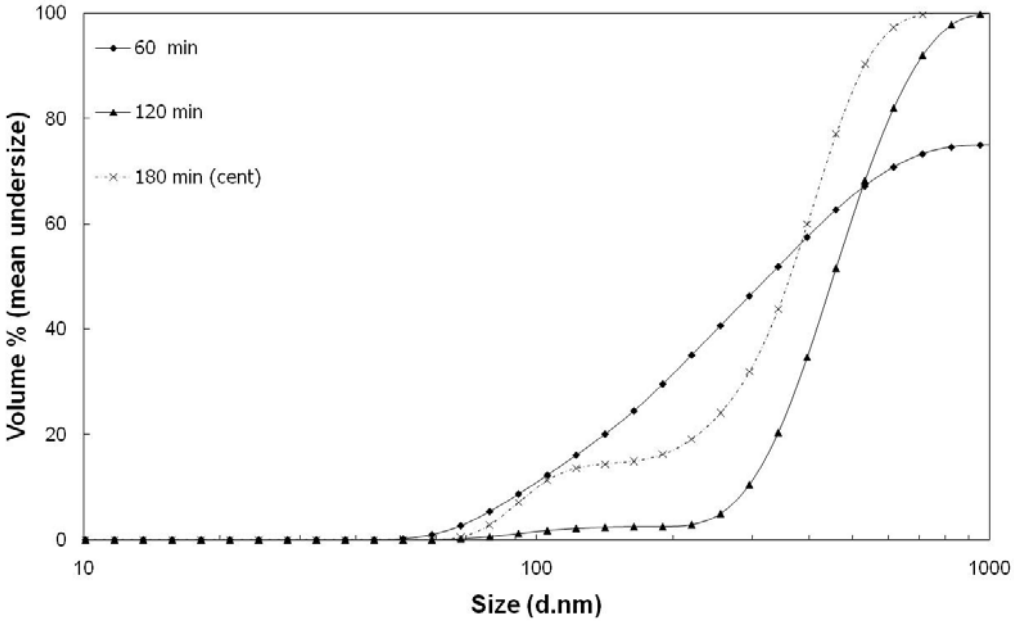

(d) MC-Ly

Figure 4.19 (Continued)

In AA grinding medium d(50) values were decreased from 190 nm to 50 nm. When MAA case was examined it is seen that d(50) values are decreased from about 200 nm to around 35 nm. It is also interesting to see that the distribution is multi-modal (i.e. three modes). Besides possible effects due to agglomerations, the fact that three different boehmitic crystallite types were observed in XRD patterns could also be used in explaining possible scaling in their agglomerative behavior. In contrast with these results in the grinding medium SA and Ly, the particle sizes are not decreased under 100 nm. Nonetheless having d(50) values already decreased to 75 nm in the pre-grinding step with Ly, calls upon the heavy agglomeration of the finely dispersed particles in this step.

To support PSA results, SEM analysis were carried out to discover extend of agglomeration occurring during the mechanochemical step. In Figure 4.20, SEM micrographs taken from the samples are given.

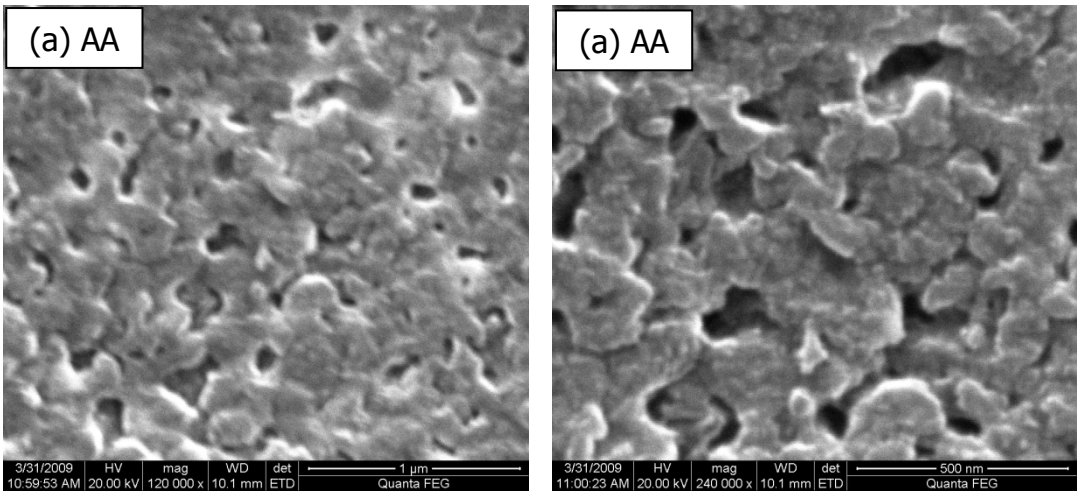

Figure 4.20 SEM micrographs of mechanochemically treated particles; **(a)** MC-AA: AA, **(b)** MC-MAA: MAA, **(c)** MC-SA: SA, **(d)** MC-Ly: Ly.

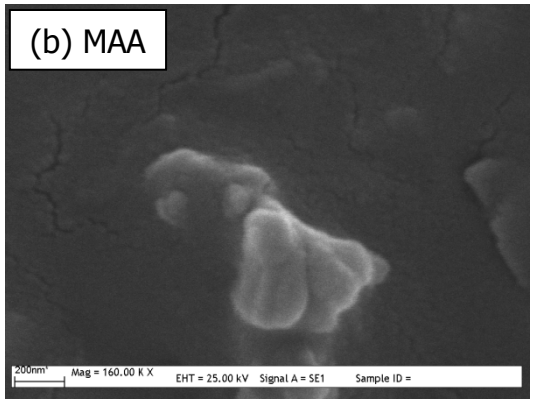

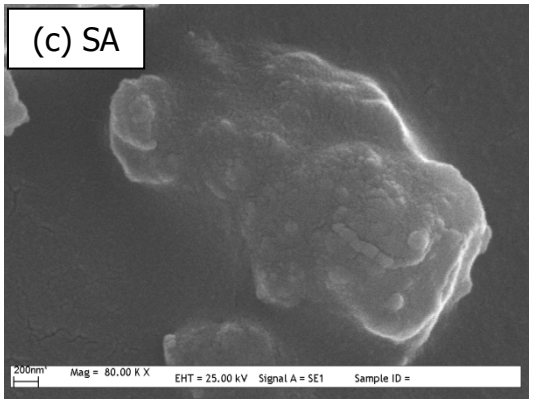

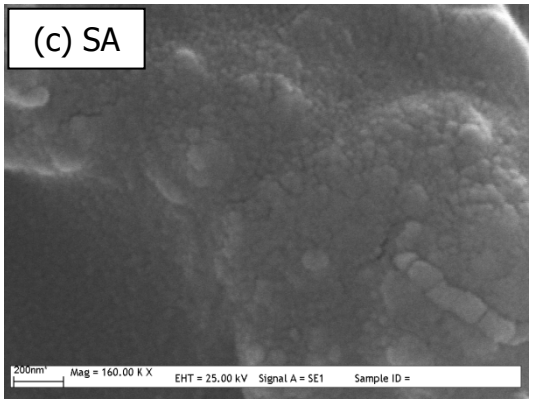

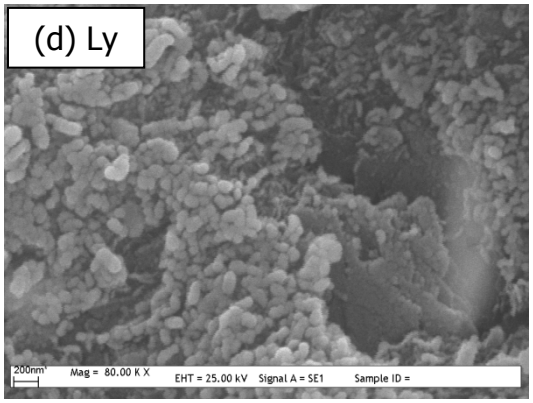

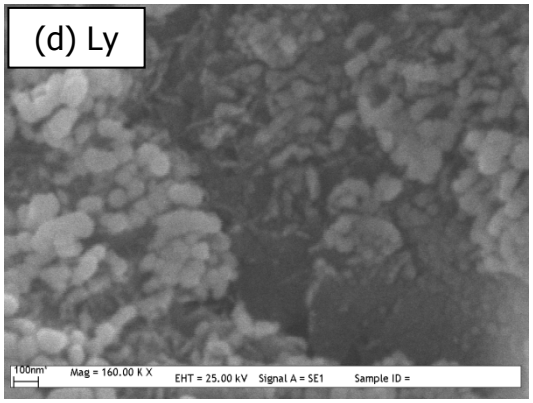

Figure 4.20 (Continued)

When SEM micrographs from AA treatment are examined, the primary alumoxane particles can be measured between 50-100 nm and even in some cases less. In MAA treated case, in a matrix resembling those of SA or Ly,

still fine particles with sizes around 100-200 nm are visible. Besides having a similar extremely fine matrix outlook, SA treated sample carried on even larger particles from inefficient pre-grinding step. These embedded particles are several hundreds of nanometers. In addition the seemingly fine matrix bears the marks of a spheroidization tendency. Although there are less remnant big particles from pre-grinding step of Ly treated sample, the spheroidization tendency in Ly treatment is remarkable and this is coherent with PSA analyses history of this sample.

To examine the molecular level effects of organic reagents used in the mechanochemical step, FT-IR spectra of the samples are taken. Results are presented in Figure 4.21. As it was explained in the preliminary FT-IR results, after the treatment in AA peaks that can be ascribed to acetate alumoxane was observed in the spectrum of MC-AA. The two peaks around 1600 cm^{-1} and 1460 cm^{-1} that can be attributed to carboxylates bonded on boehmite surfaces in bridging mode, was also observed in MAA treated sample as expected [10]. In addition to that, broad peaks around 3500 cm^{-1} and 570 cm^{-1} were formed evidencing the existence of nanosized particles. The absorption bands around 2820 cm^{-1} and 2920 cm^{-1} belong to the stretching of C-H bond. As expected in MAA and SA treated samples these were represented in larger quantities due to the larger number of associated alkyl groups. The AA treated case showed a singular large interlayer separation and a regularity in stacking. The emerging sharp peak at 3650-3700 cm^{-1} in this sample can be taken as a positive indicator of formation of a regular lattice within which free hydroxyl stretches are permitted at least for some of them.

The examination of alumina phases that can be obtained from the calcination of mechanochemically treated ODBs constitutes the next set of experiments results of which would exemplify how these novel precursors can be utilized.

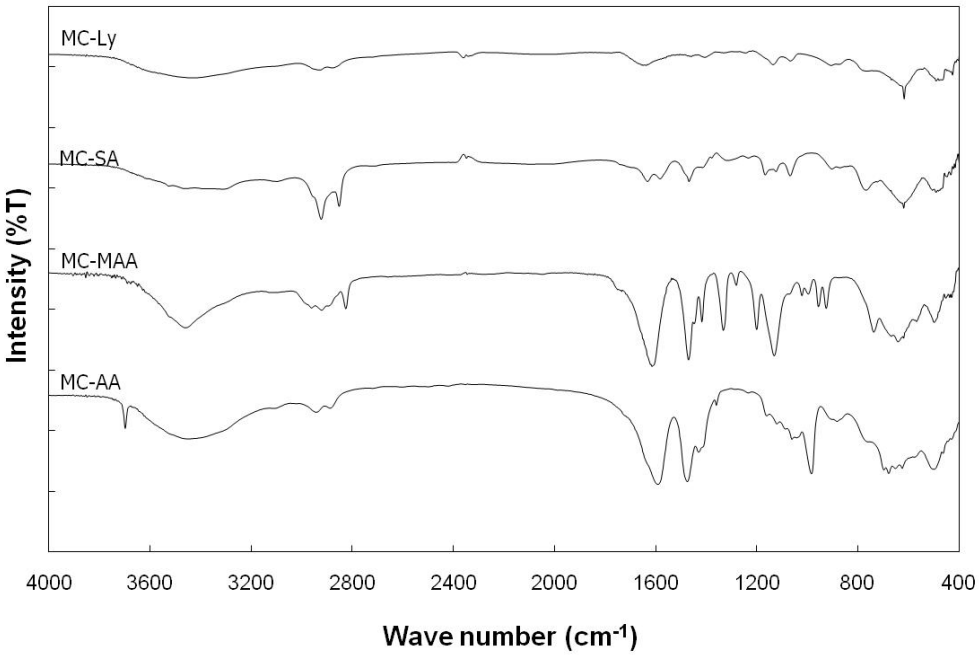

Figure 4.21 FT-IR spectra of ODB particles mechanochemically treated in AA (MC-AA), MAA (MC-MAA), SA (MC-SA) and Ly (MC-Ly).

4.5 Heat Treatment of Mechanochemically Modified ODBs

To identify possible alumina phases forming upon calcination of mechanochemically treated ODBs, ODBs were heat treated at 500°C and 1200°C for 3 hours. These calcination temperatures were chosen according to the thermal analyses plots given in Appendix D. In Appendix D, the comments on the DTA-TGA profiles of the samples are given.

XRD patterns of 500°C and 1200°C calcined products from ODBs are given with that of the similar calcination products of hydrothermally crystallized nanosized boehmite in Figures 4.22 and 4.23, respectively. Calcination at 500 °C, transformed boehmite to γ-alumina and mechanochemically treated ODBs transformed to mainly η-alumina phase, which has an amorphous

structure. These aluminas are in the group of low temperature transition aluminas and their observation confers to the expectations. The ICSD cards of various aluminas encountered in this work and their plotted presentations are given in Appendix C.

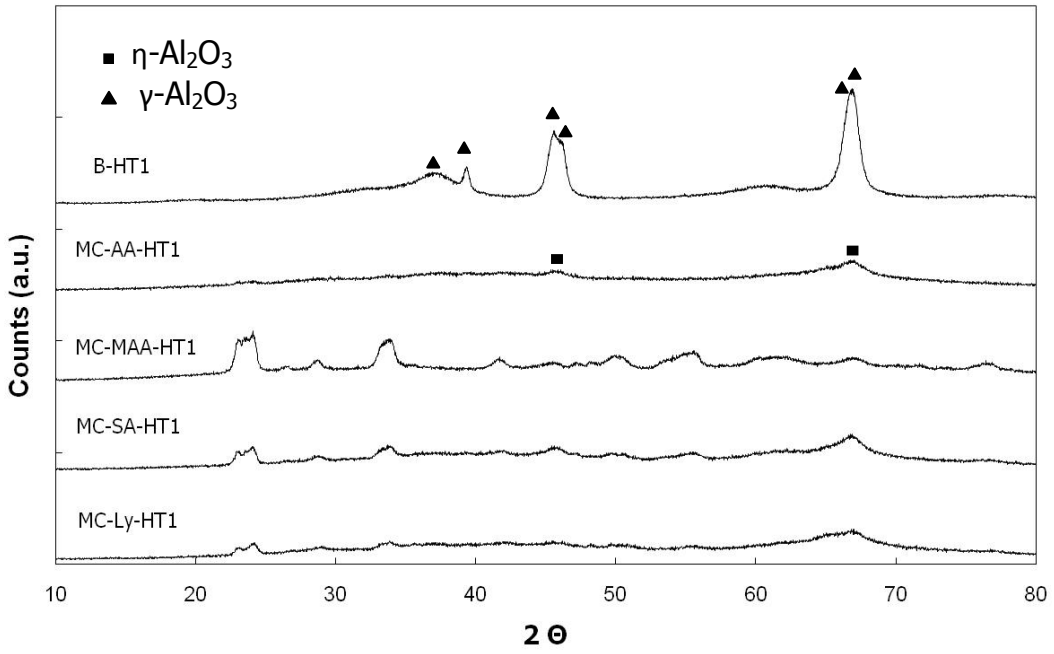

Figure 4.22 XRD patterns of mechanochemically treated ODBs and boehmite calcined at 500°C.

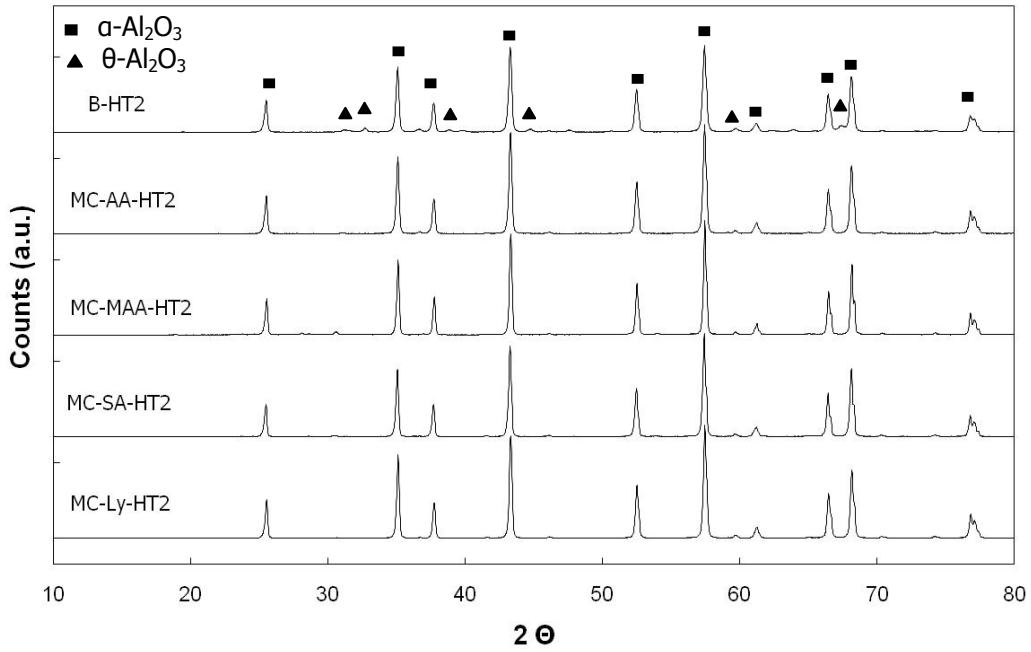

Figure 4.23 XRD patterns of mechanochemically treated ODBs and boehmite calcined at 1200°C.

Upon calcination at 1200 °C, all samples transformed into α-Al_2O_3 phase. It is known that hydrothermally produced boehmites might retain some transition alumina impurities when transformed to α-Al_2O_3 phase at high temperature, if the starting materials are gibbsite. If the gibbsite used is from a Bayer source this problem is elevated and prevents the sintering of α-Al_2O_3 phase to high density. Therefore formation of phase pure α-Al_2O_3 is a priority. With the reagent grade (Merck) ATH used in this study, existence of θ-Al_2O_3 in minor quantities was detected as marked in Figure 4.23. On the other hand, impurity level in mechanochemically treated ODBs were lower, Ly treated being the lowest. Therefore the developed glycothermal process mechanochemical treatment couple is promising in that it yields aluminas

with decreased size and higher phase purity without the need for relatively expensive bottom-up approaches.

CHAPTER 5

SUMMARY

In this study, starting from aluminum tri hydroxide (ATH) a novel alumoxane was produced by the mechanochemical treatment of glycothermally processed ATH. The production procedure was composed of three steps. As a preconditioning step of ATH for glycothermal process, wet grinding was applied in selected grinding medium. Then pre-ground ATH was fed to the pressurized reactor in ethylene glycol (EG) medium to produce the organic derivative of boehmite (ODB). As a final step, mechanochemical treatment was carried out with various organics to produce the alumoxane nano particles. The synthesized materials were characterized by using a variety of techniques including XRD, FTIR, PCS, TGA-DTA and SEM.

Firstly, preliminary studies were carried out to standardize the procedures applied to produce alumoxane. The applied pre-grinding step was optimized after the evaluation of the preliminary experiments. As the parameters concerned (rotation speed, two/one step grinding, rotation time and the selected organic reagent as a grinding medium), they were selected as 500 rpm, one step grinding with 40 minutes process time and the grinding medium was both ethylene glycol and the functional organics selected for the further mechanochemical step. The evaluation of the obtained pre-ground ATH was carried out by the particle size characterization and SEM micrographs. It was concluded that, by the pre-conditioning step, ATH was ground to nano-sized particles (≤ 500 nm). Additionally, from the XRD patterns of the pre-ground ATHs, PG-C and PG-E were the effective pre-

ground samples. Ethylene glycol (EG) and acetic acid (AA) caused considerable exfoliation on ATH's layers during the pre-grinding step.

Furthermore, the pre-conditioned ATH particles were fed into glycothermal process to obtain the poorly crystalline organic derivative of boehmite (ODB). At 250 °C, the glycothermal process was carried out for 6 hours, which was the time required for the complete transformation of ATH to ODB. The synthesized material, ODB was characterized by XRD, FTIR, SEM and PSA. The obtained GT-2, GT-3 and GT-4 ODB particles were measured around 250 nm. However, when the process was incomplete, the particle size distribution indicated a bimodal size distribution, around 100 nm and 500 nm.

As the final step, the produced ODBs were treated in carboxylic acids (e.g. acetic acid, methoxy acetic acid) mechanochemically in a high energy ball mil. After mechanochemistry step, the obtained particles (MC-1, MC-2, MC-3) were around 10-100 nm and it was concluded that the amorphous structure of ODB changed into a newly formed poorly crystalline structure from the XRD analysis.

After those preliminary studies, the pre-grinding was performed with both EG and the organic reagents (acetic acid - AA, methoxy acetic acid -MAA, stearic acid - SA and lysine – Ly). From the XRD analyses of the pre-ground ATH, it was concluded that different organic reagents used besides EG caused various exfoliation capacities on ATH. Additionally, best effective pre-grinding was succeeded by Ly which had 120 nm. However, grinding with SA caused the worst of all which had 450 nm particle sizes.

Pre-ground ATH particles were treated at 250°C in EG medium for 6 hours after the reaction conditions optimized in preliminary studies. The particle

size distribution of all ODBs indicated that an agglomeration was observed and they were composed of 200 nm particles.

It was observed from the XRD patterns of the GT-AA, GT-MAA, GT-SA and GT-Ly that in all samples digestion in the glycothermal step have been completed to a large extend. Loss of the integrity among the y-axis layers were concluded due to the loss of intensity in (020) plane.

After the final mechanochemical treatment of ODB with the organics (AA, MAA, SA and Ly), the obtained alumoxanes were charecterized with XRD, PSC, SEM and FTIR analyses. In SA and Ly treated samples the crystal structure did not change with the structure of ODB. However, in MAA and AA cases, the stacking crystalline structure on the layers along y axis was observed. The particle size of the AA and MAA treated ones were around 10-100 nm. However, the particle sizes of the alumoxanes treated with SA and Ly were not decreased under 100 nm. In addition to that, by the SEM micrographs of the final product, the heavy agglomeration of the alumoxane treated with SA and Ly was observed. With the FT-IR analyses, the carboxylate bridging on boehmite surfaces were observed.

Finally, the heat treatment was applied on the boehmite and the four different alumoxane samples. By this step, the transition aluminas they transformed were observed. While in 500 °C , η and γ alumina was observed, in 1200 °C, they all transformed to α-alumina with little phase impurity of θ-alumina was observed. The best transformation was achieved by the lysine treated alumoxane.

To sum up, with different carboxylic acids (AA, MAA, SA and Ly), glycothermally processed pre-conditioned ATH were treated. Being the general production method was the reflux method, in this study a new

technique was adapted into the production of alumoxane which was mechanochemical treatment.

CHAPTER 6

CONCLUSIONS

In this study, by the mechanochemical treatment of the glycothermally processed ATH with various organics (acetic acid - AA, methoxy acetic acid - MAA, stearic acid - SA and lysine – Ly), nano sized alumina precursor particles were produced. The produced precursor particles can be named as "alumoxane", since they have a boehmite core encapsulated with surface adsorbed and intercalated organics used in the treatment steps. The particle sizes observed were around 50 nm in MC-AA and MC-MAA cases. In contrast, in MC-SA and MC-Ly cases, the particles were heavily agglomerated and their sizes were several hundreds of nanometers. Nevertheless the agglomerates were composed of 100-200 nm primary particles.

Throughout the study, a pre-grinding step was applied as a starting process to precondition ATH particles to the further glycothermal process. After the evaluation of the preliminary grinding studies, it was found that to decrease the ATH particles required for the glycothermal process, 40 minutes of one step pre-grinding was adequate. In PG-AA, PG-MAA and PG-SA cases, the d(50) value of the particles were between 300 and 400 nm, yet in PG-Ly case, particle sizes were decreased to 75 nm.

After the preconditioning step applied on ATH, with the 6 hours of glycothermal treatment in EG medium, ATH was completely transformed to organic derivatives of boehmite (ODB). ODB particles were around 200 nm.

After 120 to 180 minutes of mechanochemical treatment of ODBs in high energy ball mill, the so-called nano-sized alumoxanes were produced. In the mechanochemical treatment cases with AA and MAA, a rearrangement of the boehmitic layers was observed along the y-axis. The poorly crystallized exfoliated and/or intercalated structure that is observed in ODBs transformed into a more ordered structure after these two mechanochemical treatment cases.

In order to identify the alumina phases that would form at high temperature the alumoxanes were heat treated and their transformational behavior were compared with that of hydrothermally produced boehmites. With the calcination at 500°C, boehmite was transformed to γ-alumina and mechanochemically treated ODBs transformed to η-alumina. In addition to that after the calcination at 1200°C, all samples were transformed to α-alumina phase. However, MC-Ly showed the highest purity when compared to the others and all other calcined alumoxanes also showed higher purity compared to calcined boehmite. Thus, taking into account the relative ease of the process as a top to bottom approach, the alumoxanes produced with the mechanochemical treatment of the glycothermally processed ATH can be considered as promising alumina precursors compared with the precursors prepared with bottom-up approaches.

CHAPTER 7

RECOMMENDATIONS

1. Throughout the grinding processes, the contamination due to the WC balls could be eliminated with using ZrO2 balls and grinding jar. In addition, the organic liquid amount in the jar should be decreased not to affect the grinding media negatively. Another ratio that can be adjusted is ball/powder weight ratio. It can be decreased from 20 to 10.
2. The produced cubic boehmites (Appendix 2) could be coated with the produced alumoxanes to obtain a precise control over size and morphology of the final aluminas in the micron size range. A control at this size range is especially needed for better sinterability of the alumina.
3. The produced novel nano-sized alumoxanes can be fed to the hydrothermal reactor as a boehmite precursor to obtain morphology controlled boehmites in the same way an aluminum alkoxide or salt is used to produce fine alumina.
4. The Lysine pretreatment was peculiar compared to any other organic used in this step. The pretreatment duration of ATH in Lysine could be extended to complete the production of alumoxane in one-step.

REFERENCES

1. K. A. Defriend, A. R. Barron, "Strengthening of porous alumina bodies using carboxylate-alumoxane nanoparticles," Journal of Materials Science 38, 927 (2003).

2. Y. Wu, Y. Zhang, X. Huang, J. Guo, "Microstructural development and mechanical properties of self-reinforced alumina with CAS addition," Journal of the European Ceramic Society 21, 581 (2001).

3. H. C. Lee, H. J. Kim, C. H. Rhee, K. H. Lee, J. S. Lee, S. H. Chung, "Synthesis of nanostructured [gamma]-alumina with a cationic surfactant and controlled amounts of water," Microporous and Mesoporous Materials 79, 61 (2005).

4. Y. K. Park, E. H. Tadd, M. Zubris, R. Tannenbaum, "Size-controlled synthesis of alumina nanoparticles from aluminum alkoxides," Materials Research Bulletin 40, 1506 (2005).

5. N. Lepot, M. K. Van Bael, H. Van den Rul, J. D'Haen, R. Peeters, D. Franco, J. Mullens, "Synthesis of platelet-shaped boehmite and [gamma]-alumina nanoparticles via an aqueous route," Ceramics International 34, 1971 (2008).

6. Y. Wu, Y. Zhang, X. Huang, J. Guo, "Preparation of platelike nano alpha alumina particles," Ceramics International 27, 265 (2001).

7. Y. Sarikaya, T. Alemdaroglu, M. s. Önal, "Determination of the shape, size and porosity of fine [alpha]-Al2O3 powders prepared by emulsion evaporation," Journal of the European Ceramic Society 22, 305 (2002).

8. M. Thiruchitrambalam, V. R. Palkar, V. Gopinathan, "Hydrolysis of aluminium metal and sol-gel processing of nano alumina," Materials Letters 58, 3063 (2004).

9. M. Mazloumi, H. Arami, R. Khalifehzadeh, S. K. Sadrnezhaad, "Studies on synthesis of alumina nanopowder from synthetic Bayer liquor," Materials Research Bulletin 42, 1004 (2007).

10. R. L. Callender, C. J. Harlan, N. M. Shapiro, C. D. Jones, D. L. Callahan, M. R. Wiesner, D. B. MacQueen, R. Cook, A. R. Barron, "Aqueous Synthesis of Water-Soluble Alumoxanes: Environmentally Benign Precursors to Alumina and Aluminum-Based Ceramics," Chemistry of Materials 9, 2418 (1997).

11. M. Inoue, "Glycothermal synthesis of metal oxides," Journal of Physics: Condensed Matter 16, S1291 (2004).

12. O. Mekasuwandumrong, V. Pavarajarn, M. Inoue, P. Praserthdam, "Preparation and phase transformation behavior of [chi]-alumina via solvothermal synthesis," Materials Chemistry and Physics 100, 445 (2006).

13. C. T. Vogelson, Y. Koide, L. B. Alemany, A. R. Barron, "Inorganic−Organic Hybrid and Composite Resin Materials Using Carboxylate-Alumoxanes as Functionalized Cross-Linking Agents," Chemistry of Materials 12, 795 (2000).

14. N. Shahid, A. R. Barron, "Solvent free synthesis of carboxylate-alumoxane nanoparticles using mechanical shear," Journal of Materials Chemistry 14, 1235 (2004).

15. M. Inoue, M. Kimura, T. Inui, "Alkoxyalumoxanes," Chemistry of Materials 12, 55 (1999).

16. M. Inoue, Y. Kondo, T. Inui, "An ethylene glycol derivative of boehmite," Inorganic Chemistry 27, 215 (1988).

17. M. Inoue, K. Kitamura, H. Tanino, H. Nakayama, T. Inui, "Alcothermal Treatments of Gibbsite: Mechanisims for the Formation of Boehmite," Clays and Clay Minerals 37, 71 (1989).

18. M. Inoue, H. Kominami, T. Inui, "Reaction of aluminium alkoxides with various glycols and the layer structure of their products," Journal of the Chemical Society, Dalton Transactions 12, 3331 (1991).

19. M. Inoue, H. Tanino, Y. Konda, T. Inui, "Formation of Organic Derivatives of Boehmite by the Reaction of Gibbsite with Glycols and Aminoalcohols," Clays and Clay Minerals 39, 151 (1991).

20. F. R. Feret, D. Roy, C. Boulanger, "Determination of alpha and beta alumina in ceramic alumina by X-ray diffraction," Spectrochimica Acta Part B: Atomic Spectroscopy 55, 1051 (2000).

21. F. S. Galasso, Structure and Properties of Inorganic Solids. International series of monographs in solid state physics (Pergamon Press, Oxford, New York, ed. 1, 1970), vol. 7, pp. 297.

22. P. S. Santos, H. S. Santos, S. P. Toledo, "Standard transition aluminas. Electron microscopy studies," Materials Research 3, 104 (2000).

23. S. V. Tsybulya, G. N. Kryukova, "Nanocrystalline transition aluminas: Nanostructure and features of x-ray powder diffraction patterns of low-temperature Al_2O_3 polymorphs," Physical Review B 77, 024112 (2008).

24. S. Değerli, "Bayer Prosesinin Ara Atık Ürünü Olan Alüminyum Hidroksit Kabuğundan Aktif Alümina Eldesi," Yıldız Technical University (2002).

25. A. R. Hind, S. K. Bhargava, S. C. Grocott, "The surface chemistry of Bayer process solids: a review," Colloids and Surfaces A: Physicochemical and Engineering Aspects 146, 359 (1999).

26. V. Isupov, L. Chupakhina, G. Kryukova, S. Tsybulya, "Fine [alpha]-alumina with low alkali: new approach for preparation," Solid State Ionics 141-142, 471 (2001).

27. Y. Y. Park, S. O. Lee, T. Tran, S. J. Kim, M. J. Kim, "A study on the preparation of fine and low soda alumina," International Journal of Mineral Processing 80, 126 (2006).

28. Y. Yoshizawa, K. Hirao, S. Kanzaki, "Fabrication of low cost fine-grained alumina powders by seeding for high performance sintered bodies," Journal of the European Ceramic Society 24, 325 (2004).

29. A. L. Penard, F. Rossignol, H. S. Nagaraja, C. Pagnoux, T. Chartier, "Dispersion of alpha-alumina ultrafine powders using 2-phosphonobutane-1,2,4-tricarboxylic acid for the implementation of a DCC process," Journal of the European Ceramic Society 25, 1109 (2005).

30. L. Jiang, L. Gao, Y. Liu, "Adsorption of salicylic acid, 5-sulfosalicylic acid and Tiron at the alumina-water interface," Colloids and Surfaces A: Physicochemical and Engineering Aspects 211, 165 (2002).

31. B. J. Briscoe, A. U. Khan, P. F. Luckham, "Optimising the dispersion on an alumina suspension using commercial polyvalent electrolyte dispersants," Journal of the European Ceramic Society 18, 2141 (1998).

32. K. A. Andrianov, A. A. Zhdanov, "Synthesis of new polymers with inorganic chains of molecules," Journal of Polymer Science 30, 513 (1958).

33. S. Pasynkiewicz, "Alumoxanes: Synthesis, structures, complexes and reactions," Polyhedron 9, 429 (1990).

34. J. L. Atwood, D. C. Hrncir, R. D. Priester, R. D. Rogers, "Decomposition of high-oxygen content organoaluminum compounds. The formation and structure of the $[Al_7O_6Me_{16}]^-$ anion," Organometallics 2, 985 (1983).

35. E. Zurek, T. Ziegler, "Theoretical studies of the structure and function of MAO (methylaluminoxane)," Progress in Polymer Science 29, 107 (2004).

36. C. J. Harlan, M. R. Mason, A. R. Barron, "Tert-Butylaluminum Hydroxides and Oxides: Structural Relationship between Alkylalumoxanes and Alumina Gels," Organometallics 13, 2957 (1994).

37. M. R. Mason, J. M. Smith, S. G. Bott, A. R. Barron, "Hydrolysis of tri-tert-butylaluminum: the first structural characterization of alkylalumoxanes $[(R_2Al)_2O]_n$ and $(RAlO)_n$," Journal of the American Chemical Society 115, 4971 (1993).

38. R. C. Mehrotra, R. Bohra, Metal Carboxylates. (Acedemic Press Inc., London, New York, 1983), pp. 396.

39. K. A. Defriend, A. R. Barron, "A flexible route to high strength alpha-alumina and aluminate spheres," Journal of Materials Science 38, 2673 (2003).

40. R. Loscutova, A. Barron, "Application of alumoxane nanoparticles as precursors for 3D alumina features," Journal of Materials Science 41, 3391 (2006).

41. K. A. Defriend, A. R. Barron, "Surface repair of porous and damaged alumina bodies using carboxylate-alumoxane nanoparticles," Journal of Materials Science 37, 2909 (2002).

42. N. Shahid, R. G. Villate, A. R. Barron, "Chemically functionalized alumina nanoparticle effect on carbon fiber/epoxy composites," Composites Science and Technology 65, 2250 (2005).

43. H.-J. Gläsel, E. Hartmann, L. Wennrich, T. Höche, M. R. Buchmeiser, "Novel Nanosized Aluminium Carboxylates: Synthesis, Characterization and Use as Nanofillers for Protective Polymeric Coatings," Macromolecular Materials and Engineering 292, 70 (2007).

44. A. M. Boczkowska, M. Ciecierska, E. Sienkiewicz, B. Pietrzykowski, A., "Urea-urethane nanocomposites obtained from modified methylalumoxane oligomers," MATERIALS SCIENCE -WROCLAW- 26; PART 2, 301 (2008).

45. C. Cook; Ronald Lee (Lakewood, Barron; Andrew Ross (Houston, TX), Gleason; Kevin Joseph (Lafayette, CO), MacQueen; David Brent (Golden, CO), Siparsky; Georgette Laila (Denver, CO), Koide; Yoshihiro (Saitama, JP), Vogelson; Cullen Taylor (Houston, TX) (United States 2002).

46. C. Cook; Ronald Lee (Lakewood, Elliott; Brian John (Superior, CO), Luebben; Silvia DeVito (Golden, CO), Myers; Andrew William (Arvada, CO), Smith; Bryan Matthew (Boulder, CO) (TDA Research, Inc. (Wheat Ridge, CO) United States, 2006).

47. A. S. Mistry, S. H. Cheng, T. Yeh, E. Christenson, J. A. Jansen, A. G. Mikos, "Fabrication and in vitro degradation of porous fumarate-based polymer/alumoxane nanocomposite scaffolds for bone tissue engineering," Journal of Biomedical Materials Research Part A 89A, 68 (2009).

48. R. A. Horch, N. Shahid, A. S. Mistry, M. D. Timmer, A. G. Mikos, A. R. Barron, "Nanoreinforcement of Poly(propylene fumarate)-Based Networks with Surface Modified Alumoxane Nanoparticles for Bone Tissue Engineering," Biomacromolecules 5, 1990 (2004).

49. S. J. Obrey, A. R. Barron, "A Chemically Functionalized Carboxylate−Alumoxane Nanoparticle Support for Olefin Polymerization Catalysts," Macromolecules 35, 1499 (2002).

50. C. D. Jones, M. Fidalgo, M. R. Wiesner, A. R. Barron, "Alumina ultrafiltration membranes derived from carboxylate-alumoxane nanoparticles," Journal of Membrane Science 193, 175 (2001).

51. J. Zhang, S. Liu, J. Lin, H. Song, J. Luo, E. M. Elssfah, E. Ammar, Y. Huang, X. Ding, J. Gao, S. Qi, C. Tang, "Self-Assembly of Flowerlike AlOOH (Boehmite) 3D Nanoarchitectures," The Journal of Physical Chemistry B 110, 14249 (2006).

52. C. Kaya, J. Y. He, X. Gu, E. G. Butler, "Nanostructured ceramic powders by hydrothermal synthesis and their applications," Microporous and Mesoporous Materials 54, 37 (2002).

53. P. K. Sharma, M. H. Jilavi, D. Burgard, R. Nass, H. Schmidt, "Hydrothermal Synthesis of Nanosize alpha-Al_2O_3 from Seeded Aluminum Hydroxide," Journal of the American Ceramic Society 81, 2732 (1998).

54. D. Mishra, S. Anand, R. K. Panda, R. P. Das, "Hydrothermal preparation and characterization of boehmites," Materials Letters 42, 38 (2000).

55. P. A. Buining, C. Pathmamanoharan, J. B. H. Jansen, H. N. W. Lekkerkerker, "Preparation of Colloidal Boehmite Needles by Hydrothermal Treatment of Aluminum Alkoxide Precursors," Journal of the American Ceramic Society 74, 1303 (1991).

56. M. Inoue, Y. Kondo, T. Inui, "The Reaction of Crystalline Aluminum Hydroxide in Ethylene Glycol," Chemistry Letters 15, 1421 (1986).

57. R. Tettenhorst, D. A. Hofmann, "Crystal chemistry of boehmite," Clays and Clay Minerals 28, 373 (October 1, 1980, 1980).

58. X. Du, Y. Wang, X. Su, J. Li, "Influences of pH value on the microstructure and phase transformation of aluminum hydroxide," Powder Technology 192, 40 (2009).

59. A. B. Kiss, G. Keresztury, L. Farkas, "Raman and i.r. spectra and structure of boehmite ([gamma]-AlOOH). Evidence for the recently discarded D172h space group," Spectrochimica Acta Part A: Molecular Spectroscopy 36, 653 (1980).

60. J. J. Fripiat, H. J. Bosmans, P. G. Rouxhet, "Proton mobility in solids. I. Hydrogenic vibration modes and proton delocalization in boehmite," The Journal of Physical Chemistry 71, 1097 (1967).

61. M. C. Stegmann, D. Vivien, C. Mazieres, "Studies on the infrared vibration mode of aluminum oxyhydrates boehmite and diaspore," Acta Part A 29A, 1653 (1973).

APPENDIX A

PARTICLE SIZE ANALYSES

A.1 Sample Preparation

In the preliminary studies particle size measurements were carried out using two types of solutions from the same sample. First solution was prepared by dispersing the filtered and dried powders in a fresh aqueous solution, pH of which was adjusted to an appropriate value using acids or bases. In such solutions dispersion was achieved by an ultrasonic horn dipped in the solution. The second type of solution used in the measurements was the centrifugate of the process solution that was separated from the powders in the final centrifugation step. These solutions were found to contain the primary particles that form after different processing steps. The advantage was that such particles were generally in a well-dispersed condition and eliminated the need for further pH and concentration adjustments. These solutions represent only the products that were ground for the longest duration.

After having problems with the dispersion quality during the preliminary experiments a standard method was applied in all measurements using both types of solutions in the measurement. Any intermediate sample taken from the grinding jar after a certain grinding duration was directly dispersed in an aqueous solution without drying and stored as such until measurement. On the other hand, the final sample that represents the longest duration was measured twice; once after direct dispersion in aqueous medium like any

other sample and a second time from the centrifugate that is collected after washing and centrifuging the final product. In the presentation of data while a straight line will mean a measurement taken from the particles dispersed in an aqueous medium, a 'dashed line' will represent a measurement taken from the centrifugate prepared as described above.

A.2 Preliminary Experiments

In Figure A.1, particle size analyses results from preliminary studies are given. Presented data are from ATH particles that are pre-ground with the PG-A, PG-B and PG-C conditions. A detailed discussion of the results from these conditions is given in Chapter 4. In each plot, the data given for 10 minutes represent the size distribution after the first step of the two-step grinding and all other time values represent the cumulative grinding times that includes the initial 10 minutes.

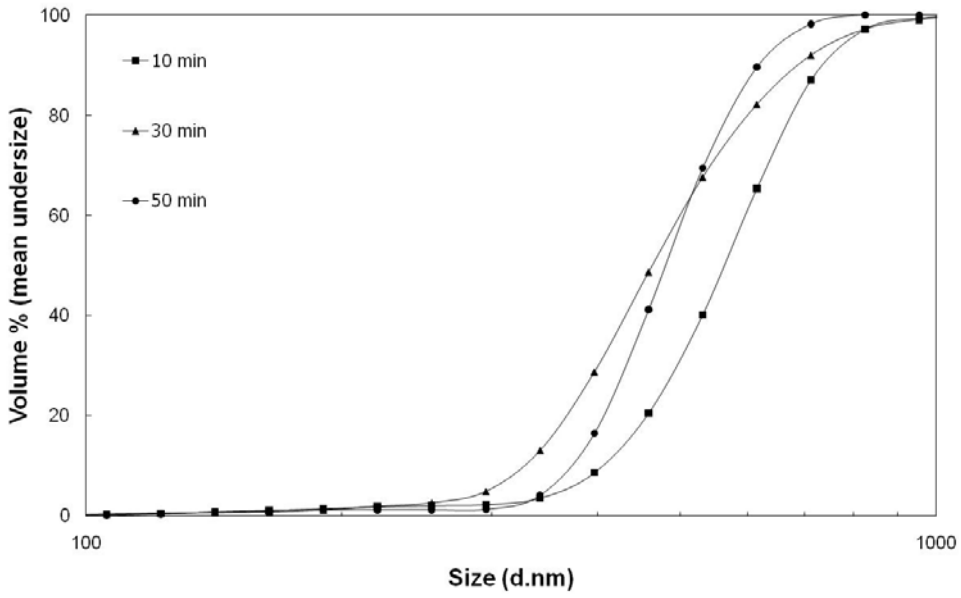

(a) PG-A

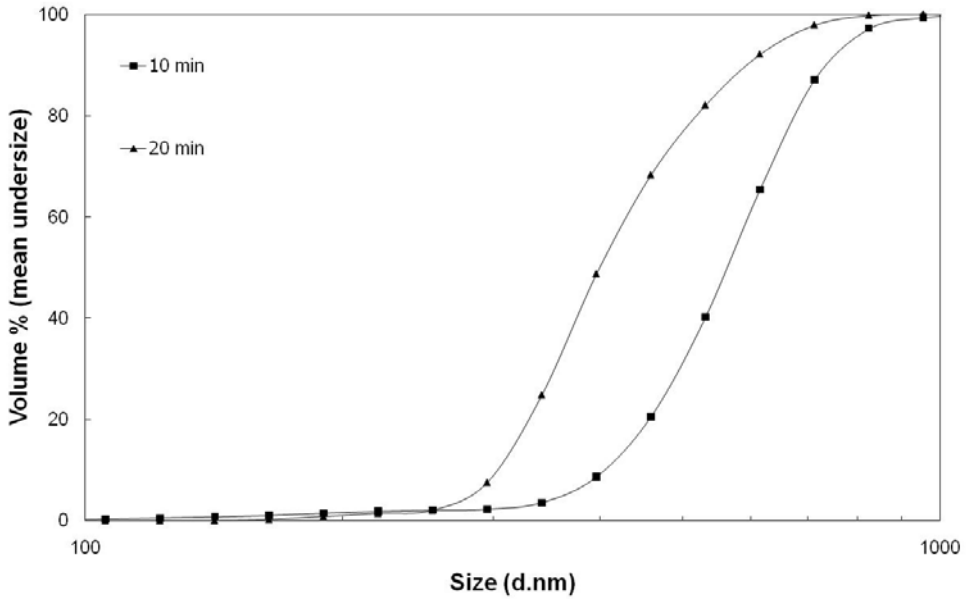

(b) PG-B

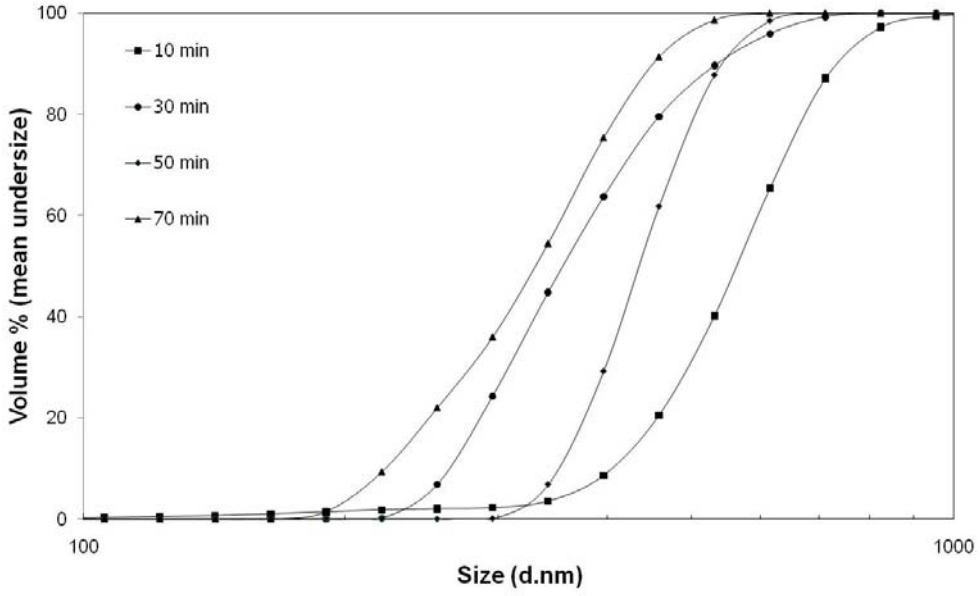

(c) PG-C

Figure A.1 Cumulative particle size distribution of ATH particles subjected to pre-grinding in the preliminary studies; **(a)** PG-A: IPOH-400 rpm, **(b)** PG-B: IPOH-500 rpm, **(c)** PG-C: EG-500 rpm.

In Figure A.2, the cumulative particle size distributions given in Figure 4.1 are plotted again along with the results obtained from the centrifugates. Results obtained from centrifugate parts gave smaller particle sizes when compared with the data obtained from dried powders. Final d(50) observed under the conditions of PG-E was 120 nm. On the other hand, it was 350 nm under the conditions of PG-F. These values are smaller than those measured from samples dispersed directly in aqueous medium. Another interesting point to note is that in some samples, with increasing time the measured sizes from the dispersed samples can get larger. For example under the grinding conditions of PG-F, after 60 minutes of grinding a d(50) value of 450 nm can be obtained. However, upon increasing the time up to 100 minutes d(50) becomes 600 nm. This is a good indication of the agglomeration among particles as the sizes get smaller with further grinding. As the sizes get smaller, the increased chemical potential would naturally lead to agglomeration. Only if the grinding medium includes a combination of organic species that effectively adsorb on the particles, this tendency can be decreased and grinding efficiency could be increased. As a conclusion, it could be said that the measurements taken from the centrifugates are more reliable in demonstrating the primary sizes that could be achieved under the grinding conditions tested. On the other hand, the measurements taken from the particle-dispersed solutions would be more representative of the state of agglomeration in the sample.

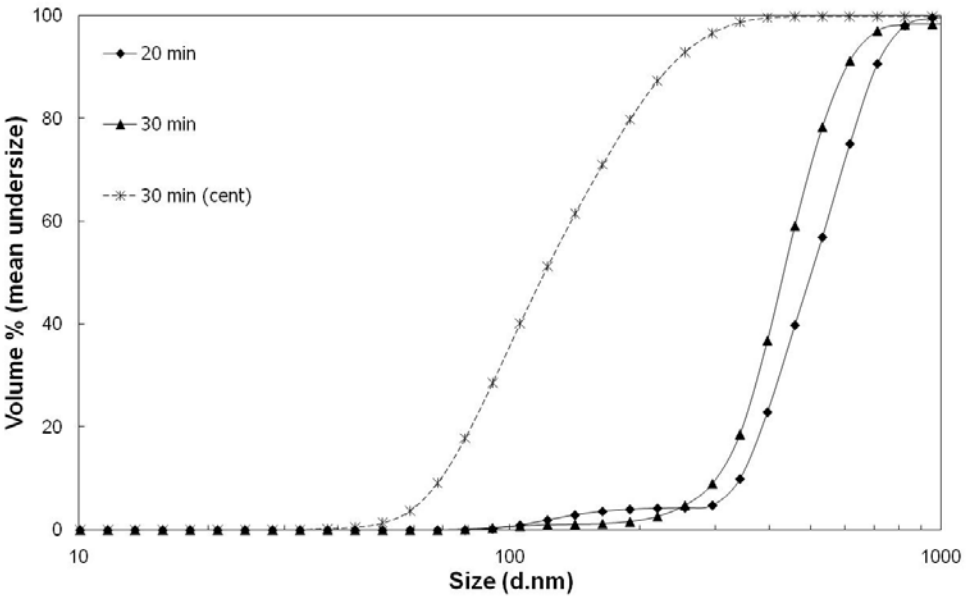

(a) PG-E

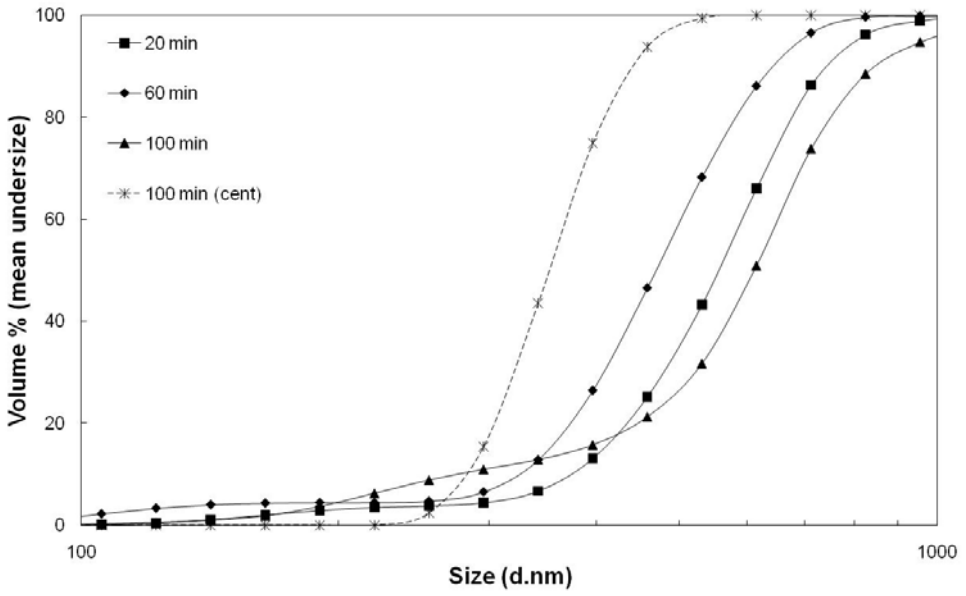

(b) PG-F

Figure A.2 Cumulative particle size distribution of ATH particles subjected to a one-step pre-grinding in the preliminary studies; **(a)** PG-E: AA and EG mixture, **(b)** PG-F: AA alone. Data in Figure 4.1 is plotted again with the results from measurements from centrifugate (given dashed lines in each plot).

In Figure A.3, cumulative particle size distribution of GT-2 obtained from its centrifugate (dashed line) is presented along with the results from direct dispersion method which was already given in Figure 4.5. Compared to the d(50) value observed in regular dispersion method, there was a decrease in the sizes measured from the centrifugate (250 nm versus 190 nm). More important is that the width of distribution is much narrower in the measurement from centrifugate. This confers to the fact that the particles are in an agglomerated state. It is highly possible that the dangling hydroxyls of surface adsorbed EG species promotes agglomeration among primary particles through the hydrogen bonding between these hydroxyl groups.

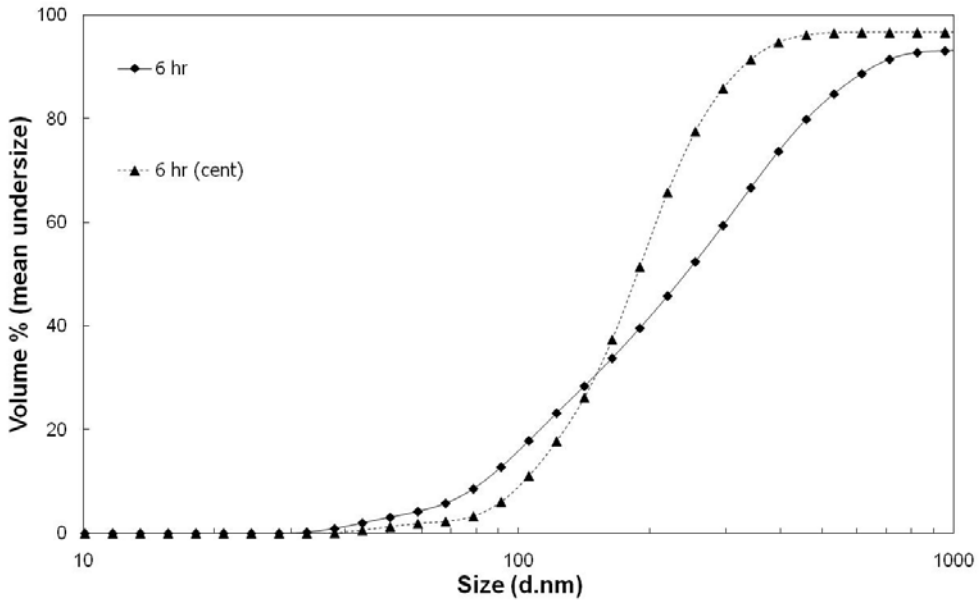

Figure A.3 Cumulative particle size distribution of ODB produced by the 6 hour glycothermal process. Data in Figure 4.5 is plotted again with the results from measurements from centrifugate (given dashed lines in the plot).

APPENDIX B

HYDROTHERMAL SYNTHESIS OF BOEHMITE

The hydrothermal synthesis of boehmite (B) starting from aluminum hydroxide (ATH) was performed within the pressurized reactor shown in Figure 3.5. Apart from the applied process parameters (temperature and time), hydrothermal process was carried out similar to the procedure applied in the glycothermal process which is summarized in Figure 3.7. The results of hydrothermal process given in this study carried out at 180°C for 5 hours. During the preparation of the precursor for the hydrothermal process, pH was adjusted (by adding NH_3 solution) in an effort to affect the morphology of the recrystallizing boehmites. Cube shaped boehmite production was achieved with a pH value around 10-11. Obtained XRD pattern of the cubic boehmite is presented in Figure B.1. Boehmite pattern is given with ATH and it can be seen that ATH-boehmite transformation is complete. To assist the reader indices of planes of crystalline ATH and B are added to the Figure B.1.

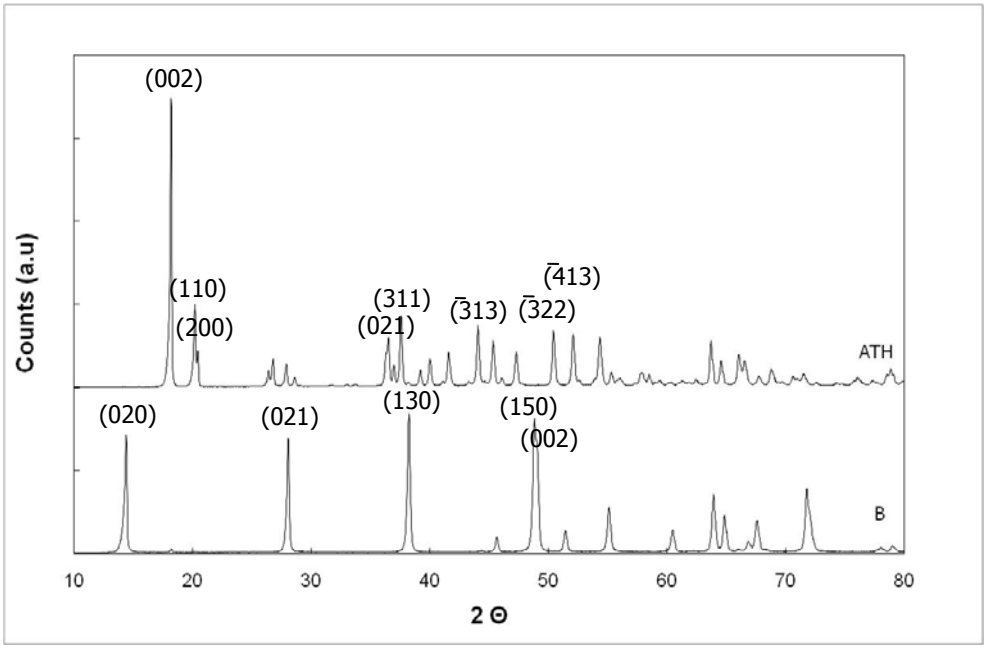

Figure B.1 XRD patterns of well-crystallizes ATH and boehmite.

.

APPENDIX C

X-RAY DIFFRACTION ANALYSES

Table C.1 ICSD cards of boehmite, ATH and transition aluminas.

AlOOH, synt		
2θ	**Intensity**	**hkl**
14.46	100	020
28.21	79.4	021
38.42	65.6	130
48.94	18.8	150
49.34	25.3	002
55.27	35.4	151
64.21	18.3	132

$Al(OH)_3$, Gibbsite		
2θ	**Intensity**	**hkl**
18.27	100	002
20.26	34.7	110
20.5	17.3	200
37.61	16.3	$\bar{3}11$
44.09	12.2	$\bar{3}13$
36.55	11.1	021
50.45	10.6	$\bar{3}14$
37.75	9.7	$\bar{2}13$
52.1	9.7	024
26.85	9.6	$\bar{1}12$

θ-Al_2O_3		
2θ	**Intensity**	**hkl**
32.79	100	002
31.21	79.4	400
36.68	78.3	111
67.42	57.3	512
38.88	52.7	310
44.8	50.7	$\bar{1}12$
31.61	45.6	$\bar{4}01$
40.02	42.5	$\bar{3}11$
63.93	0	020
67.57	30.4	$\bar{2}21$

Table C.1 (Continued)

γ-Al_2O_3			η-Al_2O_3			α-Al_2O_3		
2θ	**Intensity**	**hkl**	**2θ**	**Intensity**	**hkl**	**2θ**	**Intensity**	**hkl**
37.67	100	211	37.71	100	311	35.15	100	104
67.08	52.6	224	66.9	52.4	440	43.35	95.6	113
37.91	52.5	103	45.88	43.1	400	57.5	91.8	116
45.78	42.9	220	32	34.2	220	25.58	68.1	012
32.07	36.7	112	60.84	21.3	511	68.21	53.1	300
66.76	26.8	400				52.55	47	024
46.20	21.2	004				37.78	46.1	110
						66.52	34.8	214

Figures C.1 through C.6 give presentation of ICSD cards given in Table C.1 as a visual aid.

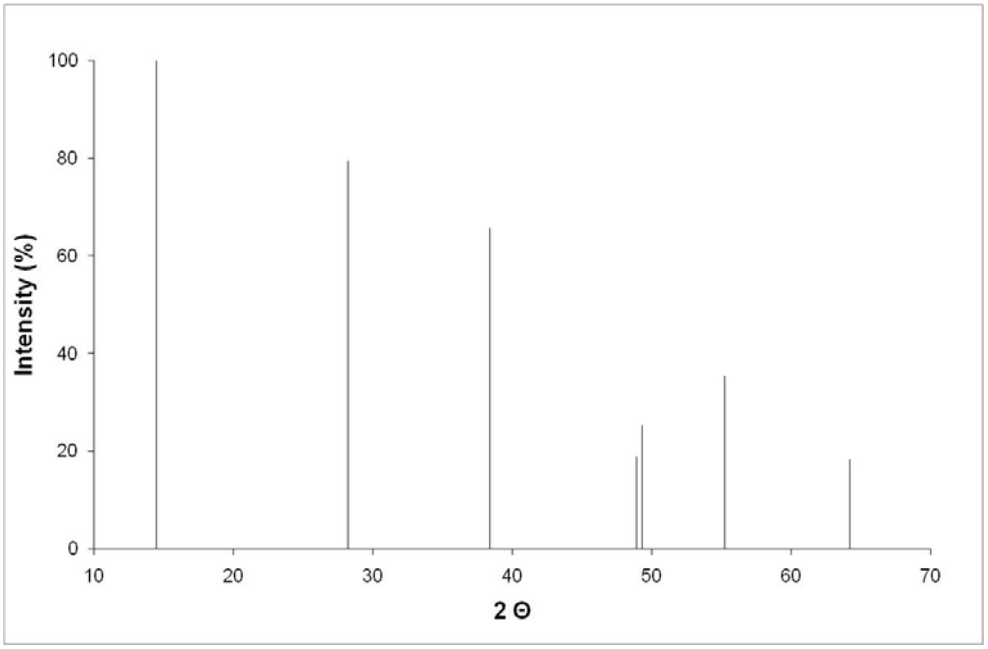

Figure C.1 XRD pattern of orthorhombic AlO(OH).

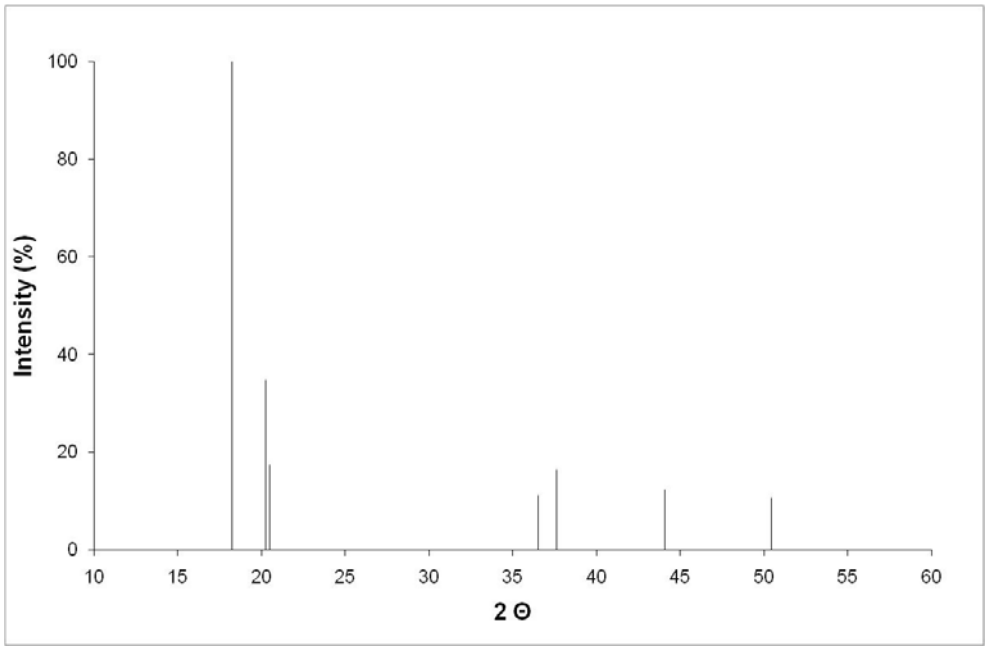

Figure C.2 XRD pattern of monoclinic gibbsite, $Al(OH)_3$.

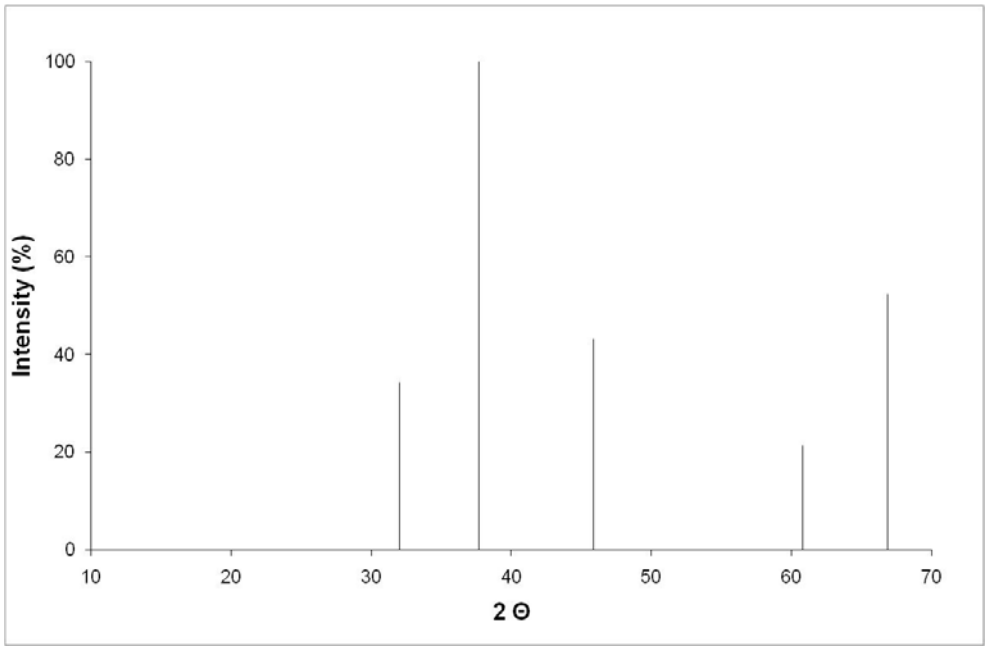

Figure C.3 XRD pattern of cubic η-alumina.

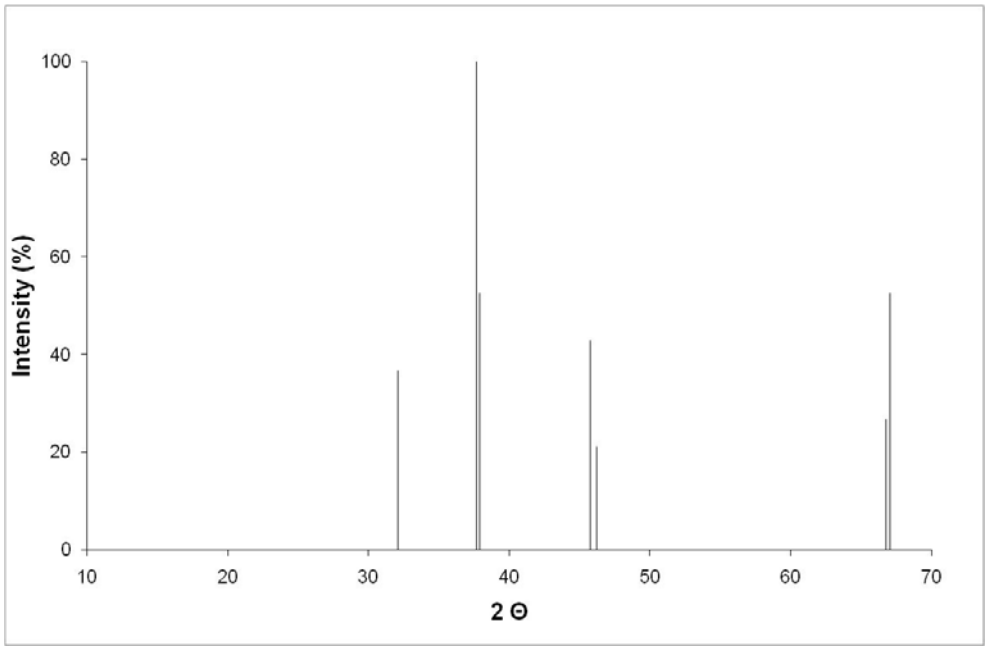

Figure C.4 XRD pattern of tetragonal γ-alumina.

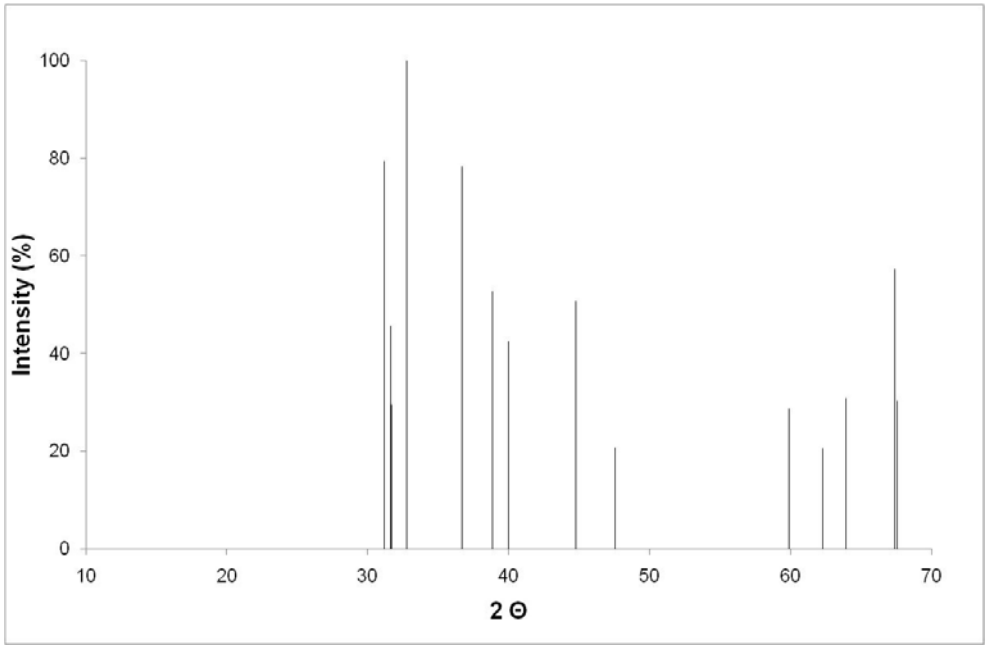

Figure C.5 XRD pattern of monoclinic Θ-alumina.

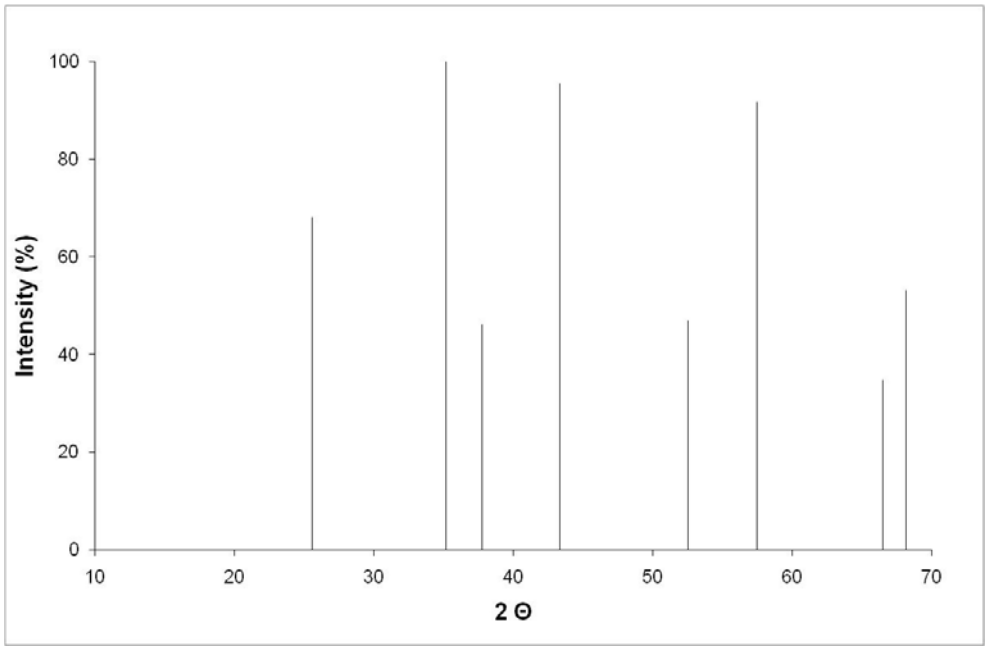

Figure C.6 XRD pattern of rhombohedral α-alumina.

APPENDIX D

THERMAL ANALYSES

Here, thermal analyses (differential thermal analysis (DTA) and thermogravimetric analysis (TGA)) results of boehmite and mechanochemically treated ODBs are given. In Figures D.1, D.2, D.3, D.4 and D.5 traces of B (boehmite), MC-AA (ODB treated with AA), MC-MAA (ODB treated with MAA), MC-SA (ODB treated with SA) and MC-Ly (ODB treated with Ly), are given respectively.

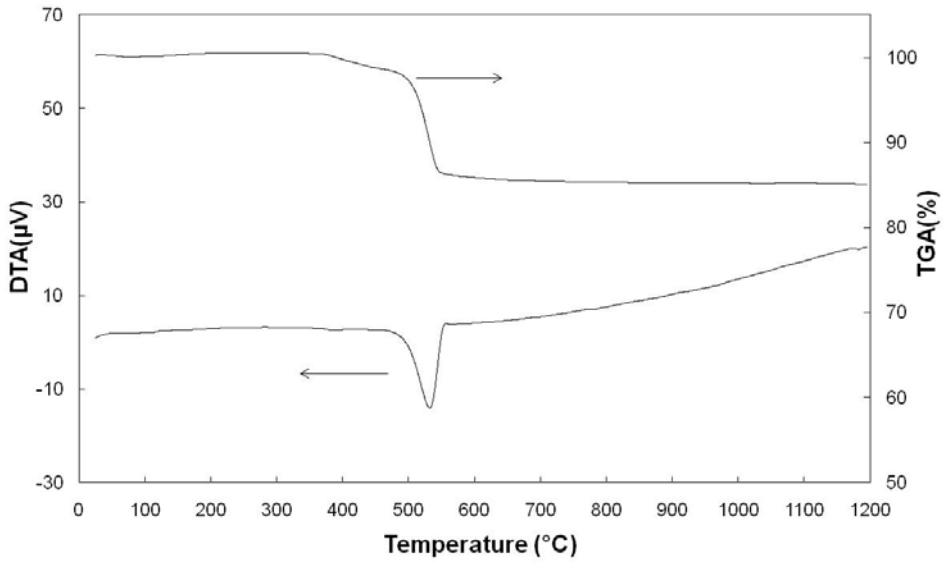

Figure D.1 DTA and TGA profiles of boehmite produced with the method described in Appendix B.

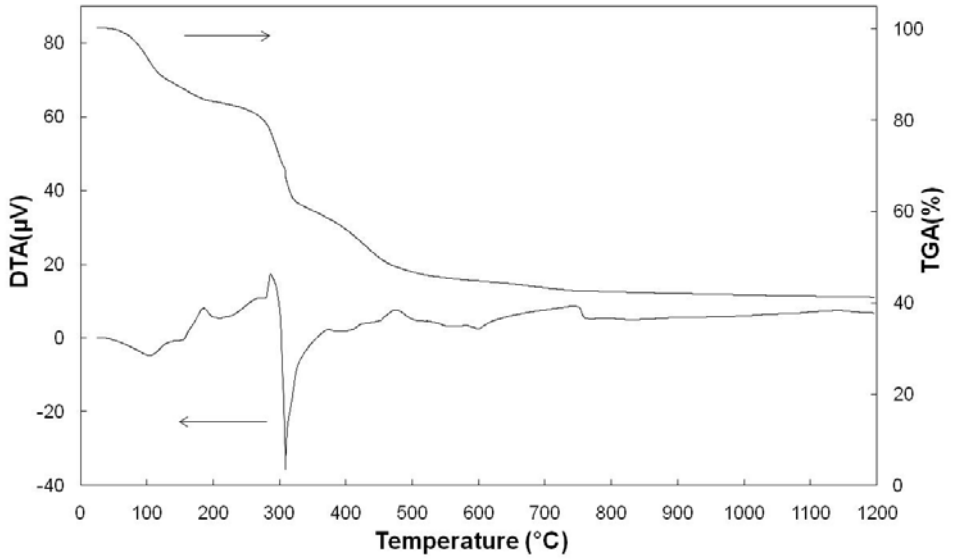

Figure D.2 DTA and TGA profiles of MC-AA (ODB treated with AA).

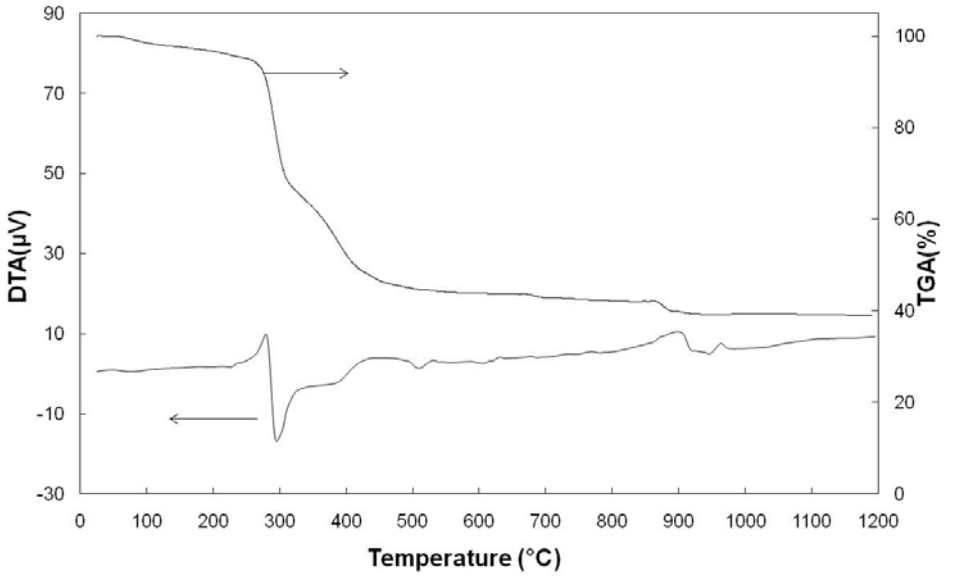

Figure D.3 DTA and TGA profiles of MC-MAA (ODB treated with MAA).

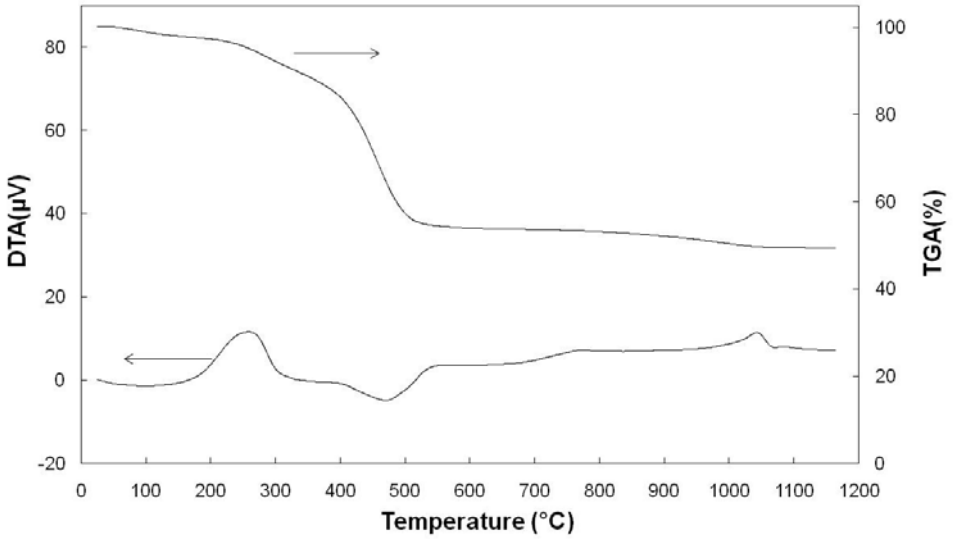

Figure D.4 DTA and TGA profiles of MC-SA (ODB treated with SA).

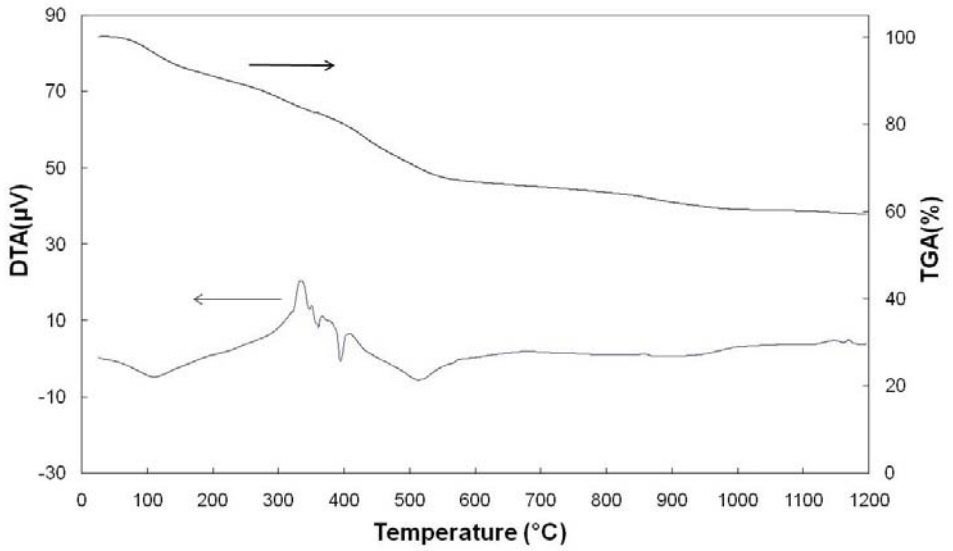

Figure D.5 DTA and TGA profiles of MC-Ly (ODB treated with Ly).

The Ly treated shows the least weight loss among all treated ODBs. The fact that the number of possible transitions is less in high temperature end of Ly treated ODB supports the observation that it shows the purest α-Al2O3 among all ODBs. In addition, the initial endothermic peak which can be observed in all ODBs do not exist in the boehmite. This lends support on the fact that all ODBs are furnished with surface adsorbed and/or intercalated organic reagents as also proved by XRD and FT-IR results. Furthermore boehmite looses its structure by the formation of water (exothermic peak around 500^{o}C). However such a loss is only evident in SA and Ly treated samples at temperatures close to 500^{o}C, but occurs at an early temperature in AA and MAA treated ones. It should be remembered that XRD results point to the preservation of boehmitic layers in SA and Ly treated samples. However the layers are regularly intercalated with AA and MAA in AA and MAA treated ones. Therefore deintercalation from the loosely stacked layers of AA and MAA treated samples occurs at a lower temperature like 300^{o}C. Besides the trace of leave is almost identical in these samples pointing to the detail that their bonding modes are similar, as was proven in FT-IR analyses. The peak denoting deintercalation in AA treated sample is sharper than that of MAA treated sample. It was also seen from XRD results that in AA there was only one type of interlayer spacing, whereas MAA displayed two additional spacing besides the standard boehmite spacing. These two observations complement each other.